NASA CR-188257

REFERENCE COPY

Final
Report

March 1981

Shuttle/Payload Contamination Evaluation Program
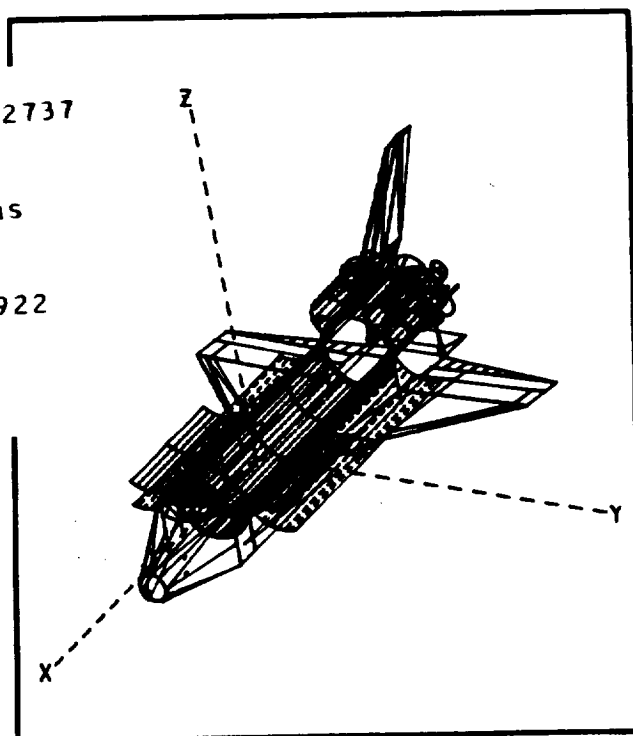
Further Model Refinement and Pre-Mission Contamination Assessment

MARTIN MARIETTA

MCR-81-510
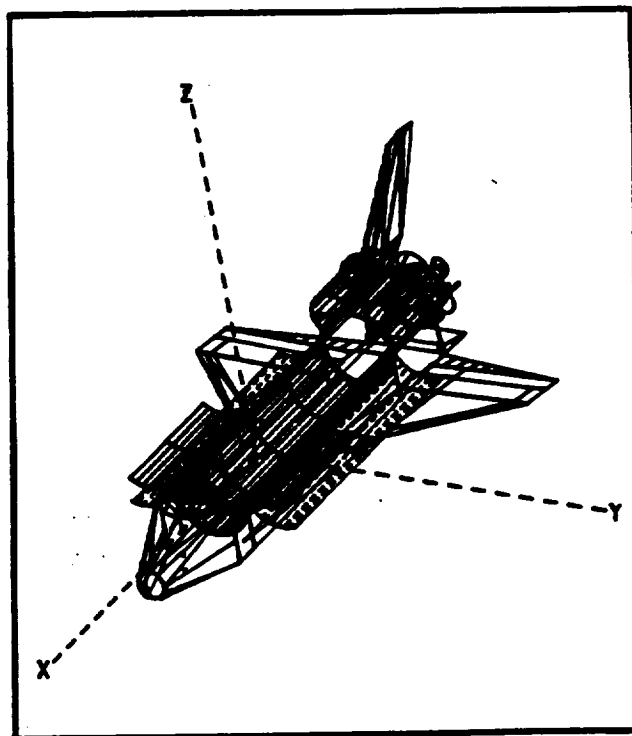Contract N.:S9-15526

Nasa C.R. 188257

Final
Report   March 1981

Shuttle/Payload Contamination Evaluation Program

Further Model Refinement and Pre-Mission Contamination Assessment

264 MR
570 CN
366 PA
808 SK

MARTIN MARIETTA

MCR-81-510
March 31, 1981

SHUTTLE/PAYLOAD CONTAMINATION
EVALUATION PROGRAM
THE SPACE COMPUTER PROGRAM
FINAL REPORT

FURTHER MODEL REFINEMENT AND
PREMISSION CONTAMINATION ASSESSMENT

Contract NAS9-15826

Authors

F. J. Jarossy
L. E. Bareiss
J. C. Pizzicaroli
N. L. Owen

Prepared for

National Aeronautics and Space Administration
Lyndon B. Johnson Space Center
Houston, Texas 77058

by

MARTIN MARIETTA CORPORATION
DENVER AEROSPACE
P. O. Box 179
Denver, Colorado 80201

CONTENTS

CONTENTS (Continued)

CONTENTS (Continued)

CONTENTS (Continued)

1.0 INTRODUCTION

This report summarizes the results of the "Shuttle Payload Contamination Evaluation (SPACE) Program Further Model Development and Refinement Program conducted for the National Aeronautics and Space Administration (NASA) Lyndon B. Johnson Space Center (JSC) under contract NAS9-15826.

The SPACE computer program was developed to provide the user with a flexible and consistent analytical tool with which to predict the external self-induced molecular contaminant environment of a spacecraft during its on-orbit operations. The SPACE computer program mathematically synthesizes the induced environment for major contaminant sources of the Shuttle Orbiter. It predicts direct flux surface deposition, return flux on surfaces with up to 2π steradian fields-of-view and molecular column densities for any modeled line-of-sight.

From its inception under NASA Contract NAS8-30452 to its delivery to JSC under the NAS9-14767 contract and updated under contract NAS9-15826, the primary goal of the SPACE computer program was to evaluate the molecular environments induced by the Space Transportation System (STS) Shuttle Orbiter and key Spacelab configurations for compliance with program contamination control requirements. These requirements have in part dictated the format and present capabilties of the SPACE program. As the STS Program approached its operational phase, an important need existed to to be able to evaluate the external self-induced molecular contaminant environment on an operational basis for a number of Shuttle Orbiter missions -- in particular the Orbital Flight Test (OFT) series that involves the Induced Environment Contamination Monitor (IECM). In order to meet these needs, the JSC SPACE program required further improvements, utility and flexibility in its code. The end product of these model improvement activities is the second version of the SPACE Program denoted as SPACE II.

1.1 Purpose

The purpose of the activity reported herein was to complete further identified improvements and create greater utility and flexibility in the SPACE Program code delivered to NASA JSC under previous contract and to conduct premission contamination analyses of the early OFT/IECM Shuttle missions.

1.2 Scope

The scope of this study activity included the following tasks:

a) update the SPACE code to include surface-to-surface contamination exchange and deposition;

b) update the SPACE code to include a summation routine for deposition

1

due to return flux and surface-to-surface deposition;

c) update the SPACE code to include an Induced Environment Contamination Monitor (IECM) representation for mission assessment purposes;

d) update the SPACE code to increase data handling and graphical presentation;

e) conduct a parametric trade study of the sensitivity and accuracy of the multi-reflect subroutine in comparison to the GBCAL routine;

f) develop OFT IECM/Shuttle Orbiter body-to-body mass transport factor files;

g) perform the necessary SPACE analysis runs to complete the in-bay and mapping mission pre-mission contamination assessments;

h) perform an IECM mission analysis and assessment for in-bay and an outside the bay mapping mission;

i) checkout the updated SPACE code delivered to NASA JSC;

j) provide user's training and liaison with JSC personnel;

k) prepare an updated User's Manual; and

l) prepare a final report.

1.3 Summary

The SPACE code has been improved to provide the user with greater utility and flexibility in performing both mission contamination analyses and parametric analyses in support of trade studies. The improvements include logic to: 1) consider direct surface-to-surface contamination exchange; 2) compute the fractional deposition of impinging flux; 3) account for the fraction of the impinging flux not deposited on surfaces (multiple reflection option) which effectively increases source emission rates; 4) provide a continuous summation of deposition due to return flux and direct flux for use with the stacked run mission analysis option; and 5) interface with the DISSPLA software plot package to provide a variety of graphical representations of the SPACE II output data.

The Shuttle Orbiter/IECM mission analyses and assessment for an IECM in-bay (OFT-1) and outside of the bay (OFT-3) mapping mission have been performed. The results of the OFT-1 analysis indicates the following for the mission parameters considered:

a) The mass spectrometer sensitivity is insufficient to detect the

2

predicted contaminant environment induced by the outgassing, early desorption, leakage, and the majority of the RCS engine sources. Several RCS engine sources were determined to be marginally detectable.

b) Several TQCM instruments are expected to detect the payload bay outgassing species environment if minimum TQCM design temperatures can be attained. Detection of the RCS engine MMHNO3 specie requires near maximum burn times. The light gas engine species (H_2O, CO_2, etc) are not expected to condense at TQCM temperatures.

c) The CQCM is expected to respond to the outgassing return flux component if the minimum design temperature ($-133^\circ C$) is attained. However, at higher temperatures ($> -100^\circ C$), the predicted deposition is below the minimum detectable level. No condensation is predicted for the early desorption, leakage, or evaporator sources due to the low predicted incident flux levels. RCS MMHNO3 deposition requires near maximum burn times.

The OFT-3 IECM instrument predictions have been developed for the baseline 24 measurement point matrix as defined by the mission analysis plan. The contamination sources evaluated include outgassing, early desorption, leakage, evaporator, and the RCS engines.

The results of the analysis show that the 24 point plan will provide sufficient data to characterize the expected sources provided that sufficient post mission support data (attitude timeline, surface temperatures, event timeline, etc) are available.

2.0 SPACE COMPUTER MODEL UPDATE

This section describes the activities performed to increase the capability and flexibility of the SPACE computer program. These activities included: 1) the development of new code to predict direct line-of-sight flux impingement on sensitive surfaces from surface and point sources, the deposition of direct and return flux on sensitive surfaces, and the increase in effective source emission rates due to multiple contaminant flux reflections; 2) the development of new code to accumulate deposition on critical surfaces for multiple stacked run mission simulation; 3) the development of new code not specifically requested in the Statement of Work (SOW) but felt to be necessary to provide analytical capability consistent with the intent of the code; 4) the development of sample cases for JSC code checkout and verification; 5) the preparation of a SPACE user's manual and; 6) providing for user's training/liason throughout the performance of the contract activity.

The original approach to upgrade the SPACE code was to modify the existing SPACE I. However the magnitude and extent of the code changes soon showed this approach to be impractical prompting a complete redesign of the code and leading to the development of the SPACE II model. A detailed description of the SPACE II model is contained in the SPACE User's Manual[1]. The remainder of this section describes the functional improvements in the code with respect to the directed task requirements.

2.1 Direct Flux/Multiple Reflection Algorithms

This section describes the development of the direct flux algorithms, the direct and return flux deposition algorithms, and the multiple reflection algorithms.

2.1.1 Direct Flux Algorithms - The capability to predict direct line-of-sight flux impingement between source and receiver has been developed and incorporated into the SPACE code. The new subroutine driver, DIRCT, computes the direct flux mass transport between any user selected receiver and any combination of surface or point sources, up to 300 total, selected by the user. The direct flux is computed from the basic mass transport function:

$$F_i = \Psi_j * TF_{j-i} \qquad (2-1)$$

where:

F_i = mass flux impinging on surface i,
Ψ_j = source function of j, and
TF_{j-i} = mass transport function between surfaces j and i.

4

The source functions for point and surface sources are essentially unchanged from SPACE I. A new input tape, TAPE 12, has been developed to store the body-to-body mass transport factors (TF_{j-i}) which are computed by the TRASYS[2] thermal radiation program. For each change in the user's spacecraft geometry configuration of a new set of TRASYS runs are required.

2.1.2 <u>Deposition Algorithms</u> - Algorithms have been developed and incorporated into the SPACE II code to compute the fraction of impinging flux that deposits on user selected critical surfaces. The algorithms are applied to both the direct flux component and the return flux component according to the following relationship:

$$D_i = F_i * S \qquad\qquad (2-2)$$

where:

D_i = deposition rate on surface i,
F_i = flux impinging on surface i, and
S = sticking coefficient.

The sticking coefficient, S, is a complex variable based on such assorted physical phenomena as the characteristics of the contaminant source, temperatures of sources and critical surfaces, source species, the transport phenomena and surface phenomena such as UV polymerization and chemical reactions. The sticking coefficient relationships currently in the SPACE II program are summarized in Table I. These are based on available ground and flight data applicable to the occurring phenomenon.

For all outgassing species the sticking coefficient is based on the source temperature (T_j) and receiver temperature (T_i). For the direct flux transport mechanism T_j is defined prior to the analysis and stored on TAPE 10. T_i may also be stored on TAPE 10 or input via namelist. Therefore the direct flux sticking coefficient can easily be computed for each pair of source/receiver nodes. However, for the return flux transport mechanism, the value of T_j is not obvious since node j is now a point (or volume) in space with a density comprising contributions from up to 300 surface/point sources at potentially 300 different temperatures.

The approach developed to compute T_j for return flux outgassing species is based upon computing on effective T_j assuming that the temperature of all sources contributing to the density at point j can be weighted by the fractional density contributed by each source or:

5

Table I. Sticking Coefficient Summary

Contaminant Source/Species	Sticking Coefficient S
Outgassing ● All Species	$(T_j - T_i)/200$* $S = 0 \quad T_i > T_j$ $S = 1 \quad (T_j - T_i) > 200$*
Engines (VCS, RCS) ● MMH-Nitrate	1.0 (i.e. $P_v \tilde{=} 0$)¶
● All Other Species **Early Desorption** ● All Species **Leakage** ● All Species **Evaporator** ● All Species	$\dfrac{F_i - E_i}{F_i}$ ¶ F_i = incident flux E_i = evaporation rate

*T_j = Source Temperature (°C); T_i = Surface of Interest Temperature (°C)

¶Langmuir - Knudsen relationship utilized to determine desorption rate of deposition

$$T_{j(eff)} = \sum_{n=1}^{300} T_n \left[\frac{\rho_n}{\rho_t}\right] \qquad (2\text{-}3)$$

where:

$T_{j(eff)}$ = effective temperature for surface j,
T_n = temperature of surface n,

ρ_T = total density at the source point $T = \sum_{n=1}^{300} \rho_n$, and

ρ_n = density contribution at the source point due to surface n.

An effective T_j is therefore determined for each point along the line-of-sight and a corresponding sticking coefficient for outgassing species can be computed based on the relationship shown in Table I.

For all other species (except MMHNO3 where S = 1) the sticking coefficient is given by an impingement rate/evaporation rate algorithm. The impingement rate is compute by SPACE while the evaporation rate for the light gas species is computed from the Langmutr-Knudsen relationship:

$$E_I = 0.0583 \left[\frac{M_I}{T_i}\right]^{\frac{1}{2}} P_{VAP} \qquad (2\text{-}4)$$

where:

E_I = evaporation rate of specie I (g/cm^2 sec),
M_I = molecular weight of specie I,
T_i = temperature of receiver node ($^\circ$K), and
P_{VAP}^i = vapor pressure of specie I at T_i (torr).

Since the evaporation rate is a function of only the receiver node temperature, the sticking coefficient calculation is straight foreward for both direct flux and return flux transport mechanism calculations.

2.1.3 _Multiple Reflections_ - A complex mass exchange occurs with a compound spacecraft configuration as mass leaves one surface, impinges on other surfaces and is partially reflected, and re-reflected within an enclosure with the possibility of partial deposition occurring at each surface contacted. Algorithms have been developed and incorporated into the SPACE II code to account for this phenomenon during the analysis stream of flux/deposition calculations.

The initial approach persued was to use the method devised by Gebhart[3] involving computing body-to-body form factors and incorporating sticking coefficients as absorptivities to account for flux losses at reflecting surfaces. Then, using the "net radiation method" equations , the resulting receiver flux is computed. The TRASYS code contains an option, GBCAL, which performs this calcuation for radiation transfer.

7

However problems were encountered in trying to modify GBCAL for mass transfer. These problems resulted from the fact that for a specific receiver, the absorptivity is unique for the single source considered (i.e., the sun) whereas the sticking coefficient for a receiver depends, for outgassing, on each source temperature and is therefore variable. A significant effort was expended attempting to modify GBCAL for mass transfer. This was successful only for a direct flux case considering the outgassing specie only, and a 38 node maximum geometry configuration. This capability was, however, incorporated into the SPACE I model and used to provide a closed form benchmark for verifying the more successful "multi-reflect" approach. The updated SPACE I code and user's manual were delivered to JSC.

The multi-reflect approach, described in detail in Appendix A, Part 1, is an interactive procedure which modifies contaminant surface source rates based upon multiple reflections of contaminant flux for complex geometries. The multi-reflect algorithm is not limited by specie, configuration size (number of nodes), or transport mechanism (both direct and return flux can be analyzed).

A comparison of the multi-reflect and GBCAL algorithms was the subject of a trade study. The specific objective was to evaluate the convergence characteristics of the interactive multi-reflect option, incorporated in SPACE II, to the closed form GBCAL option in SPACE I for typical spacecraft configurations. The results of the trade study, presented in Appendix A, Part II and Part III, showed that excellent convergence could be obtained with multi-reflect in most cases with 2 to 3 reflections with significant savings in computer run time. Therefore the multi-reflect approach is recommended for computing the effects of multiple reflections.

2.2 Deposition Summation Algorithms

The SPACE code has been modified to automatically accumulate the predicted deposition on selected critical surfaces from both direct and return flux mechanisms for multiple discrete mission intervals. This task required: 1) development of an algorithm to input the velocity vector during an orbital time slice as a function of orbital position and vehicle orientation and; 2) the development of an algorithm to maintain a running total of the deposition on a critical surface at the termination of each run within the stack comprising the entire mission simulation period.

2.2.1 Variable Velocity Vector Algorithm - An algorithm has been developed and incorporatied into the SPACE II code to form the three return flux velocity components (V_x, V_y, V_z) given three Shuttle Orbiter Euler angles. These angles are expressed as Euler rotations about the Shuttle Orbiter coordinate frame. User inputs are orbital velocity (V_t and the three Euler angles PITCH, YAW and ROLL where:

PITCH = First spacecraft rotation, CCW about Y axis,
YAW = Second spacecraft rotation, CCW about Z axis, and
ROLL = Third spacecraft rotation, CCW about X axis.

The angular relationships are shown in Figure 1. The null orientation (PITCH = YAW = ROLL = 0.) has the velocity vector coincident with the +X axis.

2.2.2 Summation Algorithm - Additional logic has been developed and incorporated into the SPACE II code to accumulate deposition for discrete mission intervals executed during any one continuous SPACE run. This involved using the current generalized code to calculate an initial deposition on each critical surface upon entry into the program. Then, during sustained stacked time slices, these deposition calculations are carried over into the next time slice. Deposition is computed for both direct and return flux transport mechanisms using existing sticking coefficient and evaporation rate algorithms. The stacked run time slice intervals are defined by the user input variables TSTART and TSTOP. This time interval is the surface source Δt used to compute deposition. Within the time slice interval, point sources can be initiated via the input variable ONTIME. The logic assumes that point sources are initiated at the end of a time slice interval. A detailed description of the summation logic is contained in Appendix B.

2.3 DISSPLA Interface

Subroutines have been developed and incorporated in the SPACE code to produce quality, professional plots of SPACE program output densities through interface with the DISSPLA system routines. Densities are stored on tapes generated by the SPACE computer program. The plot program reads the density tapes, and can create simple plots of density versus distance along a line-of-sight, isocontour plots (isodensity contours in a given plane of space), and/or carpet plots (isodensity fields in three dimensional space). Total density and density due to any source and specie may be plotted enabling the user to determine density contributions from any source or specie.

The simplist presentation (Figure 2) are log-log plots of density versus distance along a line-of-sight. Any number of log cycles may be placed on the axes; however, an excessive number of cycles will produce an unattractive plot. A maximum of six curves, corresponding to six user-defined lines-of-sight may be presented on a single plot. The user may input axis limitations, or allow the program to determine axis extremes based upon plot data.

Isocontour plots (Figure 3) present constant density in two-dimensional space, defined by a plane of the XY, XZ, or YZ axes of the local receiver coordinate system. A maximum of three isocontours may be included on one plot. Density points defining the isocontour are

9
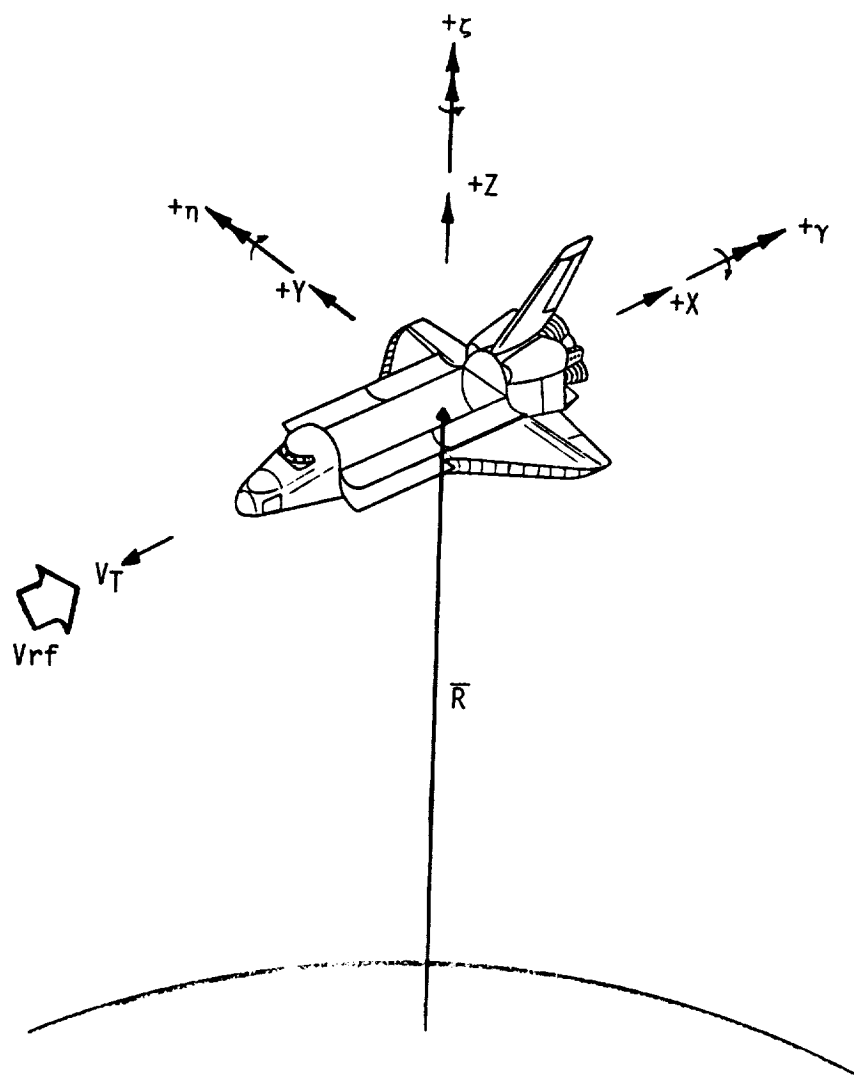
X = longitudinal axis of the Shuttle Orbiter (+ towards aft)

Y = lateral axis (+ towards right wing)

Z = lateral axis (+ away from keel)

α = roll

η = pitch

ζ = yaw

V_T = velocity vector in direction of Orbiter travel

Vfr = return flux velocity $(-V_T)$

$\overline{R}$ = radius vector from center of earth to Orbiter

Figure 1. Variable Velocity Vector Algorithm Angular Relationships

10
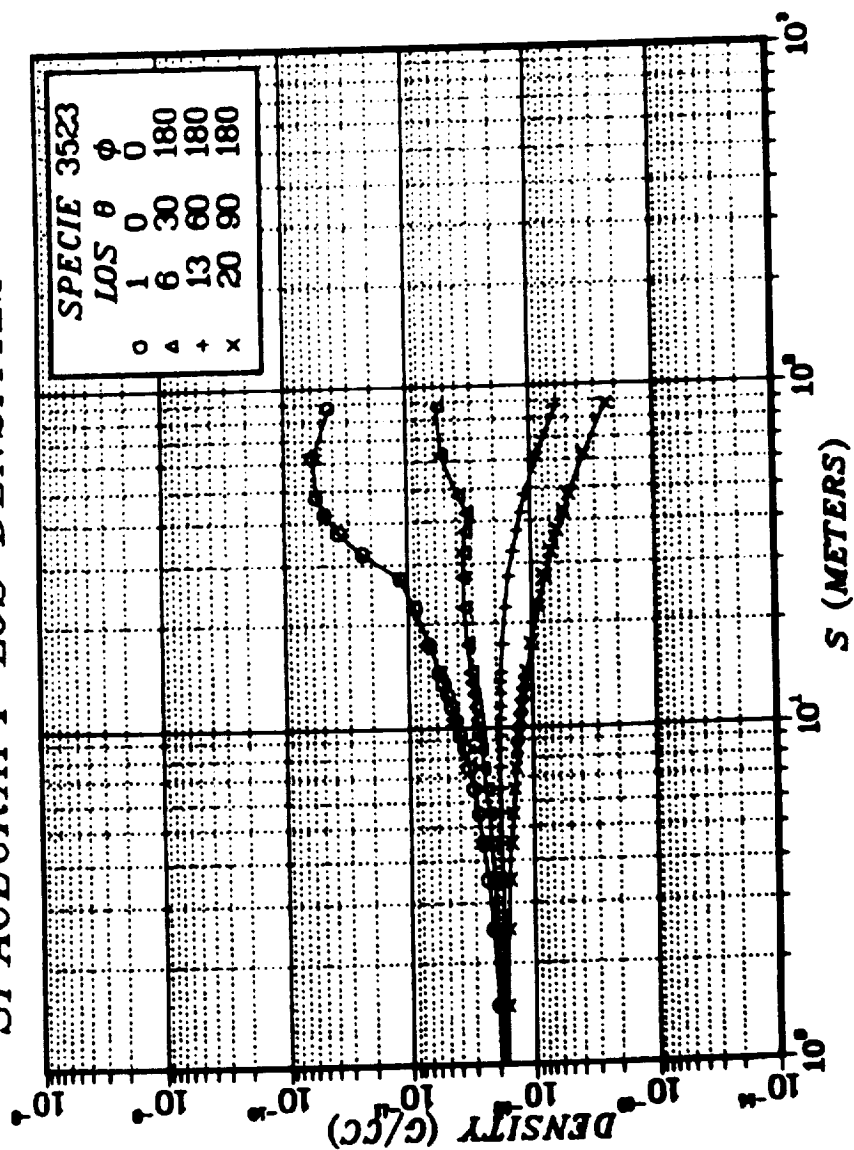
Figure 2. DISSPLA Line-of-Sight Density Sample Plot.
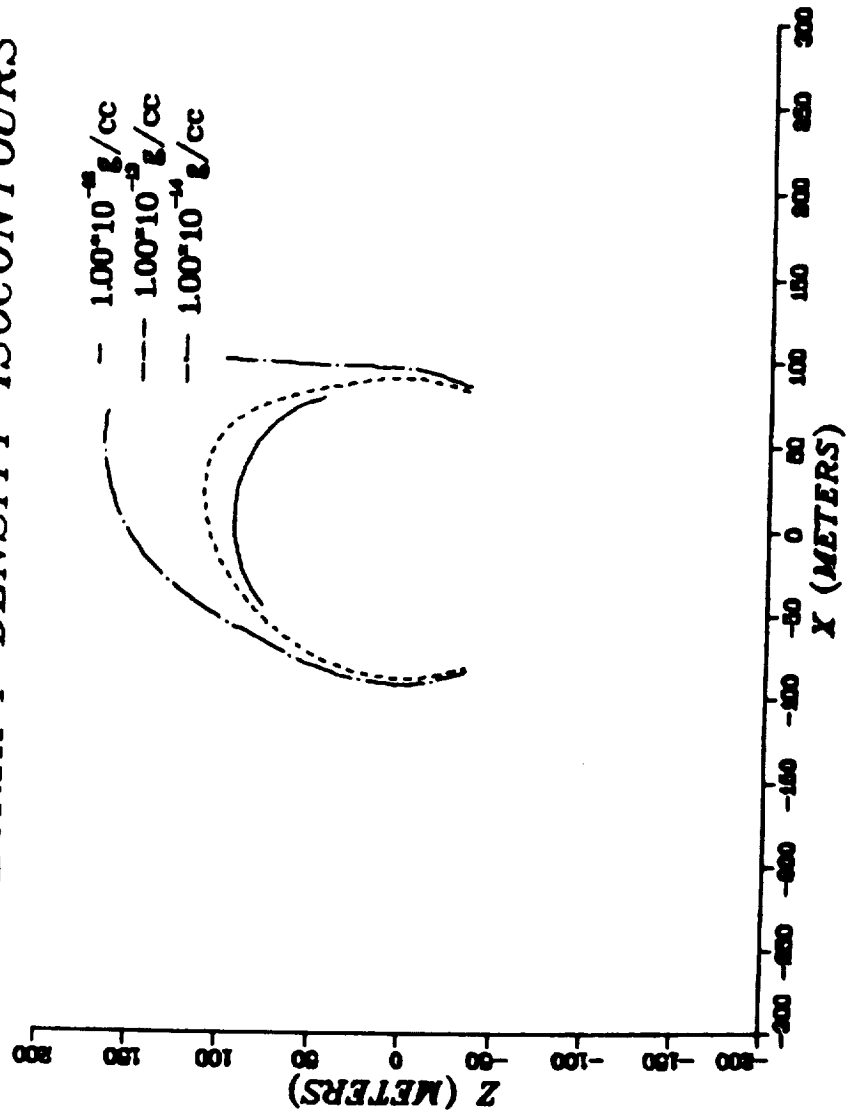
Figure 3. DISSPLA Isodensity Contour Sample Plot

12

determined by interpolation or extrapolation based upon user-defined density levels. Axes ends may be input by the user or the user may allow axes ends to default to preset values.

Carpet plots (Figure 4) depict constant density in three-dimensional space. Only one constant density surface may be drawn on a given plot because of the manner in which the grid is drawn on the plot. Density points defining and isodensity field are determined by inter-polation or extrapolation based upon user-defined density levels. Axis extremes may be input by the user or the user may allow axis ends to default to preset values.

A detailed description of the SPACE/DISSPLA interface and use of the DISSPLA option is provided in the SPACE User's Manual Supplement.[4]

2.4 General Capabilities Update

The decision to redesign the SPACE code provided the opportunity to improve the model capabilities in a variety of areas. This section summarizes these additional improvements.

2.4.1 Arbitrary Point Source Capability - The SPACE II code has been updated to include the capability to model any arbitrarily located engine, vent or point source on the Orbiter and/or payload configurations. To accomplish this, a routine was developed to determine the necessary geometrical relationships internal to the SPACE II Program, thus eliminating the need to exercise the complex TRASYS model for such calculations. This routine determines the separation distance (R) between source and receiver location and the angle (Θ) that the R vector makes with the point/vent source centerline (or surface normal). This routine, in conjunction with the hemispherical point matrix and the appropriate source plume function, will allow expeditious determination of plume density and flux levels around any given modeled configuration.

Through NAMELIST input commands, mass or number column densities (MCD/NCD), return flux (RF) and return flux deposition can be calculated for any new point source location, vent direction, plume definition, molecular specie mix and flowrate. SPACE II can interface with input flowfield tapes or input plume parameters can be developed in closed form based upon various approximation techniques and vacuum chamber test data. The SPACE II Program output reports were also expanded to include the capability to display the new vent individual specie predictions and the corresponding vent/engine name for each source evaluated.

2.4.2 Return Flux Methodology Update - The methodology for calculating contaminant return flux from ambient collisions and

SPACECRAFT ISODENSITY FIELD

$\rho = 1.00*10^{-14}$ g/cc
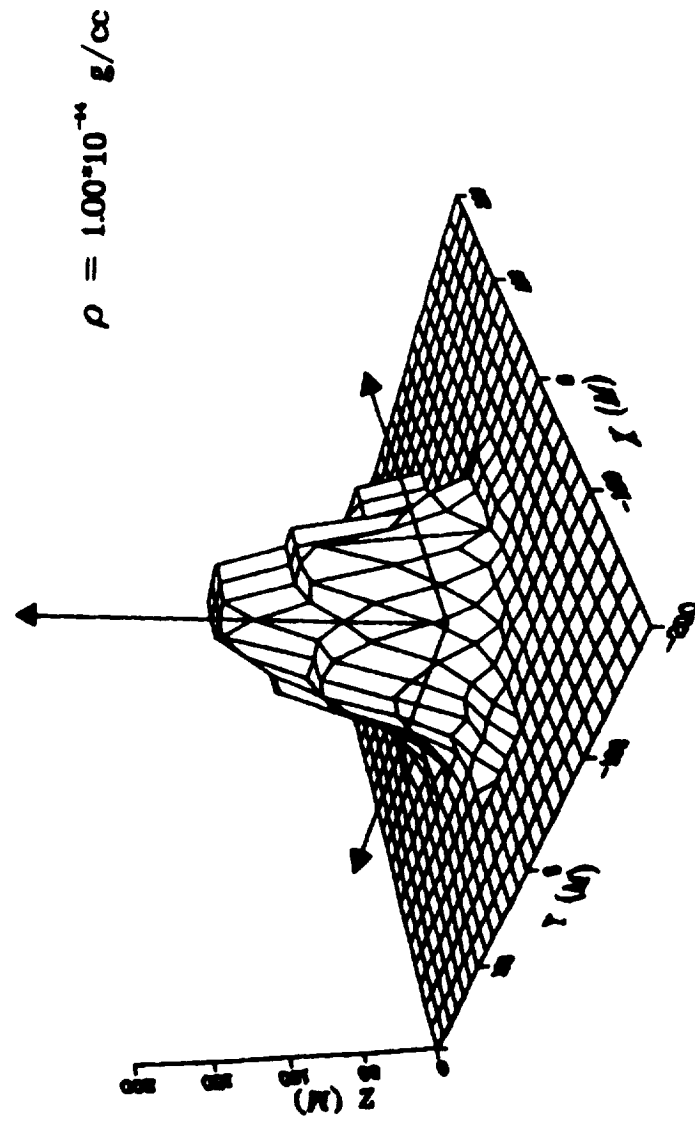
Figure 4. DISSPLA Isodensity Field Sample Plot

self-scattering was completely modified to more realistically reflect the physics involved in these transport phenomena. A modified approximation of the Boltzman Kinetic equation known as the Bhatnager/Gross/Krook model was integrated into SPACE II. This approach considers the attenuation of the returned molecular flux to a surface of interest based upon the tortuous path a returning molecule must travel from its collision center to the surface. The influence of this approach is most evident when dense environments (such as engine plumes) are being evaluated. Also included in the self-scattering option is the effect of the plume flow velocity to reduce the probability of a molecule having sufficient velocity to return. A detailed description of the BGK methodology as applied to the SPACE II Program is contained in Appendix A of the SPACE II User's Manual[1].

2.4.3 <u>Point Matrix Resolution Improvement</u> - An early in-house study indicated that significant errors in cloud density, number column density (NCD) and return flux could result when surfaces are located outside the SPACE I "point" mesh contained within the 60 degree cone above the Shuttle Orbiter. In addition, there appeared to be a large density variation near the Shuttle Orbiter that could not be resoved with the previous 5 meter mesh.

Figure 5 illustrates the extension to the original matrix of points that allows both better resolution above the Shuttle Orbiter and evaluation of return flux to surfaces inside the payload bay. As shown this includes the eight 82.5 degree lines-of-sight (LOS) necessary to complete the mass transport factor data files for the upper hemisphere of the Shuttle Orbiter and payload configurations. Nine additional points have been added to each line-of-sight between one and fifteen meters from the prime measurement point (PMP) to increase the model's resolution in the near bay vicinity. This results in a total of 25 points along each LOS. Current core storage allows 25 points to be stored. Lines-of-sight in the lower hemisphere have been truncated to account for structural interference.

The point selection logic has been extended to consider interpolation within the payload bay (lower hemisphere) so that the return flux can then be calculated to the payload bay floor.

2.4.4 <u>General Program Maintenance</u> - Basic maintenance of the Space II code was conducted throughout the contract period to correct identified program deficiencies in logic, methodology and subroutine operation. Model printout routines were improved and refined to display all new contaminant source molecular species and new vent identifiers in the appropriate output reports. Other model improvements included:

a) the addition of assorted error messages at critical points in the program flow;

15
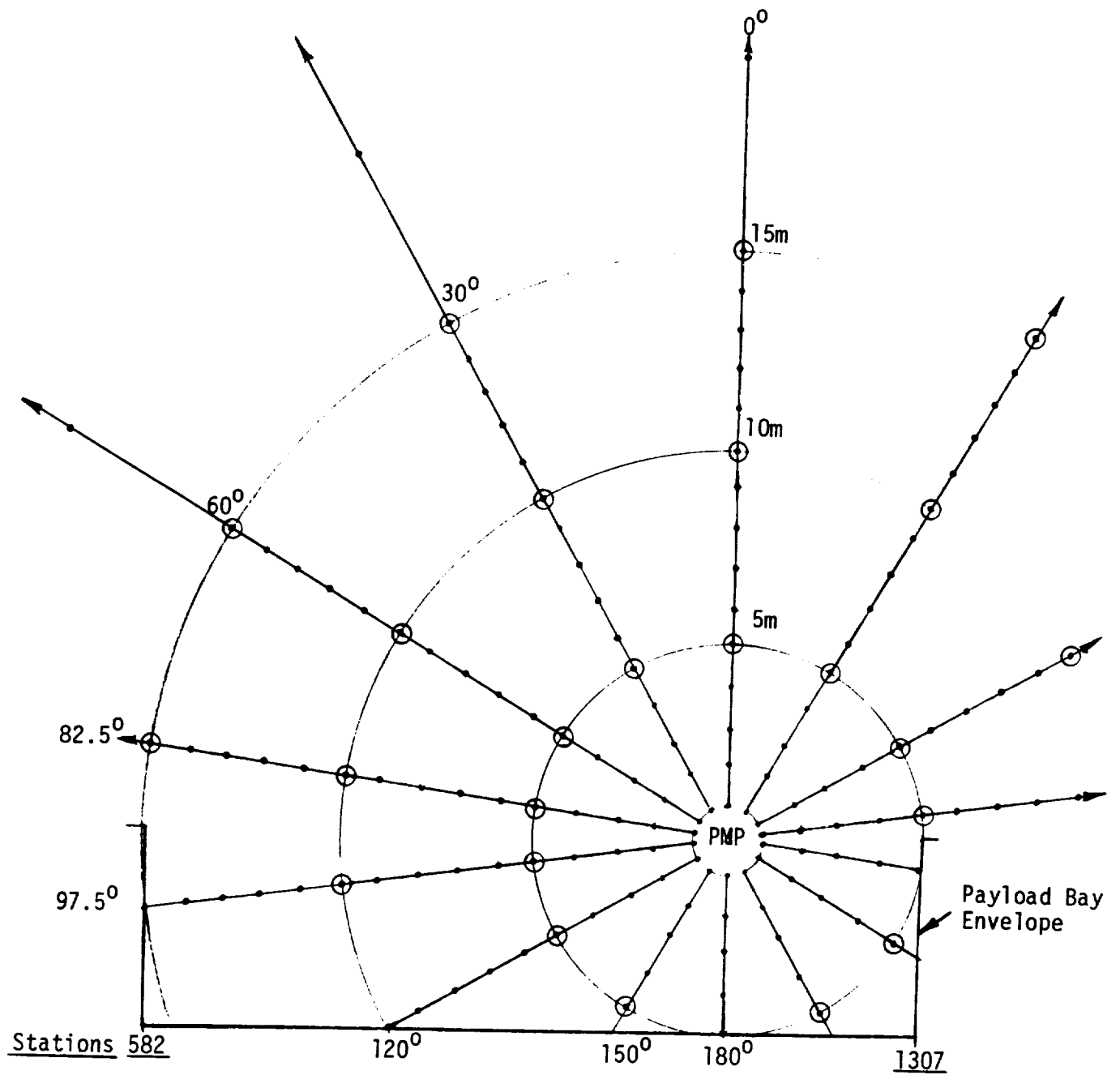
Figure 5. *Illustration of Updated Point Matrix For Return Flux Calculations*

b) the expansion of instructional comment cards in the model run stream;

c) the refinement of output report formats to include accurate surface field-of-view and "zero-valued" predictions for specific point sources; and

c) updating the Orbiter engine plume profiles based upon recent engine performance analyses.

2.4.5 Other Improvements - Other tasks performed during contract period included the following:

a) The JSC temperature conversion program was modified. The purpose of this program is to convert temperature data from JSC orbital simulation tapes into the format required for SPACE input. The code was modified to provide the flexibility to select 7 specific orbital time periods and perform the required interpolation and format conversion.

b) Programs were developed to convert TRASYS program output files into the proper format for input to SPACE. These programs perform the sorting, merging, and format modification functions required to develop SPACE mass-transport factor files TAPE 14, TAPE 15, and TAPE 12 from TRASYS' output files.

c) An algorithm was developed to limit the field-of-view of a disc receiver without the need for developing complex TRASYS geometries. The SPACE input variable FOVANG allows the user to select the field-of-view half-angle for the direct flux option. This variable eliminates contributions from sources with nodal centroids at angles greater than FOVANG degrees from the receiver normal.

2.5 Sample Cases

Sample cases have been jointly formulated by Martin Marietta and JSC to exercise the upgraded SPACE II capabilities and test the software system. The test cases will produce samples of: 1) new output reports from the deposition/multi-reflect link; 2) new output reports to demonstrate the deposition summation logic and; 3)DISSPLA plots. The sample problems formed the primary basis for model demonstration and verification at JSC. The sample problems are contained in References 1 and 4 which provide a description of the problem, a complete listing of the required model input control card and sufficient model output listings to allow the user to exercise the model for the given sample problem and verify the accuracy of the output data.

17

2.6 User's Manual

The "Shuttle/Payload Contamination Evaluation Program User's Manual", MCR-77-106, dated April 1977 and revised September 1977 was updated to reflect all modifications made to the SPACE program as a result of the tasks completed during this contract. The User's Manual was published in its entirety prior to the conclusion of the contract. (See Reference 1). Refinements and modifications to the User's Manual were made, where applicable, to facilitate the understanding of the operation of the computer code and the physics involved in the program methodology.

2.7 User's Training

User's training and liason with JSC personnel who will be operating the SPACE II program to address problems incurred in understanding and executing the program was provided. Weekly telecons were held with JSC to discuss progress and resolve problems on a real-time basis. Discussions were held at various times with JSC CSC personnel to resolve UNIVAC system level problems encountered with SPACE II program loading, segmentation, and data tape manipulation.

3.0 MISSION ANALYSIS

The SPACE II computer model was exercised to perform a contamination analysis of two Orbital Flight Test (OFT) missions; 1) OFT-1, where the (IECM) is retained in the Shuttle Orbiter bay and; 2) OFT-3, where the Remote Manipulator System (RMS) deploys the IECM to measure/map the induced contamination environment at various locations outside the payload bay. During the mission analysis, emphasis was focused on parameters measured by the five Temperature Controlled Quartz Crystal Microbalances (TQCM), the Cryogenic Quartz Crystal Microbalance (CQCM), and the Mass Spectrometer. The mission analyses were performed according to the procedures outlined in the respective mission analysis plans mutually agreed to by Martin Marietta and JSC. The remainder of this section describes the performance and results of these analyses.

3.1 General Overview

This section describes IECM geometry development and contamination source characteristics, the thermal profile used for the analyses, and the performance characteristics of the QCMs and the mass spectrometer.

3.1.1 IECM/Development Flight Instrumentation (DFI) Geometry and Source Characteristics - The IECM is designed to provide verification measurements of the particulate and molecular environment during ground operations, ascent, on-orbit, descent and post-landing for selected OFTs.

Of the ten IECM instruments shown in Figure 6 :
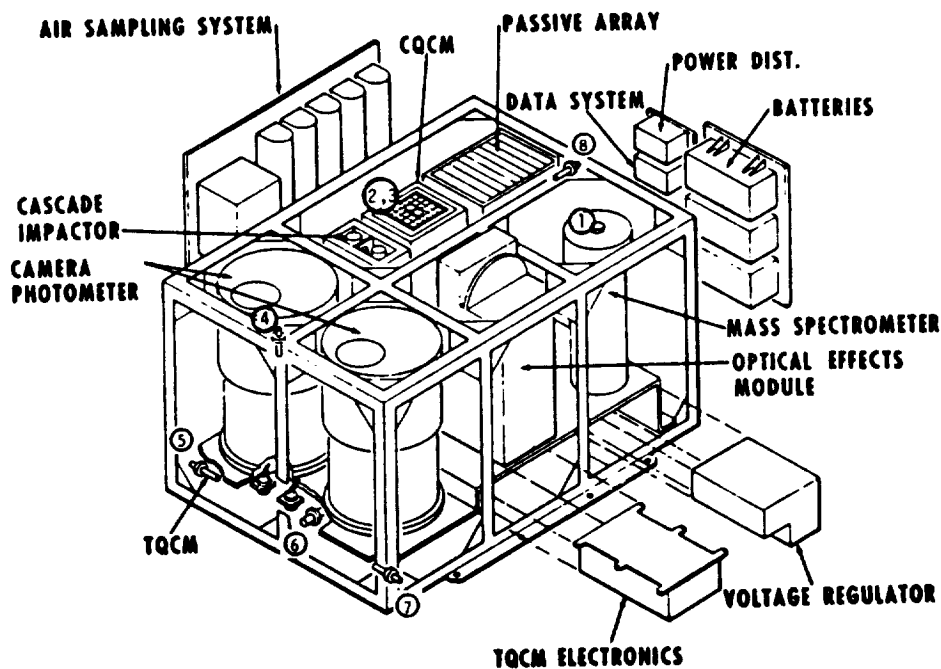
Figure 6. Induced Environment Contamination Monitor

19

the following instruments will be operational during the on-orbit periods: 1) Cascade Impactor; 2) Passive Sample Array; 3) Optical Effects Module: 4) five TQCMS; 5) CQCM; 6) Camera/Photometer; and 7) Mass Spectrometer. Location of the IECM in the payload bay is illustrated in Figure 7. As indicated, other experiments will also be flown in the bay during these OFT missions. For this study, only the IECM and the DFI geometries were considered.

Of the seven monitoring instruments listed above, the TQCMs, CQCM, and mass spectrometer are of prime importance in the current study because they are relatable to the SPACE code output. The five TQCM heads are mounted on each side of the IECM (except the bottom) and therefore face in the +X, -X, +Y, -Y, and +Z Orbiter axes. The CQCM is located on the top (+Z) side of the IECM.

The mass spectrometer has been incorporated into the IECM to perform molecular return flux measurements. The purpose of the mass spectrometer measurements is twofold. The first is to define the early desorption and outgassing molecules transported to surfaces in the Shuttle Orbiter bay for correlation to actual deposition measurements on optical and temperature-controlled surfaces. The second is to infer the gas cloud (induced atmosphere column density) through which optical experiments must look.

This instrument is designed with chevron baffles to measure collimated flux within a view angle of 0.1 sr as indicated in Figure 8. Such a narrow acceptance angle is required to reduce directional column density, identify gas scattering cross-section when pointed in the vicinity of the velocity vector (ram direction) and identify contamination sources during the RMS mode of operation when the instrument is looking back at various regions of the Shuttle.

Another facet of this task effort was to evaluate the IECM Ne/D_2O gas calibration plume. To better understand the return flux mechanism and the mass spectrometer output, an inflight calibration using Ne/D_2O will be performed. A gas release system will emit a known flux of isotopically labled water (D_2O) and neon into the collimated view of the mass spectrometer (see Figure 9). Backscattered flux, will then be monitored over a 45 minute period, while the Shuttle Orbiter rotates 180 degrees. The variation in back scattered flux, as a function of angle-of-attack, will provide the calibration needed to interpret the measurements and provide the bases for evaluating the differential scattering cross-section for 8 km/s collisions--a measurement of basic physical importance in the current return flux analytical model.

OTHER EXPERIMENTS (NOT MODELED)

OFT PALLETS

SHUTTLE DEVELOPMENT
FLIGHT INSTRUMENTATION

INDUCED ENVIRONMENT
CONTAMINATION MONITOR

AFT BULKHEAD
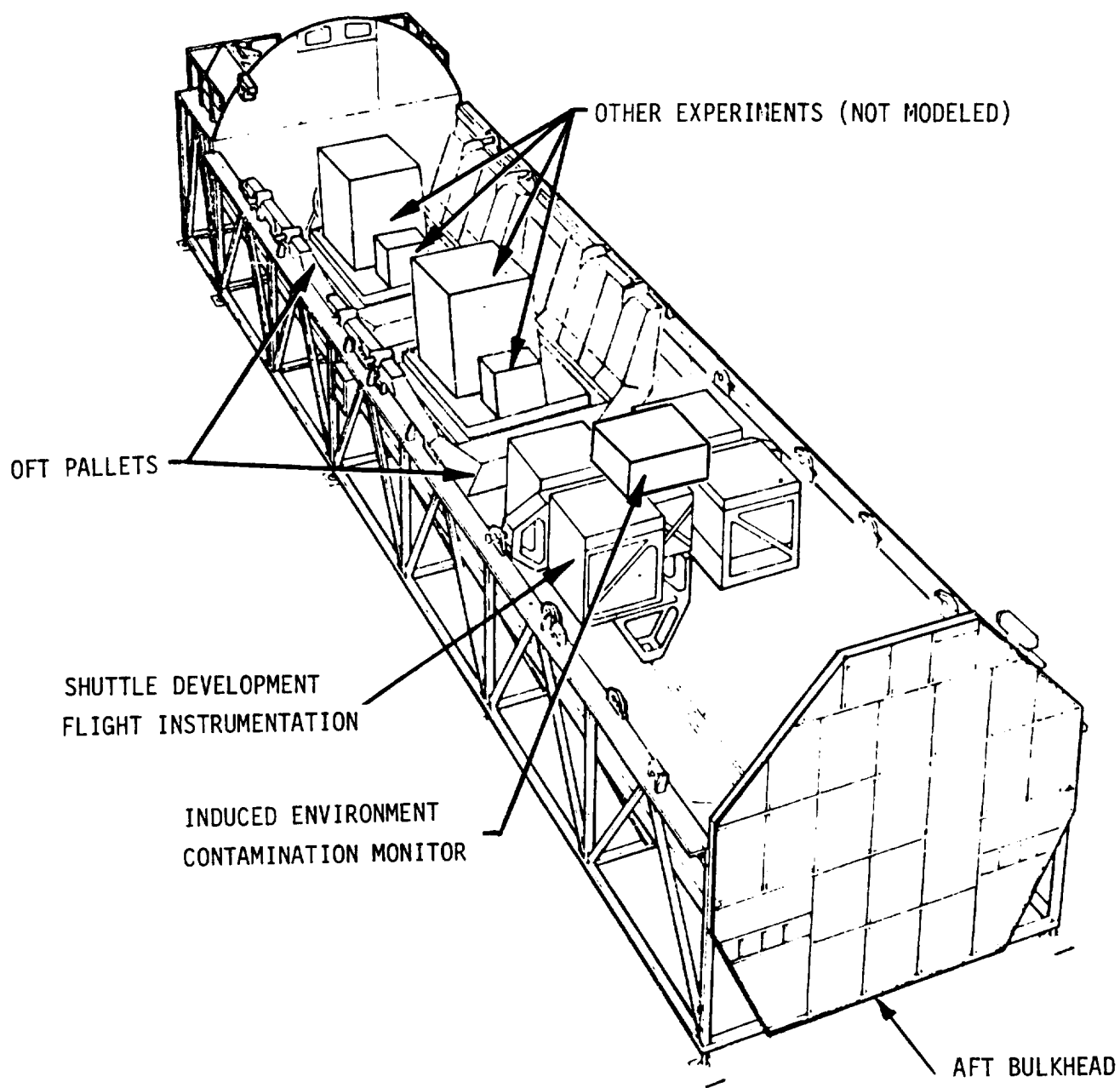
Figure 7. IECM Payload Bay Integration
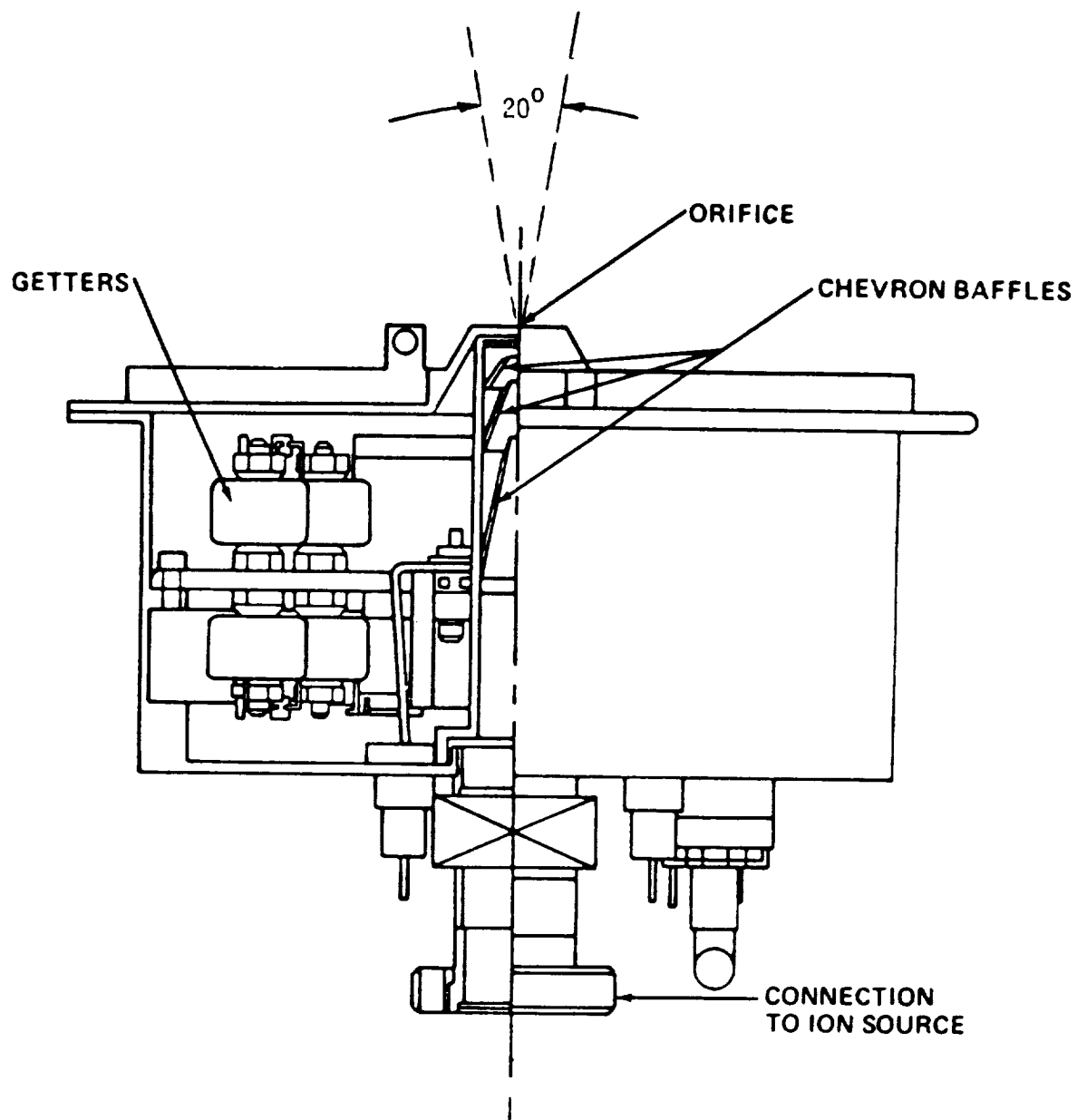
Figure 8. Mass Spectrometer Collimator Design
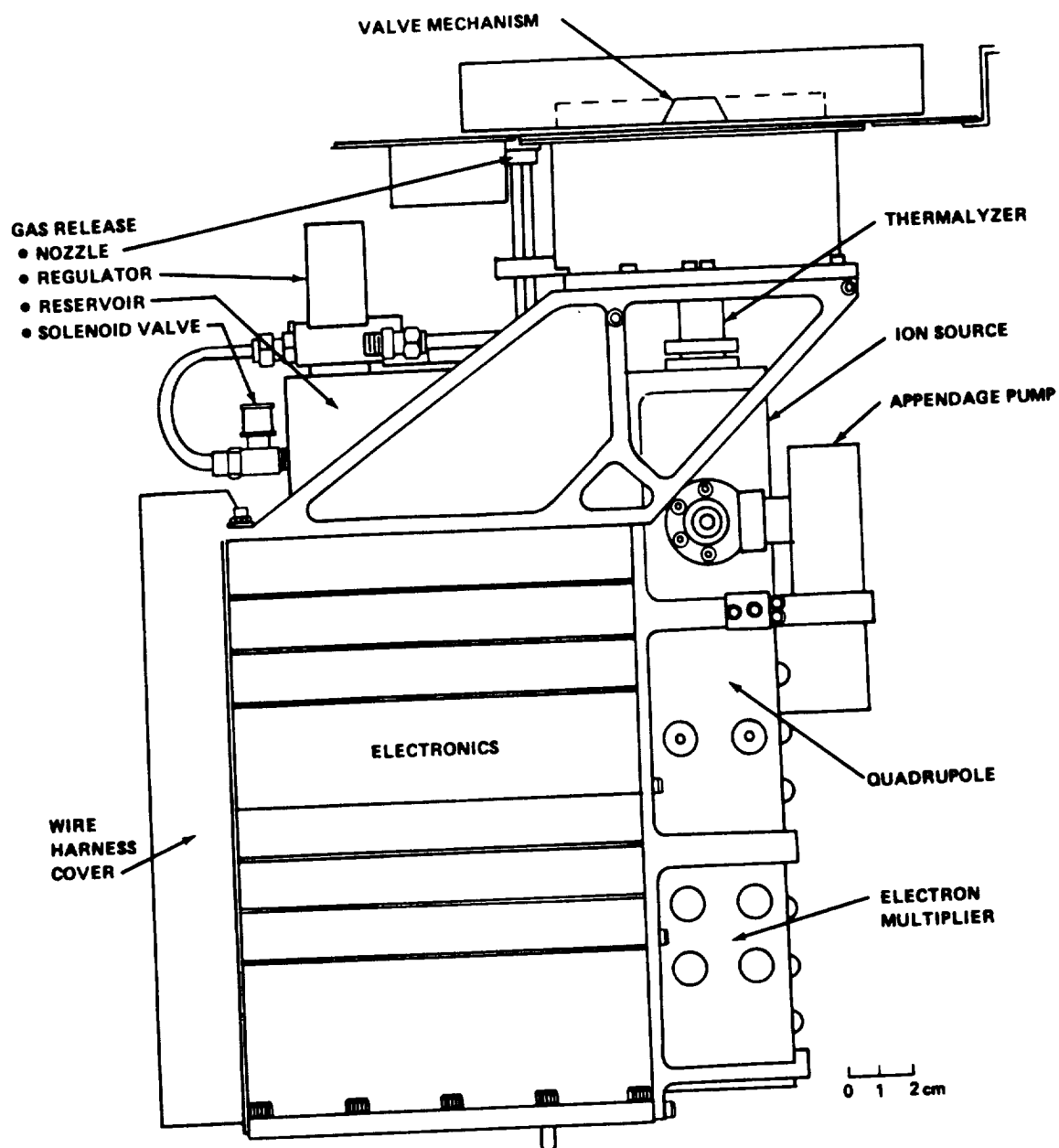
Figure 9. Simplified Schematic of Final Layout of Mass Spectrometer

The approach taken in geometrically modeling the IECM configuration was to simulate the basic housing with a six-sided box using 6 nodes. The 7 critical measuring instruments were modeled by small discs. One disc was used to represent each of the two CQCM crystals. The modeled geometry is illustrated in Figures 10 through 13. The node numbers assigned to the measuring instruments are shown in Figure 13.

The IECM was assumed to be coated with S13G-LO thermal control paint. The DFI was assumed to be coated with Chemglaze thermal control paint. The specie outgassing rates for these materials used for this analysis, at a benchmark temperature of 125°C, are shown below:

SPECIE	COATING	
	S13G-LO	CHEMGLAZE
OUT1	6.00E-10 g/cm^2 sec	4.00E-11 g/cm^2 sec
H_2O	5.42E-12 g/cm^2 sec	4.41E-9 g/cm^2 sec
N_2	8.70E-12 g/cm^2 sec	2.75E-9 g/cm^2 sec
CO_2	1.70E-11 g/cm^2 sec	2.23E-9 g/cm^2 sec
O_2	2.28E-11 g/cm^2 sec	1.05E-9 g/cm^2 sec

The internal outgassing and subsequent venting around the instrument panel penetrations were not addressed.

3.1.2 Thermal Profile - The temperature data for the Shuttle Orbiter was developed and formatted by JSC. The data consisted of Shuttle Orbiter node temperatures at eight points in a typical OFT-1 orbit for a zero degree beta angle Z local vertical (ZLV) attitude. The Martin Marietta developed Thermal Mapper Conversion Program was used by JSC to convert thermal data, derived for JSC/Rockwell thermal model nodes, to SPACE contamination model nodes. The OFT-1 temperature data mission elapsed time (hrs) points delivered by JSC to Martin Marietta were 23.85, 24.10, 24.35, 24.60, 24.85, 25.10, 25.19, and 25.35. Six time points were selected to simulated the OFT-1 orbit. These time points were 24.10, 24.35, 24.60, 24.85, 25.19, and 25.35. These points simulate a typical, approximately sinusoidal, orbital temperature cycle.

The IECM/DFI temperature data was obtained from Rockwell thermal simulation model results. The nodal temperatures for the required time points corresponding to the six time points for the Shuttle Orbiter were obtained by selecting IECM/DFI node temperatures at points in the approximately sinusoidal variation whose relative values corresponded to the relative values for the Orbiter. The

24

STARBOARD

IECM

CQCM

DFI #1

+Z TQCM

X — AFT

MASS SPECTROMETER

DFI #3

DFI #2
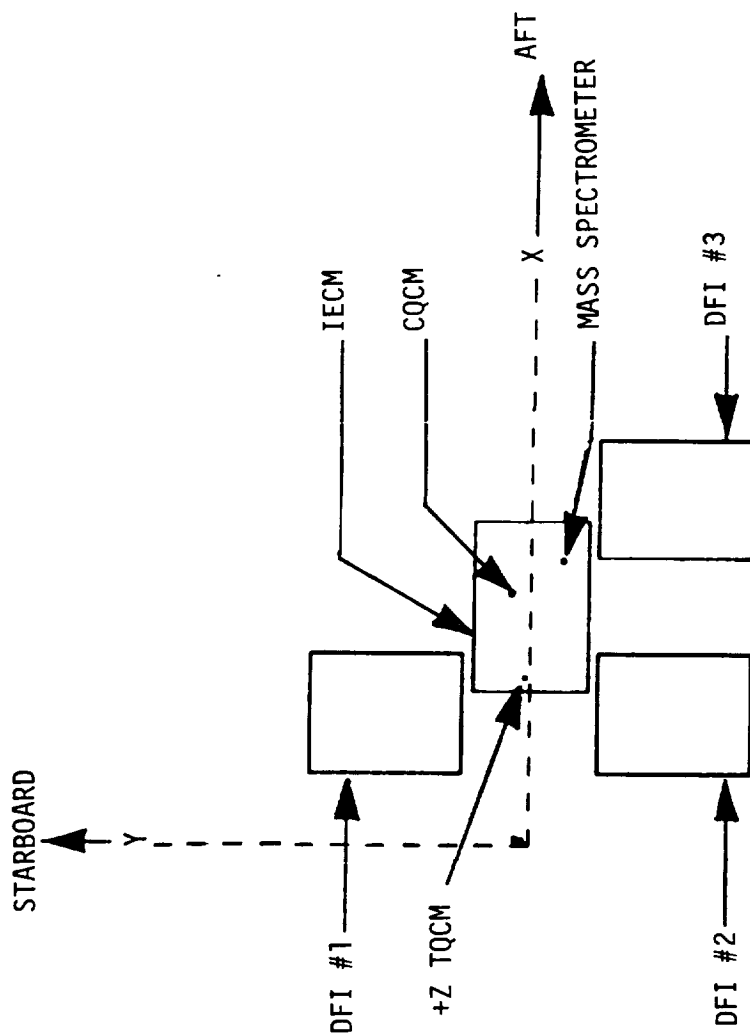
VIEW = Z-AXIS
SCALE = .0192

IECM + DFI, OFT-1 PAYLOAD

Figure 10. View Looking Downward Into Payload Bay

25
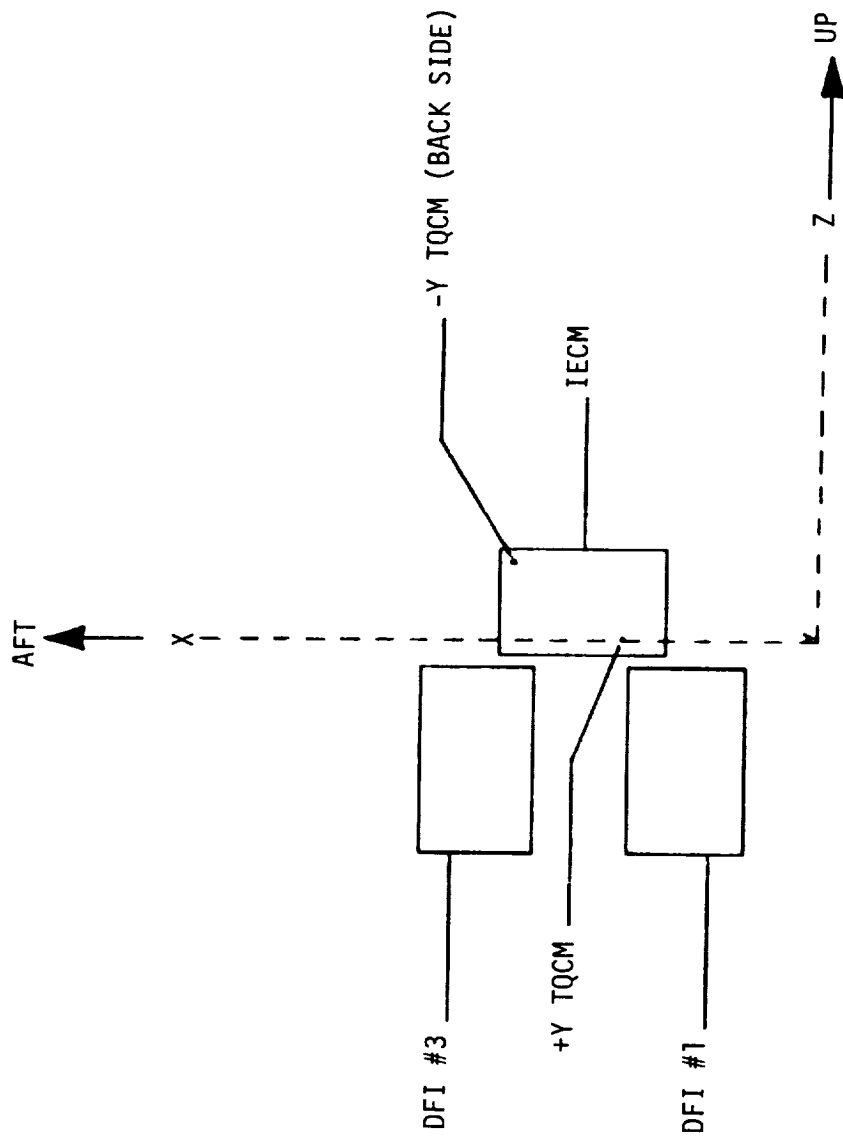
IECM + DFI, OFT-1 PAYLOAD

Figure 11. View Looking to Port Side

VIEW = Y-AXIS
SCALE = .0192

26
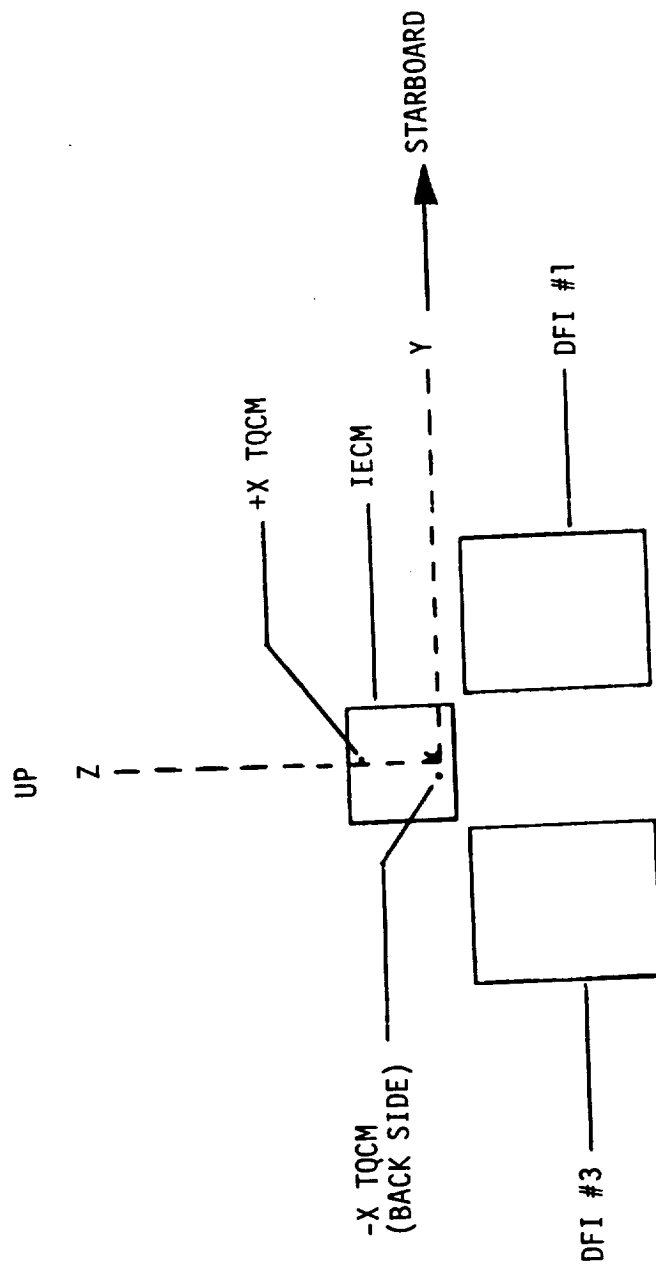
IECM + DFI, OFT-1 PAYLOAD

Figure 12. View Looking Forward

UP

Z

+Z TQCM (1050)

CQCM (1060)

MASS SPECTROMETER (1070)

-Y TQCM (1080)

DFI #2

+X TQCM (1040)

DFI #3

-X TQCM (1100)

+Y TQCM (1090)

Y

STARBOARD

DFI #1

( ) = NODE NUMBER
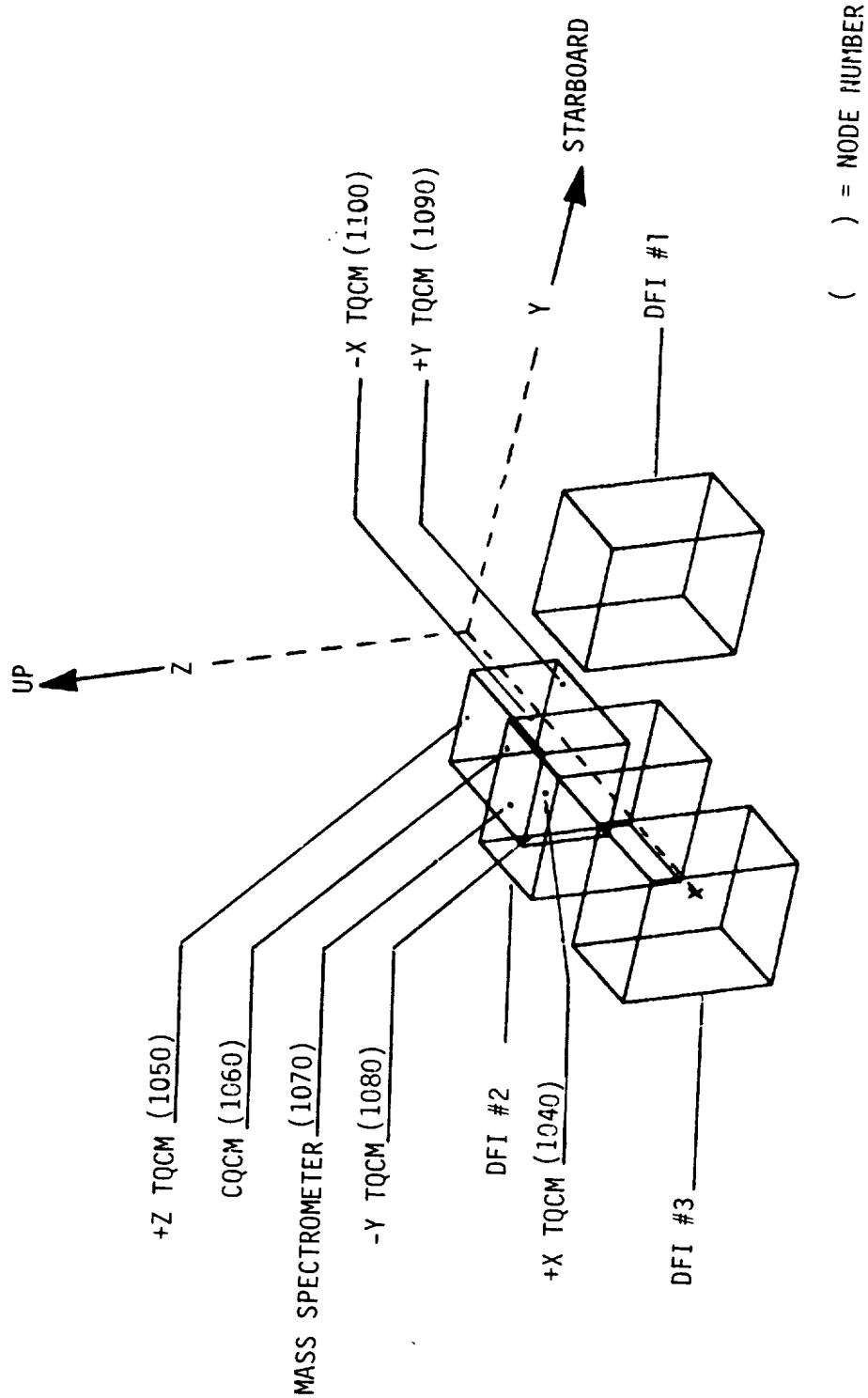
VIEW = 3-D

SCALE = .0192

IECM + DFI, OFT-1 PAYLOAD

Figure 13. View Looking Forward, Down and to Port

IECM/DFI temperatures and selected Shuttle Orbiter temperatures were plotted as a function of time. The phase of the sinusoids were matched, and the proper IECM/DFI temperatures were identified. The temperature file resulting from merging the Shuttle Orbiter and IECM/DFI temperature data is shown in Appendix C. Columns 2 through 6 were the data used for the OFT-1 analysis. Columns 2 and 5 were used for the OFT-3 analysis to approximate the maximum and minimum temperature extremes.

3.1.3 **IECM Instrument Analysis** - This subsection describes the operation and sensitivities of the IECM TQCMs, CQCMs and the mass spectrometer.

3.1.3.1 **TQCM Operation** - The TQCM crystals used in the IECM operate at a resonant frequency of 15 MHz. As designed, they will be able to detect a 1 Hz change in frequency which corresponds to a mass change of 1.56×10^{-9} g/cm^2. The TQCM transfer function analysis is presented in Appendix D, Part 2. One of the major uncertainties in the QCM data will be due to the fact that the deposit being measured must adhere tightly to the crystal surface, therefore, it will not measure particulates or volatiles which do not stick. Also, the QCM crystal has a finite limit to the amount of material it can detect. This occurs at approximately 1×10^{-4} g/cm^2. Saturation is not expected to be a concern because the TCQM will undergo periodic high temperature (80°C) cycling to desorb contamination.

The deposit may be a complex mixture of materials outgassing and engine exhaust species. It is conceivable that the deposit can chemically interact or photopolymerize and be difficult to remove. This would be observed as a permanent shift in the QCM beat frequency.

Each of the TQCM heads consists of a QCM sensor, an electronics unit and a heat sink. A two-stage bismuth-telluride thermoelectric device uses the Peltier effect to heat or cool the sensor crystals to the commanded temperature. The sensor and electronics unit are mounted directly to a toroid of gold-coated aluminum which serves as a heat sink. Platinum resistance thermometers monitor the temperatures of the crystals and the heat sink. The heat sink also serves as the mounting attachment and is bolted to the IECM frame. With this design, the IECM frame temperature determines the actual temperatures of the QCM.

The commands which the TQCM heads receive from the Data Aquisition and Command System (DACS) are temperature settings which are planned in preflight programming. These temperatures are referenced to a nominal heat sink (IECM frame) temperature of 20°C. The thermoelectric devices are designed to have the capacity to control the detector temperature to a maximum of 80°C below the heat sink temperature. For a heat sink temperature of 20°C, the lowest temperature will be -60°C.

When the heat sink goes above 20°C, DACS is programmed to disallow a command of more then the 80°C differential. This is done to avoid an excess power drain which would occur if the thermoelectric device continued to try to reach an unattainable temperature. However, in the case in which the heat sink goes below 20°C, temperatures colder than -60°C can be reached.

As soon as the "on-orbit"signal is received from the Shuttle Orbiter, the TQCM system will begin its programmed temperature sequencing. This sequence is shown in Figure 14. The first command will be for the crystals to go to 80°C for approximately 30 minutes. This will clean off the deposits from preflight and launch and establish the "clean frequency". Then the sensors will be commanded to 30°C. Then 0°C and -30°C will be commanded with an 80°C "cleanup" period between each setting. The final low temperature setting will be -60°C. After an orbit, at this low temperature, the crystals' temperatures will be raised in 30 minute steps through -30, 0 and 30 and, finally, to 80°C. This procedure is intended to permit the calculation of desorption rates between these specific temperature brackets to aid in characterizing the types of contaminants. This routine will be repeated until the on-orbit mode of the mission is completed.

All frequencies and temperatures are recorded once each minute. Unless directed otherwise, the temperature cycling, similar to that shown in Figure 14, will be used as the baseline with the IECM frame temperature of 20°C throughout the mission.

3.1.3.2 CQCM Operation - The CQCM is designed with a radiator that continually dissipates heat away from the detector crystals so that they will always seek lower temperatures. The radiator is thermally isolated from the IECM frame and electronics and consists of an array of second surface, silver-coated quartz mirrors which are attached to an aluminum plate by a thin layer of RTV 566 adhesive. The quartz mirrors provide a solar absorptance (α) of 0.06 and a thermal emittance (ϵ) of 0.8. However, the mirror properties are suject to change if contaminated. The radiator assembly has a 2π sr view of the 4°K deep space radiation sink because it is mounted flush with the top of the IECM. The CQCM head is protected from internal radiation from its surroundings by 20 layers of gold-coated Kapton (multilayer foil insulation) and is mounted in a stainless steel well enclosed on all sides (except the top). The CQCM sensitivity is similar to TQCM (Appendix D, Part 2).

When the Shuttle Orbiter attitude exposes the CQCM to direct sunlight, heat is reflected away by the second-surface silver mirrors. On specific missions, when the Orbiter payload bay is pointed away from the sun for a number of hours, the CQCM is designed to "cold soak" to cryogenic temperatures.

30

Figure 14 . TQCM Command-Temperature Sequence (One Cycle)

SUMMARY OF ON—ORBIT COMMANDS		
TIME (ELAPSED MINUTES)	COMMAND (SEEK TEMP SETTING)	MODE
0	+ 80	10
30	+ 30	9
120	+ 80	10
150	0	8
240	+ 80	10
270	- 30	7
360	+ 80	10
390	- 60	6
480	- 30	7
510	0	8
540	+ 30	9
570	REPEAT	

31

Based on the thermal analyses and laboratory simulation, it is anticipated that the CQCM will reach -133°C from 20°C after approximately 12 hours in the cold-soak mode. This 12 hour figure must be regarded as a variable however, because the time that it takes to reach a certain temperature is dependent on several factors which are difficult to predict. These are: 1) the starting temperature, which is dependent on Shuttle Orbiter activities prior to going into the cold soak; 2) the heat input from the IECM frame and 3) the cleanliness of the radiator mirrors.

The CQCM has two quartz crystal microbalance sensors which have the same viewing angle. Sensor No. 2 is insulated from the radiator by teflon washers on the hold-down screws; whereas, Sensor No. 1 uses metal washers, As a result, Sensor No. 2 will not cool down as fast as Sensor No. 1. The temperature difference between detectors will be enhanced by preflight programmed temperature cycling with an 80mW heater mounted in Sensor No.2. (The CQCM also has two other heaters; a 163 mW heater to heat the sensors for cleaning purposes and a 470 mW heater to heat the radiator mirrors for cleaning.) This time lag, or difference in sensor temperatures at a specific time, was designed into the CQCM to aid in data interpretation.

When the on-orbit signal is received, the CQCM sensors will be sampled every minute. At the beginning of a temperature sequence, the CQCM sensors will be allowed to seek their minimum temperatures for a period of 24 hours. The 80 mW heater will then be activated for a period of 6 hours followed by the 470 mW heater operation to clean the radiator for 12 hours. This sequence will be repeated until the de-orbit signal is received.

3.1.3.3 <u>Mass Spectrometer</u> - Upon receipt of an appropriate signal, or after a predetermined time, the IECM will apply power to the mass spectrometer and begin interrogating the mass spectrometer with timed signals. The mass spectrometer will turn on in an orderly sequence and the valve will open after approximately 24 seconds. From this point on, the instrument will automatically step through its sequence of of amus and provide the data to the IECM. It is presently planned to have three modes of operation for the mass spectrometer, all controlled by the IECM.

The normal mode will be for the IECM to interrogate the mass spectrometer only once every 2 seconds (i.e., the pulse count for each amu will be integrated for 2 seconds). This not only limits the amount of data which needs to be recorded, but it also provides more counts for those masses with very low pressures. Under this normal mode the mass spectrometer will step through a complete sweep from 1 to 150 amus and then alternate with an equal number of steps on the water peak (amu 18). This feature was incorporated because of the importance of water

as a contaminant for certain experiments utilizing the infrared spectrum and to try to determine the temporal fluctuation of the water cloud. It does, however, limit data on other masses to once every 10 minutes.

A fast-sweep mode can also be used by simply speeding up the interrogation rate to once every 0.2 seconds. This mode of operation is planned principally for missions when the IECM is deployed to various locations by the RMS. A faster response time is then needed to identify contamination sources when the IECM is pointed at various surfaces. The double-sweep sequence remains in operation but each mass is recorded every 1.0 minute.

A special mass mode is also available which is really an abbreviated sweep mode. In this mode, the instrument confines its sweeps to the range from 1 to 48 amus. The abbreviated sweep was incorporated into the mass spectrometer design to provide a better time resolution during the Ne/D_2O gas calibration sequence. Either the normal or fast-sweep rates can be used with the abbreviated sweep mode.

Performance Data:

Data Output - Record digital counts proportional to partial pressures

Sample Rates - 0.5/second slow scan
5/second fast scan

Resolution - ± 1 count

Accuracy - 0.2 to 0.4 percent for any counting rate above 512 counts/second

The mass spectrometer sensitivity and transfer function analysis is presented in Appendix D, Part 1.

3.2 OFT-1 Mission Analysis

This section describes the OFT-1 mission analysis activity and the resulting IECM instrument predictions.

3.2.1 Objective - The objectives of the OFT-1 mission analysis activity were to; 1) provide a preflight prediction of the outputs of various IECM contamination monitoring instruments to determine if instrument sensitivities are consistent with the expected environment and; provide a data base to allow comparison of predicted and measured contamination parameters for verification of the analytical models.

33

The approach taken to accomplish these objectives was to perform parametric analyses to determine the sensitivity of the predictions to the various parameters affecting the results. These parameters included QCM temperature, orbit position, contaminant source, and mission elapsed time (MET). This approach provided a data base containing predicted instrument outputs as a function of source and time which could be used during post flight evaluations to compare predicted and measured results for any combination of these parameters.

3.2.2 <u>Assumptions</u> - The following assumptions were used for the OFT-1 analysis:

a) return flux analysis assumed an orbital velocity vector in the -X direction (Shuttle Orbiter nose into the wind);

b) surface source temperature data was provided for a ZLV attitude, $\beta = 0^0$;

c) payload bay was empty except for IECM/DFI hardware;

d) adequate convergence of the multi-reflect option would be provided by six (6) reflections;

e) orbital altitude was 278 km; medium sunspot activity;

f) source outgassing rate time decay was negligible;

g) RCS/VCS engine combustion chamber temperature was 3000^0K; Mach number = 5; and

h) evaporator reservoir temperature was 293^0K; Mach number = 1.

3.2.3 <u>Mission Analysis Plan</u> - The OFT-1 mission analysis plan is shown in Table II. The plan outlines the type and extent of the analysis required for each IECM instrument for each contamination source. The temperature dependent sources, outgassing and early desorption, were evaluated at six separate orbital time points consistent with the available temperature data. In addition, the outgassing deposition rates on the TQCMs were determined for all four TQCM temperatures at the six orbital temperature points. Figure 15 illustrates how the orbit time was allocated to the temperature data. The six temperature points are shown together with the Δt assigned for each orbital time slice. The temperature was assumed to be constant within each time slice. Leakage is not temperature or time dependent and was therefore evaluated on an orbital basis. The evaporator and the engines flux/deposition rates were evaluated for a one second on-time. Source symmetry was assumed in many cases and will be discussed in subsection 3.2.6 for individual cases.

34

Table II. OFT-1 Mission Analysis Plan

SENSOR	SURFACE SOURCES				ENGINES			COMMENTS
	OUTGASSING	EARLY DESORPTION	LEAKAGE	EVAPORATOR	VCS	RCS	OMS	
1. Mass Spectrometer Modes - 0.2 sec/ AMU 2.0 sec/ AMU Node 1070	1 full orbit simulation; provides bounds (Max/min MCD) + rate of change; 6 time slices for temperature resolution.	3 full orbit simulations; early/late/mid mission to account for time decay; 6 time slices for temperature resolution.	1 time slice - not time or temperature dependent.	Same as leakage.	1 pulse simulation - 2 runs/ engine (w/wo reflection) 6 engines; 10 runs (no front reflection); discriminate between front/rear engines via reflection.	1 pulse simulation - assume 12 sets - reflections from 4 sets (rear out & down) - 16 runs;discriminate between reflection/no reflection.	1 - 1 sec simulation 2 engines	Possible run reduction due to symmetry considerations. All runs are return flux.
2. TQCM Node 1040 1100 Fwd 1080 Aft 1090 Right 1050 Left Top	1 full orbit flux simulation; manual computation of deposition as a function of QCM temperature/time profile; 6 time slices for temperature resolution; 6 start times for QCM temperature profile.	N/A	N/A	N/A	1 pulse simulation-MMH/NO3 only (s = 1) - no reflection 6 engines.	1 pulse simulation-MMH/NO3 only (s = 1) - no reflection; 12 sets of engines (1 run per set)	1 - 1 sec simulation 2 engines MMH/NO3 only (s = 1)	All runs are direct & return flux.
3. CQCM Node 1060	1 full orbit simulation; manual computation of deposition as a function of QCM temperature/time profile; assume -133°C minimum temperature case and adjust for actual temperature; 6 time slices for temperature resolution. 3 parametrics	3 full orbit flux simulations (H_2O, CO_2 only); manual computation of deposition same as outgassing.	1 time slice - not time/ temperature dependent; (H_2O, CO_2 only); manual computation of deposition at -133°C.	Same as leakage	Same as VCS - Mass spectrometer H_2O, CO_2, CO, MMH/NO3	Same as RCS - Mass spectrometer H_2O, CO_2, CO, MMH/NO3	Same as OMS - Mass spectrometer H_2O, CO_2, CO, MMH/NO3	All runs are direct & return flux

ASSUMED ORBITAL COVERAGE (HR:MIN:SEC)

23:58:30   24:13:30   24:28:30   24:43:30   25:01:12   25:16:30   25:28:30

TEMPERATURE DATA

MET (HR:MIN:SEC)

23:30:00   24:00:00   24:30:00   25:00:00   25:30:00
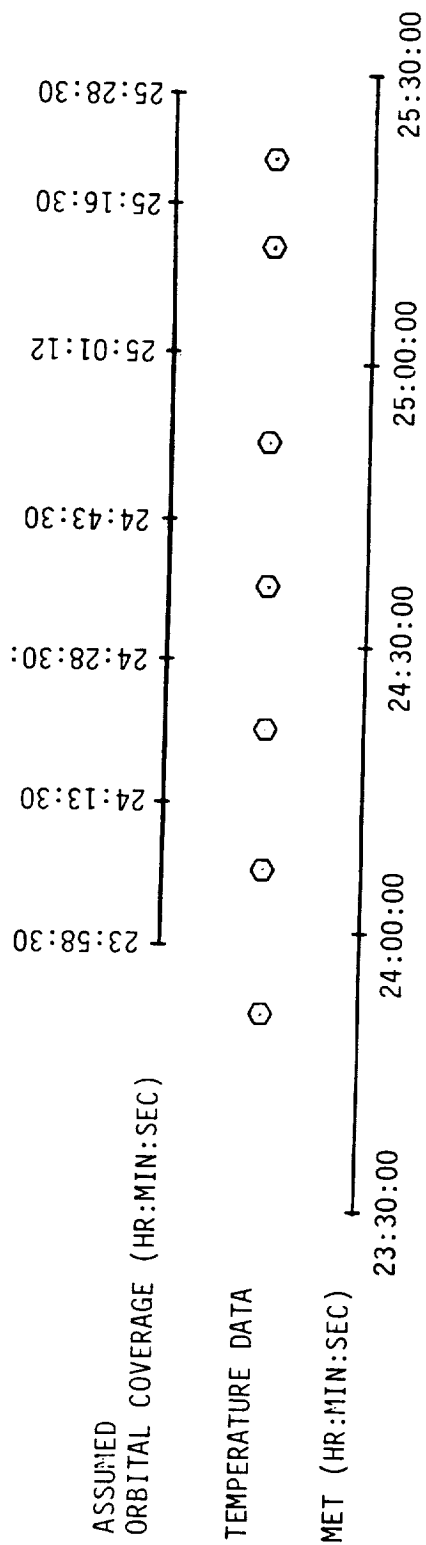
ORBITAL TIME SLICE	TAPE 10 TEMPERATURE FLAG	AVAILABLE TEMPERATURE DATA POINT	Δt(SEC)
---	MAXTMP	23:51:00	---
1	MINTMP	24:06:00	900
2	ATCODE = 1	24:21:00	900
3	ATCODE = 2	24:36:00	900
4	ATCODE = 3	24:51:00	1062
5	ATCODE = 4	25:11:24	918
6	ATCODE = 5	25:21:00	720

Figure 15. OFT-1 Temperature Profile – One Orbit

3.2.4 <u>Shuttle Orbiter/Payload Geometry</u> - The Shuttle Orbiter geometry used for the analysis is shown in Figures 16 and 17. The high resolution payload bay with filters, also shown in the figures was used to provide adequate source resolution. The location of the IECM/DFI package in the payload bay is shown in Figures 10 through 13 and Figure 18. A list of all of the surface nodes in the configuration together with their location, and source material is shown in Table III. The source functions corresponding to these materials are described in the SPACE II User's Manual, Appendix B.

The Shuttle Orbiter RCS/VCS nodal configuration is shown in Figure 19. In order to reduce the complexity of the geometry and to conserve TRASYS run time, groups of nodes were assumed to be represented by single nodes. For example, node 7125 is assumed to also represent nodes 7135 and 7115. The circled node numbers on Figure 19 were the nodes modeled and used to develop the mass transport factors.

3.2.5 <u>SPACE Input Data File Development</u> - The data files required to perform the SPACE OFT-1 mission analysis runs are described below:

a) <u>TAPE 4</u> - This data file contains a list of the nodes comprising the Shuttle Orbiter, IECM/DFI, and payload bay geometry, and the materials assigned to the nodes. A list of this data file is shown in Table III.

b) <u>TAPE 10</u> - The temperatures assigned to each node in the configuration for each of the six time slices are stored on this file. These data were described in subsection 3.1.2.

c) <u>TAPE 12</u> - This file contains the body-to-body mass transport factors generated by the TRASYS program and used by SPACE II to perform the direct flux and multi-reflect analyses. The TRASYS run inputs were developed by Martin Marietta based on the geometry configuration described in subsection 3.2.4. The TRASYS runs were performed by JSC with the output returned to Martin Marietta for formatting. A listing of TAPE 12 is on file at JSC.

d) <u>TAPE 14</u> - This data file comprises the Shuttle Orbiter point-to-body mass transport factors. The TRASYS inputs were developed by Martin Marietta. The runs were made by JSC with the output returned to Martin Marietta for Space II formatting. These data are used by SPACE for return flux and column density calculations. The size of this file (60,000 records) prohibits including a listing in this report. A listing is, however, on file at JSC.

e) <u>TAPE 15</u> - The TRASYS generated IECM/DFI/payload bay point-to-body mass transport factors are contained on this file. This

Figure 16 . Primary Shuttle Orbiter Nodal Surface Number Assignments

38

NOTE: Node numbers in parentheses indicate +Y side surfaces.

TAIL

386 (387)
388 (389)
390 (391)
393 (392)
384 (385)
382 (383)
380 (381)
399

OMS

87 (67)
94 (74)
92 (72)
97 (77)
96 (76)
90 (70)
88 (68)
86 (66)
84 (64)
82 (62)
80 (60)

ELEVON

459 (469)
458 (468)
457 (467)
456 (466)
455 (465)
454 (464)
453 (463)
452 (462)
451 (461)
450 (460)
107 (137)
119 (149)
106 (136)
104 (134)
112 (142)
110 (140)
122 (152)
118 (148)
121 (151)
102 (132)
117 (147)
100 (130)
115 (145)

WING

FUSLAG

240 (AFT)
230 (AFT)
202 (CYLINDER)
260
250
420
307
306
305
301
425
317
316
315
311
203 (CYLINDER)

RADOOR (active radiator surfaces only)

(50) 44
(54) 40
(34) 20
(36) 22
(30) 24
(32) 26

BAY

FILTERS

573
578
572
576
571
575
570
(588) (583)
(587) (584)
(581) (586)
(580)

CREW

174
175
167
169
171
165
163
160
190
(177)

WINDOWS

163
165
185
184
183
161
167
169
171
160
162
(182)
(181)
(180)
(164)
(166)
(168)
(170)
(172)

39

Figure 17. Primary Shuttle Orbiter Nodal Surface Number Assignments

UP

+Z

-Y

STARBOARD

-X

FORWARD

VIEW = 3-D
SCALE = .0052
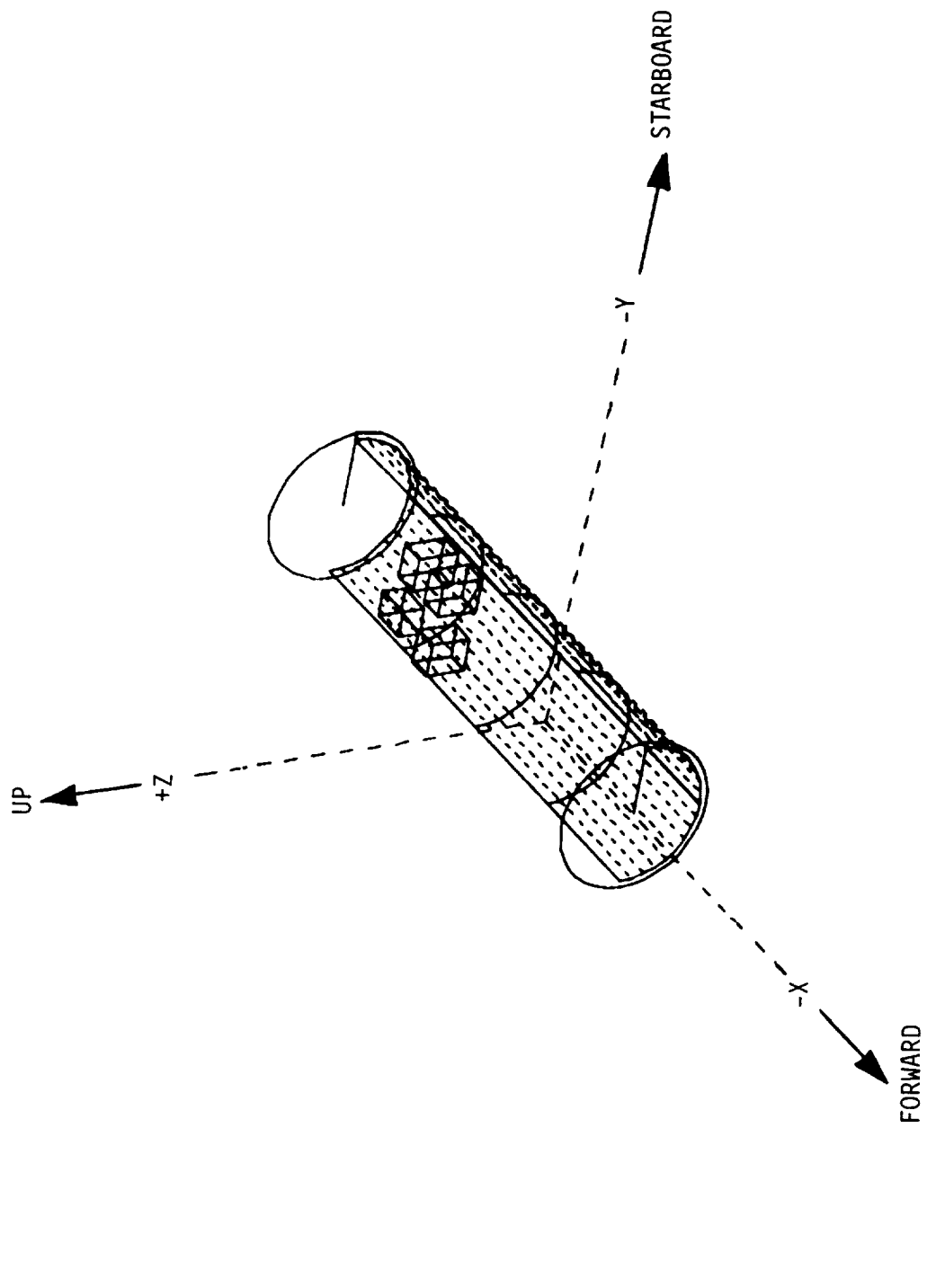
Figure 18. IEOM and DFI Integrated Into Payload Bay

1 FWD RCS MODULE, 2 AFT RCS SUBSYSTEMS IN PODS
38 MAIN THRUSTERS (14 FWD, 12 PER AFT POD)
    THRUST LEVEL = 870 LB (VACUUM)
    ISP = 289 SEC

6 VERNIER THRUSTERS (2 FWD, 2 PER AFT POD)
    THRUST LEVEL = 25 LB
    ISP = 228 SEC

PROPELLANTS: N₂O₄: OXIDIZER
             MMH: FUEL

*[THIS SIDE/OPPOSITE SIDE]

OMS THRUSTERS (9002) (9001)

PRIMARY RCS THRUSTERS (12 PER AFT POD)

VERNIER RCS THRUSTERS (2 PER AFT POD) (8258)(8358) (SIDE) (8257)(8357) (DOWN)

7211/ 7311
7231/ 7331

7213/ 7314
7233/ 7334

(7223) (324)

7243/ 7344

7215/7315 (225)(7325)
7245/7345

7246/7346 (226)(7326)
7236/7336

OMS POD

PRIMARY THRUSTER (14)

7135 (7125)
7115

(7123)(7144)
7113/7134

7126/ 7146

(7116)(8136)
(136)

7132
(7122) 7112

VERNIER THRUSTER (2) (8116)(8136)

EVAPORATOR VENT (2) (6879)(6877)

Figure 19.   Orbiter Engine/Vent Locations and Identification Numbers

41

Table III.   OFT-1 Geometry Configuration

* * *   SURFACES * * *

SEQUENCE NO.	IDENT NO.	SECTION	MATERIAL
1	20	RADOOR	TEFLON
2	22	RADOOR	TEFLON
3	24	RADOOR	TEFLON
4	26	RADOOR	TEFLON
5	30	RADOOR	TEFLON
6	32	RADOOR	TEFLON
7	34	RADOOR	TEFLON
8	36	RADOOR	TEFLON
9	40	RADOOR	TEFLON
10	42	RADOOR	TEFLON
11	44	RADOOR	TEFLON
12	46	RADOOR	TEFLON
13	50	RADOOR	TEFLON
14	52	RADOOR	TEFLON
15	54	RADOOR	TEFLON
16	56	RADOOR	TEFLON
17	21	FUSLAG	LRSI
18	23	FUSLAG	LRSI
19	25	FUSLAG	LRSI
20	27	FUSLAG	LRSI
21	31	FUSLAG	LRSI
22	33	FUSLAG	LRSI
23	35	FUSLAG	LRSI
24	37	FUSLAG	LRSI
25	41	FUSLAG	LRSI
26	43	FUSLAG	LRSI
27	45	FUSLAG	LRSI
28	47	FUSLAG	LRSI
29	51	FUSLAG	LRSI
30	53	FUSLAG	LRSI
31	55	FUSLAG	LRSI
32	57	FUSLAG	LRSI
33	202	FUSLAG	LRSI
34	203	FUSLAG	LRSI
35	230	FUSLAG	LRSI
36	240	FUSLAG	LRSI
37	241	FUSLAG	LRSI
38	250	FUSLAG	LRSI
39	260	FUSLAG	LRSI
40	301	FUSLAG	LRSI
41	305	FUSLAG	LRSI
42	306	FUSLAG	NOMEX
43	307	FUSLAG	NOMEX
44	311	FUSLAG	LRSI
45	315	FUSLAG	LRSI
46	316	FUSLAG	NOMEX
47	317	FUSLAG	NOMEX
48	420	FUSLAG	LRSI
49	425	FUSLAG	LRSI
50	60	OMS	LRSI

Table III. OFT-1 Geometry Configuration (Cont.)

51	62	OMS	LRSI
52	64	OMS	LRSI
53	66	OMS	LRSI
54	67	OMS	LRSI
55	68	OMS	LRSI
56	70	OMS	LRSI
57	72	OMS	LRSI
58	74	OMS	LRSI
59	76	OMS	LRSI
60	77	OMS	LRSI
61	80	OMS	LRSI
62	82	OMS	LRSI
63	84	OMS	LRSI
64	86	OMS	LRSI
65	87	OMS	LRSI
66	88	OMS	LRSI
67	90	OMS	LRSI
68	92	OMS	LRSI
69	94	OMS	LRSI
70	96	OMS	LRSI
71	97	OMS	LRSI
72	100	WING	NOMEX
73	102	WING	NOMEX
74	104	WING	NOMEX
75	110	WING	NOMEX
76	112	WING	NOMEX
77	115	WING	LRSI
78	117	WING	HRSI
79	118	WING	HRSI
80	119	WING	LRSI
81	121	WING	RCC
82	122	WING	RCC
83	130	WING	NOMEX
84	132	WING	NOMEX
85	134	WING	NOMEX
86	140	WING	NOMEX
87	142	WING	NOMEX
88	145	WING	LRSI
89	147	WING	HRSI
90	148	WING	HRSI
91	149	WING	LRSI
92	151	WING	RCC
93	152	WING	RCC
94	106	ELEVON	NOMEX
95	107	ELEVON	NOMEX
96	136	ELEVON	NOMEX
97	137	ELEVON	NOMEX
98	450	ELEVON	NOMEX
99	451	ELEVON	NOMEX
100	452	ELEVON	NOMEX
101	453	ELEVON	NOMEX
102	454	ELEVON	NOMEX
103	455	ELEVON	NOMEX
104	456	ELEVON	NOMEX
105	457	ELEVON	NOMEX
106	458	ELEVON	NOMEX
107	459	ELEVON	NOMEX
108	460	ELEVON	NOMEX
109	461	ELEVON	NOMEX
110	462	ELEVON	NOMEX
111	463	ELEVON	NOMEX
112	464	ELEVON	NOMEX
113	465	ELEVON	NOMEX
114	466	ELEVON	NOMEX

Table III.   OFT-1 Geometry Configuration (Cont.)

115	467	ELEVON	NOMEX
116	468	ELEVON	NOMEX
117	469	ELEVON	NOMEX
118	160	CREW	RCC
119	161	CREW	LRSI
120	162	CREW	LRSI
121	163	CREW	LRSI
122	164	CREW	LRSI
123	165	CREW	LRSI
124	166	CREW	LRSI
125	167	CREW	HRSI
126	168	CREW	HRSI
127	169	CREW	HRSI
128	170	CREW	HRSI
129	171	CREW	HRSI
130	172	CREW	HRSI
131	174	CREW	LRSI
132	175	CREW	LRSI
133	177	CREW	LRSI
134	180	CREW	WINDOW
135	181	CREW	WINDOW
136	182	CREW	WINDOW
137	183	CREW	WINDOW
138	184	CREW	WINDOW
139	185	CREW	WINDOW
140	190	CREW	LRSI
141	380	TAIL	LRSI
142	381	TAIL	LRSI
143	382	TAIL	LRSI
144	383	TAIL	LRSI
145	384	TAIL	LRSI
146	385	TAIL	LRSI
147	386	TAIL	LRSI
148	387	TAIL	LRSI
149	388	TAIL	LRSI
150	389	TAIL	LRSI
151	390	TAIL	LRSI
152	391	TAIL	LRSI
153	392	TAIL	LRSI
154	393	TAIL	LRSI
155	399	TAIL	HRSI
156	1000	DFI	CHEMGL
157	1001	DFI	CHEMGL
158	1002	DFI	CHEMGL
159	1003	DFI	CHEMGL
160	1004	DFI	CHEMGL
161	1010	DFI	CHEMGL
162	1011	DFI	CHEMGL
163	1012	DFI	CHEMGL
164	1013	DFI	CHEMGL
165	1014	DFI	CHEMGL
166	1020	DFI	CHEMGL
167	1021	DFI	CHEMGL
168	1022	DFI	CHEMGL
169	1023	DFI	CHEMGL
170	1024	DFI	CHEMGL
171	1030	IECM	S13GLO
172	1031	IECM	S13GLO
173	1032	IECM	S13GLO
174	1033	IECM	S13GLO
175	1034	IECM	S13GLO
176	1035	IECM	S13GLO
177	1040	IECM	WINDOW
178	1050	IECM	WINDOW

Table III. OFT-1 Geometry Configuration (Cont.)

179	1060	IECM	WINDOW
180	1070	IECM	WINDOW
181	1080	IECM	WINDOW
182	1090	IECM	WINDOW
183	1100	IECM	WINDOW
184	1	BAY	LINER
185	2	BAY	LINER
186	3	BAY	LINER
187	4	BAY	LINER
188	5	BAY	LINER
189	6	BAY	LINER
190	7	BAY	LINER
191	8	BAY	LINER
192	440	BAY	LINER
193	441	BAY	LINER
194	442	BAY	LINER
195	443	BAY	LINER
196	445	BAY	LINER
197	446	BAY	LINER
198	447	BAY	LINER
199	448	BAY	LINER
200	11	BAY	LINER
201	13	BAY	LINER
202	570	FILTER	FILI
203	571	FILTER	FILI
204	572	FILTER	FILI
205	573	FILTER	FILI
206	575	FILTER	FILO
207	576	FILTER	FILO
208	577	FILTER	FILO
209	578	FILTER	FILO
210	580	FILTER	FILI
211	581	FILTER	FILI
212	582	FILTER	FILI
213	583	FILTER	FILI
214	585	FILTER	FILO
215	586	FILTER	FILO
216	587	FILTER	FILO
217	588	FILTER	FILO
218	901	FUSLAG	WINDOW
219	902	FUSLAG	WINDOW
220	910	FUSLAG	WINDOW
221	911	FUSLAG	WINDOW
222	912	FUSLAG	WINDOW
223	913	FUSLAG	WINDOW
224	915	FUSLAG	WINDOW
225	916	FUSLAG	WINDOW
226	917	FUSLAG	WINDOW
227	918	FUSLAG	WINDOW
228	920	FUSLAG	WINDOW
229	921	FUSLAG	WINDOW
230	922	FUSLAG	WINDOW
231	923	FUSLAG	WINDOW

file was generated in the same manner as TAPE 14. The size of this file (~40,000 records) also prohibits its inclusion in this report, however, a listing of TAPE 14 is also on file at JSC.

3.2.6 <u>IECM Instrument Output Predictions</u> - This subsection contains the flux and deposition predictions for the mass spectrometer, TQCMs, and the CQCM. The data are presented as flux or deposition levels by specie as a function of orbit position, MET, and source as appropriate. The particular instrument outputs are not presented since the instrument response depends on the previous exposure history (e.g. see Appendix D, mass spectrometer pumping speed). However, the transfer functions can be easily applied to the flux and deposition rates to determine instrument outputs for specific conditions.

3.2.6.1 <u>Mass Spectrometer</u> - Since no surface sources lie within the mass spectrometer field-of-view (20° full cone angle, line-of-sight (LOS)parallel to +Z axis) the only applicable transport mechanism is return flux. Table IV shows the outgassing flux predictions for each of the six orbital periods. The outgassing source functions are assumed not to decay appreciably during the mission. Therefore the values shown can be applied for any orbit for the conditions specified in subsection 3.2.2.

The early desorption flux summary is shown in Table V. Since this source function has a 1/e decay time of approximately 18 hours, flux levels are shown for three orbits during the mission.

Since leakage is not time or temperature dependent, the mass spectrometer flux was computed for a single time point and is shown below:

SPECIE	LEAKAGE FLUX (mol/cm^2 sec)
H_2O	3.37E7
N_2	7.64E8
CO_2	1.29E7
O_2	2.14E8

The H_2O molecular flux contribution due to the evaporator was determined to be 1.21E10 mol/cm^2 sec for the duration of the venting period.

The RCS/VCS engine flux summary is shown in Table VI. Due to the small solid angle subtended by the mass spectrometer field-of-view,

46

Table IV. Mass Spectrometer - Outgassing Flux Summary

TIME SLICE *	FLUX $(mol/cm^2 sec)$ Outgassing
1	3.12E7 **
2	2.94E7
3	2.58E7
4	2.40E8
5	2.82E8
6	2.94E8

*see Figure 15

** 3.12E7 = 3.12×10^7

Table V. Mass Spectrometer Flux Summary - Early Desorption

MET (hrs)	TIME SLICE	FLUX (mol/cm^{2}sec)			
		H_2O	N_2	CO_2	O_2
2	1	2.65E8	1.18E10	1.99E8	3.36E9
	2	2.02E8	9.19E9	1.53E8	2.64E9
	3	8.47E7	3.95E9	6.46E7	1.13E9
	4	2.96E7	1.41E9	2.28E7	4.02E8
	5	1.62E8	7.47E9	1.23E8	2.14E9
	6	2.03E8	9.19E9	1.53E8	2.64E9
12	1	1.52E8	6.80E9	1.14E8	1.95E9
	2	1.16E8	5.27E9	8.78E7	1.51E9
	3	4.86E7	2.27E9	3.71E7	6.51E8
	4	1.70E7	8.12E8	1.31E7	2.31E8
	5	9.31E7	4.28E9	7.07E7	1.23E9
	6	1.16E8	5.27E9	8.80E7	1.52E9
25	1	7.37E7	3.03E9	5.53E7	9.45E8
	2	5.63E7	2.56E9	4.26E7	7.34E8
	3	2.36E7	1.10E9	1.80E7	3.16E8
	4	8.24E7	3.94E8	6.34E6	1.12E8
	5	4.52E7	2.08E9	3.43E7	5.95E8
	6	5.65E7	2.56E9	4.27E7	7.36E8

Table VI. Mass Spectrometer RCS/VCS Flux Summary

SPECIE	MOLECULAR FLUX (mol/cm^{2}sec)						
	7125 *	7122	7225	7226	7223	8257	8258
H_2O	3.78E11	1.03E10	9.48E10	7.09E10	7.32E10	2.04E9	2.10E9
N_2	3.58E11	1.24E10	7.82E10	8.12E10	8.31E10	2.33E9	2.39E9
CO_2	4.22E10	1.67E9	8.64E9	1.20E10	1.22E10	3.45E8	3.51E8
O_2	7.42E8	2.42E7	1.69E8	1.80E8	1.92E8	5.17E6	5.52E6
CO	1.95E11	5.30E9	3.48E10	3.56E10	3.68E10	1.02E9	1.06E9
H_2	2.81E11	7.66E9	4.25E10	1.23E10	1.25E10	3.53E8	3.59E8
H	3.15E10	8.58E8	5.13E9	1.03E9	1.05E9	2.96E7	3.02E7
MMHNO3	1.52E9	4.14E7	2.11E8	0	0	0	0

*Engine Node – see Figure 19

only the engines shown contributed appreciable densities to points within the field-of-view. Nodes 7226, 7223, 8257, and 8258 provide density contributions to the field-of-view only through reflections from the Orbiter wing. Since all impinging MMHNO3 is assumed to stick to the first collision surface, this specie is eliminated from the contaminant cloud and consequently from the return flux. The following nodal symmetry was assumed: 7225 = 7325; 7226 = 7326; 7223 = 7233; 8257 = 8357; 8258 = 8358.

The mass spectrometer Ne/D_2O calibration system was analyzed to determine the predicted return flux based on the nominal calibration sequence. The vent flowfield characteristics were extracted from Reference 5. A $\cos^2$ flowfield was assumed based on a reasonable match with the experimental data. The flow rates and half intensity beam widths are summarized below:

	Ne	D_2O
Flow Rate (g/sec)	1.18E-3	3.21E-5
Beam Width (deg)	8.4	2.2

The vent was located coplaner with the mass spectrometer receiver the X-Y plane, 9.5 cm from the centerline in the +Y direction. The Shuttle Orbiter was assumed to rotate CCW about the Y axis from the null (nose into the wind) orientation. The return flux predictions are summarized below:

PITCH ANGLE (DEGREES)	RETURN FLUX (mol/cm^2 sec)	
	Ne	D_2O
0	1.17E11	3.14E9
30 (150)	1.03E12	3.00E10
60 (120)	4.34E12	1.28E11
90	7.74E12	2.32E11

3.2.6.2 TQCM - The flux and deposition predictions for the TQCMs comprise both direct flux and return flux contributions. Multiple reflections were considered for all cases analyzed with the exceptions noted.

The integrated outgassing flux impinging on the TQCMs is shown in Table VII. These values were obtained by multiplying the instantaneous flux for each time period by the duration of the time period. Comparing the integrated flux values to the predicted deposition values provides information with respect to an integrated sticking coefficient for QCMs. These data may be useful for resolving discrepencies when comparing SPACE predictions to inflight data. The outgassing deposition predictions are shown in Tables VIII through XI for the four TQCM temperatures.

Since the minimum TQCM temperature (-60°C) is insufficient to condense any of the light gasses, the early desorption, leakage, and evaporator sources were not evaluated (re: subsection 3.2.3).

The deposition predictions for the RCS/VCS engines are shown in Table XII. Only the MMHNO3 specie was considered since the other species are light gasses and will not condense at TQCM temperatures. Multiple reflections were not considered since the MMHNO3 specie would totally condense on the first impinging surface. Since no LOS exists from any engine to any TQCM, only the return flux transport mechanism was considered. For TQCM nodes 1040 and 1050, the following symmetry is assumed: 7123 = 7144; 7116 = 7136; 7225 = 7325; 7223 = 7324; 8258 = 8358; 8116 = 8136. Symmetry is also assumed for TQCM nodes 1090 and 1080 for the various sources in the following list:

1090		1080
7125	=	7125
7122	=	7122
7123	=	7144
7116	=	7136
7225	=	7325
7223	=	7324
8258	=	8358
8116	=	8136

Table VII. *TQCM Outgassing Integrated Flux Summary*

TIME SLICE	INTEGRATED FLUX (g/cm^2)				
	1040 *	1050	1080	1090	1100
1	2.85E-9	4.47E-10	1.38E-9	1.02E-9	2.51E-9
2	2.73E-9	4.34E-10	1.31E-9	1.04E-9	2.62E-9
3	2.14E-9	3.88E-10	9.99E-10	8.60E-10	2.17E-9
4	2.35E-9	4.19E-10	1.09E-9	9.35E-10	2.29E-9
5	2.43E-9	4.12E-10	1.29E-9	9.46E-10	2.51E-9
6	1.95E-9	3.36E-10	1.02E-9	7.06E-10	2.05E-9
TOTAL	1.45E-8	2.43E-9	7.09E-9	5.51E-9	1.41E-9

*IECM node - see Figure 13

Table VIII. TQCM Deposition Summary - Outgassing, T = -60°

TIME SLICE	DEPOSITION (g/cm^2)				
	1040 *	1050	1080	1090	1100
1	9.25E-10	1.33E-10	4.73E-10	1.02E-9	2.51E-9
2	8.18E-10	1.23E-10	4.25E-10	1.04E-9	2.62E-9
3	5.31E-10	9.90E-11	2.36E-10	8.60E-10	2.17E-9
4	5.13E-10	8.82E-11	2.29E-10	9.35E-10	2.29E-9
5	6.49E-10	1.91E-10	3.64E-10	9.46E-10	2.51E-9
6	5.95E-10	1.19E-10	3.00E-10	7.06E-10	2.05E-9
TOTAL	4.03E-9	7.53E-10	2.03E-10	5.51E-9	1.41E-8

*IECM Node - see Figure 13

Table IX. TQCM Deposition Summary - Outgassing T = -30°C

TIME SLICE	DEPOSITION (g/cm^2)				
	1040 *	1050	1080	1090	1100
1	4.98E-10	6.67E-11	2.66E-10	1.45E-10	2.33E-10
2	4.18E-10	5.92E-11	2.27E-10	1.49E-10	2.73E-10
3	2.11E-10	4.27E-11	8.56E-11	7.54E-11	1.51E-10
4	1.59E-10	2.63E-11	6.52E-11	6.23E-11	1.10E-10
5	2.82E-10	5.14E-11	1.70E-10	1.01E-10	2.32E-10
6	1.65E-10	6.87E-11	1.48E-10	6.52E-11	2.13E-10
TOTAL	1.87E-9	3.15E-10	9.62E-10	5.99E-10	1.21E-9

*IECM Node - see Figure 13

Table X. TQCM Deposition Summary - Outgassing, T = 0°C

TIME SLICE	DEPOSITION (g/cm^2)				
	1040 *	1050	1080	1090	1100
1	9.86E-10	5.48E-12	8.67E-11	3.49E-11	1.68E-11
2	7.06E-11	7.69E-13	6.49E-11	3.91E-11	4.05E-11
3	1.40E-12	1.87E-13	1.18E-12	5.87E-12	8.93E-12
4	0	3.40E-13	0	4.02E-13	0
5	1.02E-10	1.86E-13	1.35E-11	9.64E-12	2.01E-11
6	5.32E-11	2.30E-11	3.67E-11	5.13E-12	4.65E-11
TOTAL	1.21E-10	3.00E-11	2.03E-10	9.50E-10	1.33E-10

*IECM Node - see Figure 13

Table XI. *TQCM Deposition Summary - Outgassing, T = +300C*

TIME SLICE	DEPOSITION (g/cm^2)				
	1040*	1050	1080	1090	1100
1	4.89E-11	0	4.66E-11	1.10E-11	0
2	2.85E-11	0	2.54E-11	5.23E-12	0
3	0	0	0	0	0
4	0	0	0	0	0
5	0	0	0	0	0
6	0	0	0	0	0
TOTAL	7.74E-11	0	7.20E-11	1.62E-11	0

*IECM Node - see Figure 13

Table XII. TQCM RCS/VCS MMHNO$_3$ Deposition

ENGINE	DEPOSITION (g/cm^{2}sec)		
	1040 *	1050	1090
7125	3.09E-11	1.23E-11	6.15E-12
7122	1.46E-11	4.98E-12	2.49E-12
7123	1.08E-11	3.99E-12	5.72E-12
7116	3.17E-12	1.54E-12	1.91E-12
7225	2.69E-12	3.51E-12	1.76E-12
7223	1.10E-13	4.06E-14	5.82E-14
8258	3.16E-15	1.17E-15	1.67E-15
8116	9.11E-14	4.43E-14	5.48E-14

*IECM Node - see Figure 13

3.2.6.3 <u>CQCM</u> - The outgassing integrated flux and deposition predictions for the CQCM are shown in Table XIII. The minimum CQCM temperature is expected to be -133°C. Two additional temperatures intermediate to the minimum CQCM temperature and the minimum TQCM temperature (-60°C) were also evaluated in case the CQCM does not attain -133°C in flight.

No light gas deposition was predicted for the CQCM at -133°C for any source. However in order to provide useful information with respect to the light gas specie sticking coefficient algorithm used by SPACE II, impinging flux values are presented. These data will be useful for evaluating this algorithm when comparing SPACE program predictions to inflight data.

The early desorption total integrated flux predictions are presented in Table XIV. The values for three mission time periods were computed due to the rapid time decay characteristic of this source.

The predicted leakage flux by specie is shown below:

SPECIE	LEAKAGE FLUX (g/cm^2 sec)
H_2O	4.21E-13
N_2	2.33E-11
CO_2	6.69E-13
O_2	9.07E-12

The predicted evaporator flux is 3.09E-10 g/cm^2 sec of H_2O.

The RCS/VCS engine predictions are shown in Table XV for the four major species. Since the sticking coefficient for MMHNO3 is 1.0, the flux values are also the deposition rates. All sources except 7226 and 8257 contribute mass directly to the CQCM field-of-view and therefore contribute the MMHNO3 specie to the return flux. The 7226 and 8257 nodes only contribute mass through reflections and therefore do not contribute MMHNO3. Symmetry is assumed for the following sources: 7123 = 7144; 7116 = 7136; 7225 = 7325; 7223 = 7324; 7226 = 7326; 8257 = 8357; 8258; 8258 = 8358.

3.2.7 <u>Results Summary</u> - From the transfer function analysis described in Appendix D, minimum sensitivity levels can be identified for the instruments. For the TQCM/CQCM assume a minimum detectable frequency change of 1 Hz. This results in a minimum detectable deposition value of 1.56 x 10^{-9} g/cm^2.

Table XIII. CQCM Integrated Flux and Deposition Summary - Outgassing

TIME SLICE	INTEGRATED FLUX (g/cm^2)	DEPOSITION (g/cm^2)		
		T = -85^oC	T = -100^oC	T = -133^oC
1	4.57E-10	1.89E-10	2.22E-10	3.02E-10
2	4.38E-10	1.77E-10	2.09E-10	2.84E-10
3	3.88E-10	1.48E-10	1.77E-10	2.42E-10
4	4.26E-10	1.41E-10	1.72E-10	2.45E-10
5	4.21E-10	2.42E-10	2.73E-10	3.41E-10
6	3.43E-10	1.61E-10	1.86E-10	2.45E-10
TOTAL	2.47E-9	1.06E-9	1.24E-9	1.93E-9

Table XIV. CQCM Integrated Flux Summary - Early Desorption

MET (hrs)	TIME SLICE	INTEGRATED FLUX (g/cm^2)
2	1	1.98E-7
	2	1.54E-7
	3	6.71E-8
	4	2.89E-8
	5	1.27E-7
	6	<u>1.24E-7</u>
	TOTAL	6.99E-7
12	1	1.14E-7
	2	8.86E-8
	3	3.85E-8
	4	1.66E-8
	5	7.31E-8
	6	<u>7.11E-8</u>
	TOTAL	4.01E-7
25	1	5.51E-8
	2	4.30E-8
	3	1.87E-8
	4	8.04E-9
	5	3.55E-8
	6	<u>3.45E-8</u>
	TOTAL	1.95E-7

Table XV. *CQCM RCS/VCS Flux Summary*

ENGINE	MASS FLUX ($g/cm^2 sec$)			
	H_2O	CO_2	CO	MMHNO3
7125	1.81E-9	4.77E-10	1.13E-9	1.23E-11
7122	7.36E-10	1.94E-10	4.60E-10	4.98E-12
7123	5.59E-10	1.56E-10	3.61E-10	3.99E-12
7116	1.65E-10	5.94E-11	1.26E-10	1.54E-12
7225	4.54E-10	1.37E-10	3.09E-10	3.51E-12
7223	1.50E-9	6.53E-10	1.22E-9	4.06E-14
7226	1.43E-9	6.34E-10	1.17E-9	0
8257	4.11E-11	1.82E-11	3.36E-11	0
8258	4.31E-11	1.88E-11	3.51E-11	1.17E-15

For the mass spectrometer, assume that the minimum detectable count rate, providing minimum acceptable accuracy is 50 counts/sec. Then from Appendix D, Part 1, the minimum detectable flux, for an unexposed collimator is given by:

$$F_i = \frac{50}{S_i * 1.90E-6}$$

where:

F_i = molecular flux of specie i incident on mass spectrometer aperture(mol/cm^2 sec) and

S_i = sensitivity of the mass spectrometer for specie i (counts/sec/mol/cm^3).

For the various species considered by the SPACE code, the following sensitivities can be determined.

SPECIE	SENSITIVITY (counts/sec/mol/cm³)	MINIMUM DETECTABLE FLUX (mol/cm²sec)
OUT	1.69E-3*	1.56E10
H_2O	9.46E-4	2.77E10
N_2	1.05E-3	2.51E10
CO_2	1.42E-3	1.85E10
O_2	1.13E-3	2.33E10
CO	1.05E-3	2.51E10
H_2	4.20E-4	6.27E10
H	3.99E-4	6.60E10
MMHNO3	3.10E-3*	8.49E9

* These are estimates based on the parent molecule shown since the cracking patterns of these complex species are not defined.

Based on these assumptions for the minimum detectability levels for the instruments an assessment of the capability of these instruments to detect the various sources can be performed.

Mass Spectrometer - The maximum value predicted for outgassing flux occurs in slice 6 and is 2.94E8 mol/cm^2 sec. This value is below the minimum detectability level. The maximum predicted values for early desorption flux occur for the MET = 2 hr. case and time slice 1. The flux for all species, H_2O, N_2, CO_2, O_2 are also below the minimum detectable levels. The predicted flux levels for leakage are several orders of magnitude below the minimum detectable levels. The predicted flux levels for the RCS/VCS engines exceed the minimum detectable levels for several engines and species. However, pulse lengths for the RCS vary from 40 msec to 150 seconds and for the VCS are 40 msec. The detectability of the RCS engines will depend on the pulse duration. The detectability of the VCS engine is questionable.

The minimum detectable flux for both calibration species (Ne/D_2O) is 1.9E11 mol/cm^2 sec. The predicted Ne and D_2O specie flux exceed this level for all pitch angles greater than 10^0 and 70^0 respectively.

TQCM - The predicted outgassing orbital deposition levels for the 1040, 1090, and 1100 TQCMs are above the minimum detectable level for a temperature of -60°C. The predicted deposition levels are 2.6, 3.5, and 9.0 times the minimum level respectively for an exposure period of 90 minutes. For a temperature of -30°C, only the 1040 TQCM is above the minimum detectable level for a 90 minute exposure. For 0°C, and 30°C none of the predicted deposition levels are above the limit.

The MMHNO3 deposition levels from the RCS engines require near maximum burn times to be detectable. The VCS engine deposition levels are well below detectable limits on a pulse basis. At best, 4.3E5 pulses would be required from the 8116 VCS node to be detectable with the 1040 TQCM.

CQCM - The predicted outgassing deposition levels for a full orbit at the nominal -133°C temperature exceeds the minimum detectable level. However, the predicted orbit deposition for -100°C and -85°C are below the detectable level.

No deposition is predicted for the early desorption, leakage, or evaporator source species.

RCS MMHNO3 deposition requires at best, 130 seconds cumulative burn time (7125) to be detectable. The next best case is 313 seconds cumulative burn time (7122). The VCS engines require unreasonable cumulative burn times to exceed the minimum detectable levels.

3.2.8 <u>OFT-1 Post Mission Analysis Requirements Assesment</u> - The results described provide a detailed assessment of the expected response of the IECM instruments to the Shuttle Orbiter contamination environment for OFT-1. The predictions are limited by the assumptions described in subsection 3.2.2 The most critical assumptions relate to the assumed Shuttle Orbiter attitude which directly resolves into surface temperature predictions and velocity vector orientation. Surface temperatures directly relate to source rates and outgassing sticking coefficients. Velocity vector orientation directly relates to return flux predictions which in some cases, exceed direct flux predictions. The probability of the OFT-1 mission parameters duplicating those used for this analysis is very low.

The approach used to perform the OFT-1 post flight IECM data analysis would greatly depend on the available data. If, as anticipated, data were available for the entire mission, the analysis approach would be to simulate selected portions of the mission which provided IECM data which could be used to assess SPACE II source transport, and deposition algorithms. Based on the predictions described in subsection 3.2.6, the TQCM/CQCM instruments would be the most likely to detect contamination deposition. The mass spectrometer is not expected to respond to the predicted environment. However, the inherent modularity and flexibility of the SPACE model will expedite resolution of discrepencies between measured and predicted parameters.

3.3 OFT-3 Mission Analysis

This section describes the OFT-3 mission analysis activity and resulting IECM instrument predictions.

3.3.1 <u>Objective</u> - The objective of the OFT-3 mission analysis activity is to analyze and assess the measurement of direct molecular flux with a TQCM and the mass spectrometer instruments of the IECM placed with the Remote Manipulator System (RMS) at various locations and viewing directions outside of the payload bay. The purpose of these measurements is to: 1) determine the actual direct contamination flow and characteristic emission and reflection rates from specific major Orbiter sources and at locations above the payload bay and 2) verify and update the SPACE II model source, transport mechanism, and deposition algorithms.

The approach used to accomplish these objectives was to develop predictions for the 1050 TQCM and the 1070 mass spectrometer at 24 locations above and outside of the payload bay. Flux impingement and deposition rates were developed for the TQCM. Flux impingement rates within the 0.1 steradian field-of-view were developed for the mass spectrometer.

3.3.2 <u>Assumptions</u> - The following assumptions were used for

the OFT-3 analysis:

a) IECM measurements would be made for a Shuttle Orbiter attitude which would prevent the return flux transport mechanism from contributing to the measured values (i.e. only the direct flux transport mechanism was considered);

b) the temperature data on the OFT-1 TAPE 1C (ZLV attitude, $\beta = 0^{\circ}$) were assumed to be representative of the OFT-3 surface temperatures; the assumed TQCM temperature was $-60^{\circ}C$.

c) the payload bay was assumed to be empty except for the DFI hardware;

d) adequate convergence of the multi-reflect option would be provided by 6 reflections;

e) source outgassing rate time decay was assumed to be negligible; and

f) the mass spectrometer collimator was not previously exposed.

3.3.3 <u>Mission Analysis Plan</u> - The OFT-3 mission analysis plan is contained in Appendix E. The plan outlines the objective, groundrules, and approach to be used for the analysis. Also included in Appendix E is the IECM location and orientation data for the 24 measurement points defined by JSC. The Shuttle Orbiter contamination sources to be considered were outgassing, early desorption, leakage, evaporators, and the RCS/VCS engines.

3.3.4 <u>Shuttle Orbiter/Payload Geometry</u> - The Shuttle Orbiter and DFI geometry used for this analysis was the same as for the OFT-1 analysis and is described in subsection 3.2.4. The IECM was removed from the payload bay. The TQCM was represented by a single disc and the mass spectrometer was represented by a cylinder/disc/point geometry (Figure 20) for the purposes of developing the body-to-body mass transport factors. The complex geometry of the mass spectrometer simulation was required to limit the field-of-view of the instrument to a 20° full cone angle. The point represents the instrument aperture and the cylinder/disc provide the shadowing required to limit the field-of-view. Since the acceptance angle of the TQCM is very large (155°), it was approximated by a single disc without shadowing since the relative projected area of the disc for angles greater than 78° is small resulting in small effective viewfactors for sources at or greater than this angle. This simplification resulted in a substantial reduction in TRASYS mass transport factor run times. The locations and orientations of the simplified IECM geometry are shown in Appendix E, Part 2.
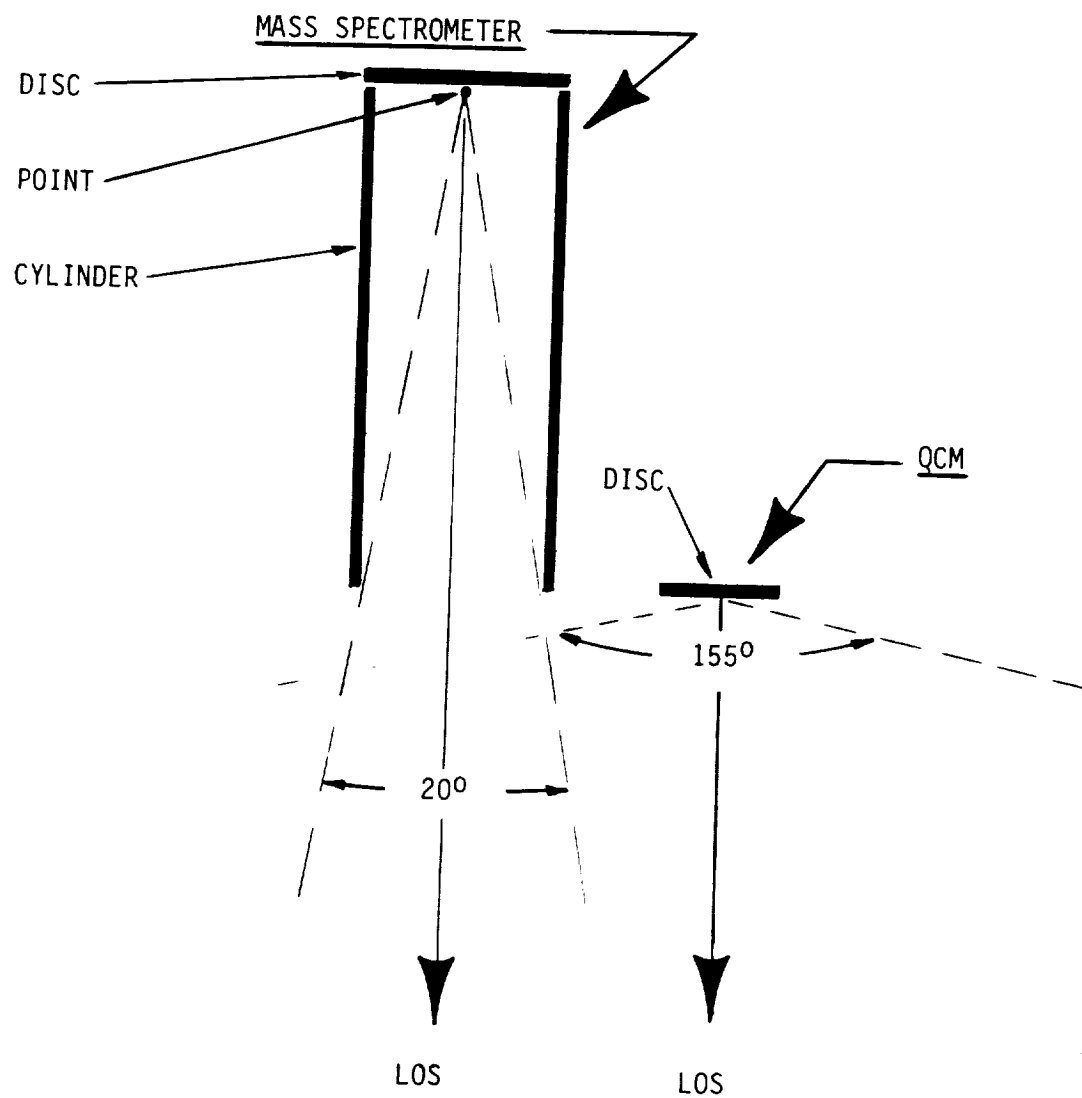
Figure 20. Mass Spectrometer/TQCM TRASYS Simulation

3.3.5 SPACE Input Data File Development - The data files required
to perform the OFT-3 mission analysis runs are described below:

TAPE 4   - This data file is a list of the nodes comprising the
               Shuttle Orbiter, DFI, and payload bay geometry and the
               materials assigned to the nodes. This file is the same
               as that used for the OFT-1 analysis except that the IECM
               nodes were removed (see Table III).

TAPE 10   - The temperatures assigned to the various nodes comprising
               the geometry are stored on this file. For the OFT-3
               analysis the MINTMP (hot) and ATCODE = 3 (cold) files
               described in subsection 3.1.2 were used to bound the
               outgassing and early desorption source rates.

TAPE 12   - This file contains the body-to-body mass transport
               factors generated by the TRASYS program and used by
               SPACE for direct flux and multiple reflection calculations.
               The mass transport factors were computed from the
               TQCM/mass spectrometer nodes to the Shuttle Orbiter/DFI
               nodes for each of the 24 measurement points. These
               mass transport factors were then merged with the
               Shuttle Orbiter/DFI mass transport factors (less the
               deleted IECM nodes) used for the OFT 1 analysis to
               provide the proper TAPE 12 file for OFT-3 analysis.

TAPE 14/15 - These files were not utilized since no return flux runs
             were required.

3.3.6 IECM Instrument Output Predictions - This subsection
contains the flux and deposition predictions for the 1050 TQCM and the
1070 mass spectrometer. The data are tabulated for each of the 24
measurement points by source and specie in the following table:

Source	Table
Outgassing/Early Desorption	
Hot Case	XVI
Cold Case	XVII
Leakage	XVIII
Evaporators	XIX
Engines	XX to XXVI

The values corresponding to the mass spectrometer (MS) are mass flux
predictions. The values corresponding to the TQCM are deposition rates.
The specific engines corresponding to the node numbers

67

Table XVI. Outgassing/Early Desorption Predictions - Hot case

MEAS. POINT	RECVR. NODE	DEPOSITION RATE/FLUX (g/cm^2 sec)								
		OUT	H_2O	N_2	CO_2	O_2	CO	H_2	H	$MMHNO_3$
1	MS TQCM	1.65E-13 3.34E-12	2.01E-13	1.26E-13	1.02E-13	4.85E-14				
2	MS TQCM	1.32E-13 1.54E-12	1.47E-13	9.21E-14	7.42E-14	3.50E-14				
3	MS TQCM	2.35E-13 2.15E-12	2.73E-13	1.17E-13	1.38E-13	6.51E-14				
4	MS TQCM	1.74E-13 2.95E-12	2.13E-13	1.33E-13	1.08E-13	5.11E-13				
5	MS TQCM	1.66E-13 3.43E-12	1.97E-13	1.24E-13	1.00E-13	4.78E-14				
6	MS TQCM	1.43E-13 3.60E-12	1.68E-13	1.06E-13	8.57E-14	4.08E-14				
7	MS TQCM	1.28E-13 3.81E-12	1.47E-13	9.23E-14	7.49E-14	3.56E-14				
8	MS TQCM	1.54E-13 3.86E-12	1.90E-13	1.19E-13	9.65E-14	4.57E-14				
9	MS TQCM	2.70E-13 3.80E-12	3.47E-13	2.10E-13	1.76E-13	8.30E-14				
10	MS TQCM	3.05E-13 3.41E-12	4.60E-13	2.80E-13	2.32E-13	1.10E-13				
11	MS TQCM	1.19E-12 3.60E-12	1.90E-12	1.19E-12	9.59E-13	4.01E-13				
12	MS TQCM	2.94E-13 4.82E-12	3.54E-13	2.22E-13	1.80E-13	8.45E-14				

Table XVI. Outgassing/Early Desorption Predictions - Hot Case (Cont.)

DEPOSITION RATE/FLUX (g/cm² sec)

MEAS. POINT	RECVR. NODE	OUT	H_2O	N_2	CO_2	O_2	CO	H_2	H	$MMHNO_3$
13	MS TQCM	1.48E-13 5.05E-12	1.78E-13	1.12E-13	9.06E-13	4.31E-14				
14	MS TQCM	1.69E-13 5.42E-12	1.96E-13	1.23E-13	9.96E-14	4.74E-14				
15	MS TQCM	1.11E-12 4.79E-12	1.77E-12	1.11E-12	8.93E-13	4.22E-13				
16	MS TQCM	4.56E-13 6.49E-12	6.96E-13	4.35E-13	3.51E-13	1.66E-13				
17	MS TQCM	5.63E-14 1.08E-11	6.64E-14	4.16E-14	3.38E-14	1.61E-14				
18	MS TQCM	1.93E-13 9.08E-12	2.94E-13	1.84E-13	1.49E-13	7.07E-14				
19	MS TQCM	5.94E-13 9.31E-12	8.61E-13	5.30E-13	4.34E-13	2.05E-13				
20	MS TQCM	1.64E-12 2.51E-11	2.26E-12	1.41E-12	1.14E-12	5.31E-13				
21	MS TQCM	1.59E-12 2.47E-11	2.20E-12	1.37E-12	1.11E-12	5.24E-13				
22	MS TQCM	1.65E-12 1.99E-11	2.28E-12	1.43E-12	1.15E-12	5.44E-13				
23	MS TQCM	2.42E-11 2.73E-11	5.05E-12	3.16E-12	2.55E-12	1.20E-12				
24	MS TQCM	1.48E-12 2.30E-11	1.89E-12	1.10E-12	9.53E-13	4.51E-13				

Table XVII. Outgassing/Early Desorption Predictions – Cold Case

MEAS. POINT	RECVR. NODE	DEPOSITION RATE/FLUX (g/cm² sec)								
		OUT	H2O	N2	CO2	O2	CO	H2	H	MMHNO3
1	MS TQCM	1.04E-13 2.67E-12	1.31E-13	8.22E-14	6.66E-14	3.17E-14				
2	MS TQCM	1.32E-13 1.29E-12	1.47E-13	9.21E-14	7.43E-14	3.51E-14				
3	MS TQCM	2.03E-13 1.77E-12	2.66E-13	1.67E-13	1.34E-13	6.35E-14				
4	MS TQCM	1.39E-13 2.37E-12	1.72E-13	1.07E-13	8.69E-14	4.12E-14				
5	MS TQCM	1.02E-13 2.75E-12	1.25E-13	7.82E-14	6.34E-14	3.01E-14				
6	MS TQCM	8.68E-13 2.88E-12	1.05E-13	6.56E-14	5.32E-14	2.53E-14				
7	MS TQCM	7.59E-13 3.04E-12	8.75E-14	5.48E-14	4.45E-14	2.12E-14				
8	MS TQCM	1.15E-13 3.08E-12	1.44E-13	9.03E-14	7.31E-14	3.41E-14				
9	MS TQCM	2.26E-13 3.03E-12	2.96E-13	1.85E-13	1.50E-13	7.08E-14				
10	MS TQCM	2.89E-13 2.71E-12	4.73E-13	2.74E-13	2.21E-13	1.04E-13				
11	MS TQCM	9.56E-13 2.86E-12	1.68E-12	1.05E-12	8.50E-13	4.01E-13				
12	MS TQCM	1.82E-13 3.62E-12	2.28E-13	1.43E-13	1.16E-13	5.50E-14				

Table XVII. Outgassing/Early Desorption Predictions - Cold Case (cont.)

DEPOSITION RATE/FLUX (g/cm^2 sec)

MEAS. POINT	RECVR. NODE	OUT	H2O	N2	CO2	O2	CO	H2	H	MMHNO3
13	MS	9.17E-14	1,15E-13	7.18E-14	5.82E-14	2.77E-14				
	TQCM	3.79E-12								
14	MS	1.01E-13	1.17E-13	7.33E-14	5.94E-14	2.83E-14				
	TQCM	4.03E-12								
15	MS	9.08E-13	1.58E-12	9.91E-13	7.99E-13	3.78E-13				
	TQCM	3.55E-12								
16	MS	4.21E-12	6.47E-13	4.05E-13	3.26E-13	1.54E-13				
	TQCM	5.09E-12								
17	MS	3.44E-14	4.20E-14	2.52E-14	2.04E-14	9.72E-15				
	TQCM	8.47E-12								
18	MS	1.63E-13	2.51E-13	1.57E-13	1.27E-13	6.03E-14				
	TQCM	7.11E-12								
19	MS	4.96E-13	7.49E-13	4.69E-13	3.78E-13	1.79E-13				
	TQCM	7.30E-12								
20	MS	1.51E-12	2.14E-12	1.34E-12	1.08E-12	5.11E-13				
	TQCM	2.05E-11								
21	MS	1.47E-12	2.09E-12	1.30E-12	1.05E-12	4.97E-13				
	TQCM	2.00E-11								
22	MS	1.11E-12	1.68E-12	1.05E-12	8.48E-13	4.01E-13				
	TQCM	1.61E-11								
23	MS	1.82E-12	4.60E-12	2.88E-12	2.32E-12	1.10E-12				
	TQCM	2.09E-11								
24	MS	1.09E-12	1.47E-12	9.15E-13	7.38E-13	3.49E-13				
	TQCM	1.76E-11								

Table XVIII. Leakage Predictions

MEAS. POINT	RECVR. NODE	OUT	DEPOSITION RATE/FLUX (g/cm² sec)							
			H_2O	N_2	CO_2	O_2	CO	H_2	H	$MMHNO_3$
1	MS TQCM		2.47E-11	1.84E-9	2.46E-11	5.70E-10				
2	MS TQCM		1.47E-13	9.23E-14	7.42E-14	3.51E-14				
3	MS TQCM		1.17E-11	8.60E-9	1.16E-11	2.64E-10				
4	MS TQCM		2.31E-11	1.72E-9	2.30E-11	5.30E-10				
5	MS TQCM		1.96E-11	1.45E-9	1.95E-11	4.52E-10				
6	MS TQCM		1.37E-11	1.02E-9	1.37E-11	3.16E-10				
7	MS TQCM		6.65E-12	4.88E-10	6.58E-12	1.55E-10				
8	MS TQCM		3.48E-12	2.47E-10	3.39E-12	7.98E-11				
9	MS TQCM		3.12E-12	2.09E-10	2.95E-12	6.76E-11				
10	MS TQCM		1.45E-12	7.43E-11	1.22E-12	2.38E-11				
11	MS TQCM		3.01E-12	8.45E-11	2.07E-12	2.76E-11				
12	MS TQCM		3.86E-11	2.80E-9	3.84E-11	8.86E-10				

Table XVIII. Leakage Predictions – (Cont.)

MEAS. POINT	RECVR. NODE	OUT	DEPOSITION RATE/FLUX (g/cm² sec)							
			H_2O	N_2	CO_2	O_2	CO	H_2	H	$MMHNO_3$
13	MS TQCM		1.94E-11	1.44E-9	1.93E-11	4.46E-10				
14	MS TQCM		6.55E-12	4.70E-10	6.46E-12	1.51E-10				
15	MS TQCM		4.81E-12	2.29E-10	3.94E-12	7.57E-11				
16	MS TQCM		7.42E-13	3.90E-12	3.97E-13	1.24E-12				
17	MS TQCM		1.74E-12	1.26E-10	1.71E-12	4.05E-11				
18	MS TQCM		3.52E-12	2.42E-10	3.38E-12	7.79E-11				
19	MS TQCM		2.48E-12	1.22E-10	2.05E-12	3.93E-11				
20	MS TQCM		2.27E-12	2.35E-12	1.15E-12	8.30E-13				
21	MS TQCM		2.21E-12	2.29E-12	1.12E-12	8.07E-13				
22	MS TQCM		2.29E-12	1.66E-12	1.15E-12	6.16E-13				
23	MS TQCM		5.05E-12	3.63E-12	2.55E-12	1.35E-12				
24	MS TQCM		1.90E-12	1.49E-12	9.57E-13	5.46E-13				

Table XIX. Evaporator Predictions

MEAS. POINT	RECVR. NODE	OUT	H_2O	N_2	CO_2	O_2	CO	H_2	H	$MMHNO_3$
					DEPOSITION RATE/FLUX (g/cm^2 sec)					
1	MS TQCM		6.56E-13							
2	MS TQCM		7.23E-17							
3	MS TQCM		4.19E-13							
4	MS TQCM		7.16E-13							
5	MS TQCM		5.67E-13							
6	MS TQCM		4.76E-13							
7	MS TQCM		6.28E-13							
8	MS TQCM		3.26E-12							
9	MS TQCM		6.90E-12							
10	MS TQCM		1.08E-8							
11	MS TQCM		1.75E-8							
12	MS TQCM		1.04E-12							

Table XIX. Evaporator Predictions (Cont.)

MEAS. POINT	RECVR. NODE	OUT	DEPOSITION RATE/FLUX (g/cm^2 sec)							
			H_2O	N_2	CO_2	O_2	CO	H_2	H	MMHNO3
13	MS TQCM		5.22E-13							
14	MS TQCM		1.21E-12							
15	MS TQCM		2.48E-9							
16	MS TQCM		3.93E-9							
17	MS TQCM		1.02E-12							
18	MS TQCM		3.24E-12							
19	MS TQCM		6.72E-9							
20	MS TQCM		1.97E-10							
21	MS TQCM		1.92E-10							
22	MS TQCM		4.31E-8							
23	MS TQCM		2.03E-9							
24	MS TQCM		8.02E-9							

Table XX. RCS Engine 7116 Predictions

MEAS. POINT	RECVR. NODE	OUT	DEPOSITION RATE/FLUX (g/cm² sec)							
			H_2O	N_2	CO_2	O_2	CO	H_2	H	$MMHNO_3$
1	MS TQCM		2.30E-12	3.33E-12	6.19E-13	7.94E-15	1.46E-12	1.35E-13	7.94E-15	
2	MS TQCM		6.11E-16	8.84E-16	1.65E-16	2.13E-18	3.88E-16	3.59E-16	2.13E-18	
3	MS TQCM		1.58E-12	2.28E-12	4.24E-13	5.43E-15	1.00E-12	9.24E-14	5.43E-15	
4	MS TQCM		2.64E-12	3.82E-12	7.10E-13	9.11E-15	1.68E-12	1.55E-13	9.11E-15	
5	MS TQCM		1.64E-12	2.38E-12	4.42E-13	5.67E-15	1.04E-12	9.64E-14	5.67E-15	
6	MS TQCM		1.14E-12	1.65E-12	3.07E-13	3.94E-15	7.25E-13	6.29E-14	3.94E-15	
7	MS TQCM		3.22E-13	4.66E-13	8.65E-14	1.11E-15	2.04E-13	1.88E-14	1.11E-15	
8	MS TQCM		9.53E-13	1.38E-12	2.56E-13	3.29E-15	6.05E-13	5.59E-14	3.29E-15	
9	MS TQCM		2.30E-12	3.30E-12	6.19E-13	7.94E-15	1.46E-12	1.35E-13	7.94E-15	
10	MS TQCM		9.22E-13	1.34E-12	2.48E-13	3.18E-15	5.85E-13	5.41E-14	3.18E-15	
11	MS TQCM		1.77E-11	2.56E-11	4.95E-12	6.09E-14	1.22E-11	1.04E-12	6.07E-14	
12	MS TQCM		3.53E-12	5.12E-12	9.51E-13	1.22E-14	2.24E-12	2.07E-13	1.22E-14	

Table XX. RCS Engine 7116 Predictions – (Cont.)

MEAS. POINT	RECVR. NODE	OUT	DEPOSITION RATE/FLUX (g/cm² sec)							
			H_2O	N_2	CO_2	O_2	CO	H_2	H	MMHNO3
13	MS TQCM		1.78E-12	2.58E-12	4.78E-13	6.13E-15	1.13E-12	1.04E-13	6.13E-15	
14	MS TQCM		3.18E-13	4.61E-13	8.57E-14	1.10E-15	2.02E-13	1.87E-14	1.10E-15	
15	MS TQCM		2.11E-11	3.06E-11	5.68E-12	7.28E-14	1.34E-11	1.24E-12	7.28E-14	
16	MS TQCM		7.07E-13	1.02E-12	1.90E-13	2.44E-15	4.49E-13	4.14E-14	2.44E-15	
17	MS TQCM		5.86E-14	8.50E-14	1.58E-14	2.02E-16	3.72E-14	3.44E-15	2.02E-16	
18	MS TQCM		1.85E-13	2.68E-13	4.97E-14	6.37E-16	1.17E-13	1.08E-14	6.37E-16	
19	MS TQCM		6.29E-12	9.10E-12	1.69E-12	2.17E-14	3.79E-12	3.69E-13	2.17E-14	
20	MS TQCM		5.53E-11	8.01E-11	1.49E-11	1.91E-11	3.51E-11	3.24E-12	1.91E-13	
21	MS TQCM		5.38E-11	7.79E-11	1.45E-11	1.86E-13	3.41E-11	3.15E-12	1.86E-13	
22	MS TQCM		3.07E-12	4.44E-12	8.24E-13	1.06E-14	1.94E-12	1.80E-13	1.06E-14	
23	MS TQCM		2.59E-11	3.76E-11	6.98E-12	8.95E-14	1.65E-11	1.52E-12	8.95E-14	
24	MS TQCM		2.71E-12	3.93E-12	7.30E-13	9.36E-15	1.72E-12	1.59E-13	9.36E-15	

Table XXI. RCS Engine 7123 Predictions

MEAS. POINT	RECVR. NODE	OUT	DEPOSITION RATE/FLUX (g/cm² sec)							
			H_2O	N_2	CO_2	O_2	CO	H_2	H	$MMHNO_3$
1	MS TQCM		1.45E-11	2.10E-11	3.89E-12	4.99E-14	9.18E-12	8.49E-13	4.99E-14	
2	MS TQCM		2.20E-14	3.19E-14	5.94E-15	7.81E-17	1.40E-14	1.29E-15	7.70E-17	
3	MS TQCM		8.93E-11	1.29E-10	2.40E-11	3.08E-13	5.67E-11	3.23E-12	3.08E-13	
4	MS TQCM		6.52E-11	9.44E-11	1.75E-11	2.25E-13	4.14E-11	3.82E-12	2.25E-13	
5	MS TQCM		1.05E-11	1.53E-11	2.83E-12	3.64E-14	6.69E-12	6.18E-13	3.63E-14	
6	MS TQCM		7.33E-12	1.06E-11	1.97E-12	2.53E-14	4.65E-12	4.29E-13	2.53E-14	
7	MS TQCM		2.10E-12	3.04E-12	5.64E-13	7.24E-15	1.33E-12	1.23E-13	7.24E-15	
8	MS TQCM		4.05E-12	5.87E-12	1.09E-12	1.40E-14	2.57E-12	2.37E-13	1.40E-14	
9	MS TQCM		9.30E-12	1.35E-11	2.50E-12	3.21E-14	5.90E-12	5.45E-13	3.21E-14	
10	MS TQCM		7.20E-12	1.02E-11	1.89E-11	2.42E-14	4.46E-12	4.12E-13	2.42E-14	
11	MS TQCM		5.49E-11	7.95E-11	1.48E-11	1.89E-13	3.49E-11	3.22E-12	1.89E-13	
12	MS TQCM		2.26E-11	3.28E-11	6.09E-11	7.81E-13	1.44E-11	1.33E-12	7.81E-14	

Table XXI. RCS Engine 7123 Predictions (Cont.)

DEPOSITION RATE/FLUX (g/cm^2 sec)

MEAS. POINT	RECVR. NODE	OUT	H$_2$O	N$_2$	CO$_2$	O$_2$	CO	H$_2$	H	MMHNO3
13	MS TQCM		1.14E-11	1.65E-11	3.06E-12	3.93E-14	7.23E-12	6.68E-13	3.93E-14	
14	MS TQCM		2.11E-12	3.06E-12	5.68E-13	7.29E-14	1.34E-12	1.24E-13	7.29E-15	
15	MS TQCM		6.62E-11	9.59E-11	1.78E-11	2.28E-13	4.12E-11	3.88E-12	2.28E-13	
16	MS TQCM		5.55E-12	8.03E-12	1.49E-12	1.91E-14	3.52E-12	3.25E-13	1.91E-14	
17	MS TQCM		4.18E-13	6.05E-13	1.12E-13	1.44E-15	2.65E-13	2.45E-14	1.44E-15	
18	MS TQCM		9.92E-13	1.44E-12	2.67E-13	3.43E-15	6.30E-13	5.82E-14	3.42E-15	
19	MS TQCM		2.41E-11	3.50E-11	6.49E-12	8.32E-13	1.53E-11	1.41E-12	8.32E-14	
20	MS TQCM		1.69E-10	2.83E-10	5.26E-11	6.74E-13	1.24E-10	1.15E-11	6.74E-13	
21	MS TQCM		1.90E-10	2.76E-10	5.12E-11	6.56E-13	1.21E-10	1.12E-11	6.56E-13	
22	MS TQCM		4.29E-12	6.21E-12	1.15E-12	1.48E-14	2.72E-12	2.51E-13	1.48E-14	
23	MS TQCM		3.47E-11	5.03E-11	9.34E-12	1.20E-13	2.20E-11	2.03E-12	1.20E-13	
24	MS TQCM		4.89E-12	7.08E-12	1.32E-12	1.69E-14	3.10E-12	2.87E-13	1.69E-14	

Table XXII. RCS Engine 7223 Predictions

MEAS. POINT	RECVR. NODE	OUT	DEPOSITION RATE/FLUX (g/cm² sec)							
			H_2O	N_2	CO_2	O_2	CO	H_2	H	$MMHNO_3$
1	MS / TQCM		5.27E-11	7.63E-11	1.42E-11	1.82E-13	3.34E-11	3.09E-12	1.82E-13	
2	MS / TQCM		3.36E-15	4.85E-15	1.03E-15	4.74E-17	2.20E-15	2.24E-16	2.66E-16	
3	MS / TQCM		3.01E-11	4.37E-11	8.11E-12	1.04E-13	1.91E-11	1.77E-12	1.04E-13	
4	MS / TQCM		5.35E-11	7.74E-11	1.44E-11	1.84E-13	3.93E-11	3.13E-12	1.84E-13	
5	MS / TQCM		4.60E-11	6.67E-11	1.24E-11	1.59E-12	2.92E-11	2.70E-12	1.59E-13	
6	MS / TQCM		3.78E-11	5.47E-11	1.02E-11	1.30E-13	2.40E-11	2.22E-12	1.30E-13	
7	MS / TQCM		4.50E-11	6.52E-11	1.21E-11	1.55E-13	2.86E-11	2.64E-12	1.55E-13	
8	MS / TQCM		3.68E-10	5.33E-10	9.90E-11	1.27E-12	2.33E-10	2.16E-11	1.27E-12	
9	MS / TQCM		8.37E-10	1.21E-9	2.25E-10	2.89E-12	5.31E-10	4.91E-11	2.89E-12	
10	MS / TQCM		1.96E-8	2.84E-8	5.28E-8	6.76E-11	1.24E-8	1.15E-9	6.76E-11	
11	MS / TQCM		3.11E-7	4.50E-7	8.36E-9	1.07E-9	1.97E-7	1.82E-8	1.07E-9	
12	MS / TQCM		8.60E-11	1.25E-10	2.31E-11	2.97E-13	5.46E-11	5.04E-12	2.97E-13	

Table XXII. RCS Engine 7223 Predictions (Cont.)

MEAS. POINT	RECVR. NODE	OUT	DEPOSITION RATE/FLUX (g/cm² sec)							
			H_2O	N_2	CO_2	O_2	CO	H_2	H	$MMHNO_3$
13	MS TQCM		4.33E-11	6.27E-11	1.16E-11	1.49E-13	2.75E-11	2.57E-12	1.49E-13	
14	MS TQCM		8.58E-11	1.24E-10	2.31E-11	2.96E-13	5.45E-11	5.03E-12	2.96E-13	
15	MS TQCM		2.40E-7	3.47E-7	6.45E-8	8.27E-10	1.52E-7	1.41E-8	8.27E-10	
16	MS TQCM		5.44E-8	7.88E-8	1.46E-8	1.88E-10	3.45E-8	3.19E-9	1.88E-10	
17	MS TQCM		7.07E-11	1.02E-10	1.90E-11	2.44E-13	4.49E-11	4.14E-12	2.44E-13	
18	MS TQCM		6.75E-11	9.77E-11	1.81E-11	2.33E-13	4.28E-11	3.95E-12	2.33E-13	
19	MS TQCM		3.30E-8	4.78E-8	8.88E-9	1.14E-10	2.09E-8	1.93E-9	1.14E-10	
20	MS TQCM		1.68E-8	2.43E-8	4.51E-9	5.78E-11	1.06E-8	9.83E-10	5.78E-11	3.60E-9
21	MS TQCM		1.63E-8	2.36E-8	4.39E-9	5.26E-11	1.03E-8	9.56E-10	5.62E-11	6.46E-9
22	MS TQCM		7.21E-7	1.05E-6	1.94E-7	2.49E-9	4.58E-7	4.23E-8	2.49E-9	1.46E-8
23	MS TQCM		1.25E-7	1.81E-7	3.35E-8	4.30E-10	7.91E-8	7.31E-9	4.30E-10	8.43E-9
24	MS TQCM		1.67E-6	2.42E-6	4.49E-6	5.75E-8	1.06E-6	9.78E-8	5.75E-9	6.18E-7

Table XXIII. RCS Engine 7226 Predictions

MEAS. POINT	RECVR. NODE	DEPOSITION RATE/FLUX (g/cm² sec)								
		OUT	H_2O	N_2	CO_2	O_2	CO	H_2	H	$MMHNO_3$
1	MS		1.67E-11	2.42E-11	4.50E-12	5.78E-14	1.06E-11	9.18E-13	5.77E-14	
	TQCM									
2	MS		6.46E-16	9.05E-16	3.42E-16	4.72E-17	4.97E-16	7.36E-17	2.01E-17	
	TQCM									
3	MS		1.29E-11	1.86E-11	3.46E-12	4.46E-14	8.16E-12	7.54E-13	4.44E-14	
	TQCM									
4	MS		2.02E-11	2.93E-11	5.44E-12	6.98E-14	1.28E-11	1.19E-12	6.98E-14	
	TQCM									
5	MS		1.48E-11	2.14E-11	3.99E-12	5.13E-14	9.41E-12	8.70E-13	5.12E-14	
	TQCM									
6	MS		1.32E-11	1.91E-11	3.54E-12	4.55E-14	8.36E-12	7.72E-13	4.55E-14	
	TQCM									
7	MS		2.17E-11	3.15E-11	5.85E-12	7.51E-14	1.38E-11	1.27E-12	7.50E-14	
	TQCM									
8	MS		1.16E-10	1.69E-10	3.13E-11	4.02E-13	7.39E-11	6.83E-12	4.02E-13	
	TQCM									
9	MS		2.38E-10	3.44E-10	6.39E-11	8.19E-12	1.51E-10	1.39E-11	8.19E-13	
	TQCM									
10	MS		4.21E-7	6.10E-7	1.13E-7	1.45E-9	2.67E-7	2.47E-8	1.45E-9	
	TQCM									
11	MS		4.04E-7	5.85E-7	1.09E-7	1.39E-9	2.56E-6	2.37E-8	1.39E-9	
	TQCM									
12	MS		2.56E-11	3.71E-11	6.88E-12	8.85E-14	1.62E-11	1.50E-12	8.83E-14	
	TQCM									

Table XXIII. RCS Engine 7226 Predictions (Cont.)

MEAS. POINT	RECVR. NODE	OUT	DEPOSITION RATE/FLUX (g/cm^2 sec)							
			H_2O	N_2	CO_2	O_2	CO	H_2	H	MMHNO3
13	MS									
	TQCM		1.29E-11	1.87E-11	3.47E-12	4.46E-14	8.19E-12	7.57E-13	4.45E-14	
14	MS									
	TQCM		4.41E-11	6.39E-11	1.19E-11	1.52E-13	2.80E-11	2.59E-12	1.52E-13	
15	MS									
	TQCM		8.16E-8	1.18E-7	2.19E-8	2.81E-10	5.98E-8	4.98E-9	2.81E-10	
16	MS									
	TQCM		7.47E-7	1.08E-6	2.01E-7	2.58E-9	4.74E-7	4.38E-8	2.58E-9	
17	MS									
	TQCM		3.43E-11	4.96E-11	9.22E-12	1.18E-13	2.17E-11	2.01E-12	1.18E-13	
18	MS									
	TQCM		4.46E-11	6.46E-11	1.20E-11	1.54E-13	2.83E-11	2.62E-12	1.54E-13	
19	MS									
	TQCM		1.86E-7	2.69E-7	5.00E-8	6.41E-10	1.18E-7	1.09E-8	6.41E-10	
20	MS									
	TQCM		8.84E-9	1.28E-8	2.38E-9	3.05E-11	5.68E-9	5.18E-10	3.05E-11	
21	MS									
	TQCM		8.60E-9	1.25E-8	2.31E-9	2.96E-11	5.45E-9	5.04E-10	2.96E-11	
22	MS									
	TQCM		1.18E-6	1.71E-6	3.17E-6	4.06E-8	7.47E-7	6.91E-8	4.06E-9	
23	MS									
	TQCM		8.44E-8	1.22E-7	2.27E-8	2.91E-10	5.35E-8	4.95E-9	2.91E-10	
24	MS									
	TQCM		3.13E-7	4.53E-7	8.41E-8	1.08E-9	1.98E-7	1.83E-8	1.08E-9	

Table XXIV. RCS Engine 7125 Engine Predictions

MEAS. POINT	RECVR. NODE	OUT	H2O	N2	CO2	O2	CO	H2	H	MMHNO3
1	MS TQCM		1.39E-12	2.02E-12	3.74E-13	4.83E-15	8.83E-13	8.16E-14	4.81E-15	3.93E-7
2	MS TQCM		2.74E-8	3.96E-8	7.36E-9	9.44E-11	1.74E-8	1.60E-9	9.44E-11	4.67E-7
3	MS TQCM		2.86E-8	4.15E-8	7.71E-9	9.88E-11	1.82E-8	1.68E-9	9.88E-11	4.56E-7
4	MS TQCM		1.08E-12	1.57E-12	2.91E-13	3.76E-15	6.87E-13	6.35E-14	3.74E-15	4.31E-7
5	MS TQCM		1.32E-12	1.91E-12	3.55E-13	4.58E-15	8.37E-13	7.74E-14	4.56E-15	3.79E-7
6	MS TQCM		1.06E-12	1.54E-12	2.86E-13	3.69E-15	6.75E-13	6.23E-14	3.68E-15	3.48E-7
7	MS TQCM		6.72E-13	9.73E-13	1.81E-13	2.34E-15	4.26E-13	3.94E-14	2.32E-14	2.76E-7
8	MS TQCM		2.36E-13	3.42E-13	6.35E-13	8.25E-13	1.50E-13	1.39E-19	8.19E-16	2.06E-7
9	MS TQCM		1.59E-13	2.30E-13	4.28E-14	5.57E-16	1.01E-13	9.32E-15	5.51E-16	1.38E-7
10	MS TQCM		8.06E-14	1.17E-13	2.17E-14	2.84E-16	5.11E-14	4.73E-15	2.80E-16	
11	MS TQCM		6.90E-14	9.99E-14	1.86E-14	2.44E-16	4.38E-14	4.05E-15	2.40E16	8.00E-8
12	MS TQCM		2.50E-12	3.62E-12	6.73E-13	8.64E-15	1.59E-12	1.47E-13	8.65E-15	1.12E-7

DEPOSITION RATE/FLUX (g/cm^2 sec)

Table XXIV. RCS Engine 7125 Predictions (Cont.)

DEPOSITION RATE/FLUX (g/cm^2 sec)

MEAS. POINT	RECVR. NODE	OUT	H2O	N2	CO2	O2	CO	H2	H	MMHNO3
13	MS TQCM		1.12E-11	1.62E-11	3.01E-12	3.86E-14	7.11E-12	6.57E-13	3.86E-14	9.78E-8
14	MS TQCM		8.71E-12	1.26E-11	2.34E-12	3.00E-14	5.53E-12	5.11E-13	3.00E-14	
15	MS TQCM		2.92E-12	4.23E-12	7.86E-13	1.01E-14	1.85E-12	1.71E-13	1.01E-14	
16	MS TQCM		8.08E-13	1.17E-12	2.17E-13	2.79E-15	5.13E-13	4.74E-14	2.79E-15	
17	MS TQCM		2.49E-12	3.61E-12	6.71E-13	8.60E-15	1.58E-12	1.45E-13	8.60E-15	
18	MS TQCM		6.07E-12	8.79E-12	1.63E-12	2.09E-14	3.85E-12	3.56E-13	2.09E-14	
19	MS TQCM		3.40E-12	4.92E-12	9.14E-13	1.17E-14	2.16E-12	1.99E-13	1.71E-14	
20	MS TQCM		3.95E-12	5.72E-12	1.66E-12	1.36E-14	2.50E-12	2.31E-13	1.36E-14	
21	MS TQCM		3.84E-12	5.56E-12	1.03E-12	1.32E-14	2.44E-12	2.25E-13	1.32E-14	
22	MS TQCM		7.91E-13	1.15E-12	2.13E-13	2.73E-15	5.02E-13	4.64E-14	2.73E-15	
23	MS TQCM		1.40E-12	2.03E-12	3.78E-13	4.84E-15	8.91E-13	8.23E-14	4.84E-15	
24	MS TQCM		9.46E-13	1.37E-12	2.54E-13	3.26E-15	6.00E-13	5.54E-14	3.26E-15	

Table XXV. RCS Engine 7122 Predictions

MEAS. POINT	RECVR. NODE	DEPOSITION RATE/FLUX (g/cm² sec)								
		OUT	H_2O	N_2	CO_2	O_2	CO	H_2	H	$MMHNO_3$
1	MS TQCM		9.61E-17	1.33E-16	6.32E-17	5.44E-12	1.00E-9	9.25E-11	5.44E-12	
2	MS TQCM		1.74E-9	2.52E-9	4.69E-10	6.00E-12	1.10E-9	1.02E-10	6.00E-12	
3	MS TQCM		1.80E-12	2.61E-12	4.85E-13	6.21E-15	1.14E-12	1.06E-13	6.21E-15	
4	MS TQCM		8.18E-17	1.13E-16	5.44E-17	1.18E-18	6.81E-17	1.17E-17	1.18E-18	
5	MS TQCM		9.32E-17	1.29E-16	6.25E-17	1.35E-18	7.79E-17	1.34E-17	1.35E-18	
6	MS TQCM		7.66E-17	1.06E-16	5.23E-17	1.13E-18	6.46E-17	1.12E-17	1.13E-18	
7	MS TQCM		5.20E-17	7.14E-17	3.76E-17	8.27E-19	4.51E-17	8.07E-18	8.27E-19	
8	MS TQCM		2.01E-17	2.73E-17	1.63E-17	3.68E-19	1.85E-17	3.50E-18	3.68E-19	
9	MS TQCM		1.60E-17	2.14E-17	1.45E-17	3.35E-19	1.56E-17	3.11E-18	3.35E-19	
10	MS TQCM		9.73E-18	1.29E-17	9.22E-18	2.08E-19	9.77E-18	1.98E-18	2.08E-19	
11	MS TQCM		9.62E-18	1.27E-17	9.77E-18	2.30E-19	9.48E-18	2.09E-18	2.30E-19	
12	MS TQCM		1.74E-16	2.40E-16	1.14E-16	2.45E-18	1.44E-16	2.46E-17	2.45E-18	

Table XXV. RCS Engine 7122 Predictions (Cont.)

DEPOSITION RATE/FLUX (g/cm^2 sec)

MEAS. POINT	RECVR. NODE	OUT	H_2O	N_2	CO_2	O_2	CO	H_2	H	MMHNO3
13	MS TQCM		3.05E-16	4.43E-16	9.35E-17	1.23E-18	2.00E-16	2.03E-17	1.23E-18	
14	MS TQCM		2.32E-16	3.35E-16	6.85E-17	8.98E-19	1.50E-16	1.49E-17	8.98E-19	
15	MS TQCM		7.54E-17	1.09E-16	2.12E-17	2.75E-19	4.83E-17	4.62E-18	2.75E-19	
16	MS TQCM		2.11E-17	3.05E-17	5.74E-18	7.39E-20	1.34E-18	1.25E-18	7.39E-19	
17	MS TQCM		6.38E-17	9.73E-17	1.85E-17	2.41E-19	4.11E-17	4.01E-18	2.41E-19	
18	MS TQCM		1.44E-16	2.08E-16	4.06E-17	5.27E-19	9.21E-17	8.83E-18	5.27E-19	
19	MS TQCM		8.07E-17	1.17E-16	2.76E-17	2.93E-19	5.17E-16	4.93E-18	2.93E-19	
20	MS TQCM		1.08E-16	1.57E-15	2.98E-17	3.85E-19	6.90E-17	6.49E-18	3.85E-19	
21	MS TQCM		1.05E-16	1.52E-16	2.90E-17	3.74E-19	6.71E-17	6.32E-18	3.74E-19	
22	MS TQCM		2.01E-17	2.91E-17	5.45E-18	7.00E-20	1.28E-17	1.19E-18	7.00E-20	
23	MS TQCM		3.72E-17	5.38E-17	1.03E-16	1.33E-19	2.38E-17	2.25E-18	1.33E-19	
24	MS TQCM		2.54E-17	3.68E-17	7.01E-18	9.64E-20	1.62E-17	1.53E-17	9.04E-19	

Table XXVI. RCS Engine 7225 Predictions

MEAS. POINT	RECVR. NODE	OUT	DEPOSITION RATE/FLUX (g/cm² sec)							
			H_2O	N_2	CO_2	O_2	CO	H_2	H	MMHNO3
1	MS TQCM		1.68E-9	2.43E-9	4.52E-10	5.79E-12	1.07E-9	9.84E-11	5.79E-12	
2	MS TQCM		5.45E-15	7.58E-15	1.67E-15	3.70E-17	3.67E-15	3.63E-16	2.92E-17	
3	MS TQCM		6.40E-10	9.25E-10	1.73E-10	2.21E-12	4.07E-10	3.76E-11	2.21E-12	
4	MS TQCM		1.41E-9	2.04E-9	3.80E-10	4.87E-12	8.97E-10	8.28E-11	4.87E-12	
5	MS TQCM		1.58E-9	2.28E-9	4.25E-10	5.45E-12	1.00E-9	9.27E-11	5.45E-12	
6	MS TQCM		1.33E-9	1.92E-9	3.59E-10	4.60E-12	8.47E-10	7.83E-10	4.60E-12	
7	MS TQCM		1.44E-9	2.07E-9	3.92E-10	5.02E-12	9.23E-10	8.53E-11	5.02E-12	
8	MS TQCM		1.98E-9	2.83E-9	5.41E-10	6.93E-12	1.27E-9	1.18E-10	6.93E-12	
9	MS TQCM		1.83E-9	2.62E-9	4.99E10	6.40E-12	1.18E-9	1.09E-10	6.40E-12	
10	MS TQCM		9.44E-8	1.34E-7	2.59E-8	3.32E-10	6.10E-8	5.64E-9	3.32E-10	
11	MS TQCM		2.05E-9	2.81E-8	5.94E-9	7.61E-11	1.39E-8	1.29E-9	7.61E-11	
12	MS TQCM		2.87E-9	4.16E-9	7.74E-10	9.92E-12	1.82E-9	1.69E-10	9.92E-12	

Table XXVI. RCS Engine 7225 Predictions (Cont.)

MEAS. POINT	RECVR NODE	OUT	H_2O	N_2	CO_2	O_2	CO	H_2	H	$MMHNO3$
13	MS TQCM		1.45E-9	2.09E-9	3.89E-9	4.99E-12	9.18E-10	8.49E-11	4.99E-12	
14	MS TQCM		2.44E-9	3.49E-9	6.67E-10	8.55E-12	1.57E-9	1.45E-10	8.55E-12	
15	MS TQCM		1.74E-8	7.38E-8	5.03E-9	6.45E-11	1.18E-8	1.10E-9	6.46E-11	
16	MS TQCM		3.55E-7	5.05E-7	9.72E-8	1.25E-9	2.29E-7	2.12E-8	1.75E-9	
17	MS TQCM		1.32E-9	1.90E-9	3.56E-10	4.56E-12	8.39E-10	7.76E-11	4.56E-12	
18	MS TQCM		1.47E-9	2.12E-9	3.97E-10	5.09E-12	9.37E-10	8.66E-11	5.09E-12	
19	MS TQCM		6.82E-9	9.50E-9	1.91E-9	2.45E-11	4.50E-9	4.17E-10	2.45E-11	
20	MS TQCM		1.54E-8	2.16E-8	4.38E-9	5.61E-10	1.03E-8	9.54E10	5.61E-11	
21	MS TQCM		1.50E-8	2.10E-8	4.26E-9	5.46E-11	9.98E-9	9.28E-10	5.46E-11	
22	MS TQCM		3.46E-8	4.72E-8	9.98E-9	1.28E-10	2.34E-8	2.17E-9	1.28E-10	
23	MS TQCM		3.70E-8	4.09E-8	8.73E-9	1.12E-10	2.05E-8	1.90E-9	1.12E-10	
24	MS TQCM		7.02E-8	9.50E-8	2.07E-8	2.65E-10	4.84E-8	4.51E-9	2.65E-10	

DEPOSITION RATE/FLUX $(g/cm^2\ sec)$

in the tables are defined in Figure 19.

3.3.7 <u>Results Summary</u> - The dwell time at each position required for the TQCM to accumulate sufficient deposition to exeed the minimum detectable limit (1.56E10-9 g/cm^2) can be computed from :

$$t_{DWELL} + \frac{1.56E-9}{\dot{D}}$$

where:

t_{DWELL} = minimum dwell time (seconds) and

$\dot{D}$ = predicted depostion rate (g/cm^2 sec) .

The dwell time for each of the 24 points for measurement of the outgassing specie are summarized in Table XXVII. No deposition is predicted from any of the light gas species from the early desorption, leakage, evaporator, or engine sources.

The MMHNO3 specie will deposit on the TQCM for several measurement points from the 7223 and 7125 nodes. The RCS engine deposition per pulse depends on the pulse duration which is variable from 40 m sec to 150 second. The total exposure times for the applicable measurement points for these two RCS engine nodes are summarized in Table XXVII. The table shows that the 7223 engine must pulse up to 11 times, assuming minimum pulse length, for the deposition to exceed the minimum detectable limit. However, for all measurement points receiving direct flux from the 7125 engine, even a single pulse will exceed the minimum detectable limit. In fact, for measurement point numbers 2 and 3, a cumulative burn time of 200 seconds will saturate the TQCM. Since MMHNO3 deposits are assumed permanent, saturation would render the TQCM useless for the remaining measurements. Therefore careful planning is required to prevent TQCM saturation.

The mass spectrometer sensitivity is based on the instantaneous molecular density in the detector volume. Assuming a 50 count/sec. minimum count rate, from subsection 3.2.7, the following minimum detectable flux levels can be determined:

SPECIE	MINIMUM DETECTABLE FLUX (g/cm^2 sec)
OUT	2.59E-12 *
H_2O	8.28E-13
N_2	1.17E-12

90

Table XXVII. *TQCM Dwell Time Summary*

MEASUREMENT POINT	DWELL TIME (sec)			
	OUTGASSING		MMHNO3	
	HOT CASE	COLD CASE	7223	7125
1	467	584		0.004
2	1013	1210		0.003
3	726	881		0.003
4	529	658		0.004
5	455	567		0.004
6	433	542		0.004
7	409	513		0.006
8	404	506		0.008
9	411	515		0.011
10	457	576		
11	433	545		0.020
12	324	431		0.014
13	309	412		0.016
14	288	387		
15	326	439		
16	240	306		
17	144	184		
18	172	219		
19	168	214		
20	62	76	0.433	
21	63	78	0.241	
22	78	97	0.106	
23	57	75	0.185	
24	68	89	0.025	

(Continued)

CO_2	1.35E-12
O_2	1.24E-12
CO	1.17E-12
H_2	2.08E-13
H	1.10E-13
$MMHNO3$	6.06E-13 *

* These are estimates based on the parent molecule shown since the cracking patterns of these complex molecules are unknown.

Comparing the minimum detectable levels to the predicted flux levels for the mass spectrometer, the following observations can be made for predicted detectability of the various Shuttle Orbiter sources:

Outgassing - Point 23, Hot Case, approaches the minimum detectable level and may be marginally detectable.

Early Desorption - For both temperature cases, the flux levels shown for points 11, 15 and 19 through 24, approach or exceed the minimum detectable levels. The flux levels shown apply to a MET of 25 hours. If the mapping activity is performed at an earlier time in the mission, the flux levels would be substantially higher. For example, for a MET = 2 hrs. the predicted flux levels would be approximately 3.5 times higher. The number of measurement points providing flux levels exceeding the minimum detectable level would therefore increase.

Leakage - The leakage source characteristics are best measured from points 1 through 15. Unfortunately, the leakage specie flux levels equal or exceed the early desorption levels for all measurement points for the flux levels shown. Although the leakage sources exist only in the payload bay their substantial magnitude together with the multiple reflection phenomenon results in their specie presence affecting nearly all Shuttle Orbiter surfaces. Of course, the relative magnitudes of the predicted leakage and early desorption flux are functions of MET.

Evaporator - Evaporator source characteristics are best observed at measurement points 22 and 24. The predicted flux levels result in a predicted count rate of 2.6E6 counts/sec and 4.8E5 counts/sec. These count rates are less than the maximum calibration rate (2.5E7 counts/sec). Two additional points, 10 and 11, will also provide comparable count rates. The effects of the evaporator will be detectable at lower levels at various other points and will effectively mask the early desorption and leakage H_2O specie. Thus measurements of these other sources

92

from specific points, should be suspended during evaporator venting cycles.

Engines - Flux from the various engines can be measured from a variety of points. Since direct line-of-sight impingement from any engine to the mass spectrometer is prohibited, all flux values represent reflected mass. Maximum flux levels will occur at different points for different engines depending primarily on the geometrical relationship between the engine, the mass spectrometer and the first reflecting surface.

The VCS engines were not run as individual sources since they are assumed to be scalable, to corresponding RCS engines by total mass flow for direct flux calculations. The assumed correspondence is; 8116 = 7116; 8257 = 7226; 8258 = 7223, and:

$$(VCSFLUX) = 0.029 * (RCS FLUX).$$

3.3.8 OFT-3 Post Mission Analysis Requirements Assessment - The results described provide a detailed assessment of the expected response of the IECM, TQCM and mass spectrometer instruments for the baseline 24 point measurement matrix. The predictions are limited to the assumptions described in subsection 3.3.2. Obviously if the attitude and thermal parameters for OFT-3 are not the same as the model inputs the predictions will not agree with the measurements. The outgassing and early desorption source rates are a direct function of surface temperature. The TQCM deposition is a direct function of crystal temperature. If the mass spectrometer is oriented so as to allow direct impingement of the ambient flux in the aperture, sensitivity will be reduced and the transfer function will be modified. The sensitivity of the predictions to these variables has been discussed previously. The probability of the OFT-3 mission duplicating the analysis inputs is low.

The approach for performing the post flight analysis for OFT-3 depends on the available data. If, as anticipated, data were available for the 24 measurement points, the post flight analyses would require that predictions be recomputed based on the actual mission parameters. The parameters include source node temperatures, Shuttle Orbiter orientation with respect to the velocity vector, measurement history of the mass spectrometer, TQCM temperature, and other parameters directly and indirectly influencing the instrument response. If new measurement points are selected, new mass transport factor files will be required to be developed using TRASYS. This would require determining the precise coordinates and attitude of the IECM during the measurement period. If the 24 point measurement program, or a subset, is followed, the rerun requirements would be minimal providing that the input data were available in the proper form. If the measurement plan is not followed, additional geometrical modeling would be required which could substantially increase the rerun requirements.

93

Resolution of discrepencies between measured and predicted values will be expedited by the inherent modularity and flexibility of the SPACE model. Surface source rates as a function of time and temperature are directly accessable in block data files. Point source mass distribution functions are also available in block data files. These parameters can be adjusted temporarily through namelist inputs for parametric analyses to investigate output sensitivity. Source and TQCM temperatures can also be adjusted via namelist inputs to account for revised thermal profiles. The direct flux transport mechanism has been extensively verified through laboratory testing and is therefore not expected to require modification. All other mission parameters can be adjusted via namelist input or simple code modifications as determined by flight data analysis.

4.0 CONCLUSIONS

Table XXVIII and XXIX summarize the Statement of Work (SOW) task compliance referencing each SOW task item to a specific paragraph in the report. Since this study was performed in two stages both the basic and follow-on contract SOW are addressed.

The SPACE code has been improved to provide the user with greater utility and flexibility in performing both mission contamination analyses and parametric analyses to support trade study activities. As a result of these improvements computer runtimes have increased. The increase in the number of lines-of-sight in the point matrix (from 17 to 50) to provide for higher density resolution in the vicinity of the spacecraft, the capability to compute column densities and return flux from random lines-of-sight , and the incremental approach for computing return flux required to account for flux attenuations are the primary reasons for the increase in computer run times.

The SPACE II code has been checked out to the maximum extent practical within the constraints of the program. As with all large, complex, systems level codes, when the code is applied to specific analyses, code updates may be required. The modular design and inherent flexibility of the code will permit updates and modifications with minimum effort and impact on the basic code structure.

The Shuttle Orbiter/IECM mission analysis and assessment for an IECM in-bay (OFT-1) and outside of the bay (OFT-3) mapping mission have been performed. The results of the OFT-1 analysis indicate the following:

a) The mass spectrometer sensitivity is insufficient to detect the predicted contaminant environment induced by the outgassing, early description, leakage, and the majority of the RCS engine sources. Several RCS engine sources were determined to be marginally detectable (see subsections 3.2.6.1 and 3.2.7).

b) Several TQCM instruments are expected to detect the payload bay outgassing species environment if minimum TQCM design temperatures can be attained. Detection of the RCS engine MMHNO3 specie requires near maximum burn times. Light gas species (H_2O, CO_2, etc) are not expected to condense at TQCM temperatures.

c) The CQCM is expected to repond to the outgassing return flux component if the minimum design temperature ($-133^{\circ}C$) is attained. However, at higher temperatures ($>-100^{\circ}C$), the predicted deposition is below the minimum detectable level. No condensation is predicted for the early desorption, leakage, or evaporator sources due to the low predicted incident flux levels. RCS MMHNO3 deposition requires near maximum burn times.

95

Table XXVIII. Basic Contract Task Compliance Summary

SOW TASK REQUIREMENTS	FINAL REPORT SECTION REF.

4.1 Direct Flux Deposition with Multiple Reflections
   a) Direct Flux Algorithms
   b) Multiple Reflections Algorithms
   c) Viewfactors - TAPE12
   d) Direct Flux Deposition Algorithms
	2.1
	2.1
	3.2.5, 3.3.5
	2.2

4.2 Deposition Summation DELETED	

4.3 IECM Model Development
   a) Develop IECM Geometry/Sources
   b) Develop IECM Viewfactors
   c) Orbiter Wing Node Resolution Analysis
   d) Model Neon/Water Vent
	3.1.1
	3.2.5, 3.3.5
	3.3.6
	3.1.1

4.4 Update Data Handling and Presentation
   a) Increase LOS Resolution
   b) Develop DISSPLA Interface Capability
	2.4
	2.3

4.5 Mission Analysis and Assessment
   a) OFT-1 Mission Analysis
   b) OFT-3 Mission Analysis
   c) Perform Instrument Input/Output Analysis
   d) Assess Post Mission Analyses Effort
	3.2
	3.3
	3.1.3
	3.2.7, 3.3.7

4.6 Develop Sample Cases and Verify JSC SPACE Code	2.5
4.7 Update User's Manual	2.6
4.8 Final Report	---

Table XXIX. *Follow-On Contract Task Compliance Summary*

SOW TASK REQUIREMENTS	FINAL REPORT SECTION REF.

4.1 Deposition Summation
    a) Develop Variable Velocity Vector Algorithm
    b) Develop Return Flux Deposition Algorithm
    c) Develop Deposition Summation Algorithm
	2.2
	2.2
	2.2

4.2 GBCAL/Multireflect Trade Study	2.1

4.3 Body-to-Body Viewfactor Development
    a) Perform OFT-1 TRASYS Runs
    b) Perform OFT-3 TRASYS Runs
	3.2.5.3
	3.3.5.3

4.4 IECM Mission Analysis SPACE Runs
    a) Perform OFT-1 SPACE Runs
    b) Perform OFT-3 SPACE Runs
	3.2.6
	3.3.6

4.5 Provide User's Training	2.7
4.6 Update User's Manual	2.6

The tabulated OFT-1 IECM instrument predictions provide a substantial data base for comparison to measured values. The predictions however are limited by the assumptions required to bound the analyses. The applicabilty of the data base will depend on the OFT-1 mission parameters and how well they compare to the assumed mission profile. It is anticipated that the post-mission analysis activity will require that the SPACE II code be reapplied to simulate specific IECM instrument measurement conditions. The improved capability of the SPACE II code developed during the course of this program will permit an accurate and expedicious simulation of any desired measurement situation.

The OFT-3 IECM instrument predictions have been developed for the baseline 24 measurement point matrix as defined by the mission analysis plan. The contamination sources evaluated include outgassing, early desorption , leakage, evaporator, and the RCS engines. The results of the analyses show that the 24 point plan will provide sufficient data to characterize the expected sources provided that sufficient post-mission support data (attitude timeline, surface temperatures, event timeline, etc) are available. The preferred measurement points for specific sources are those points where the mass spectrometer flux levels are maximized or the TQCM dwell times are lowest. An optimized subset of the 24 point matrix was not developed since the specific time history of the instruments and the mission variables have a significant impact on instrument sensitivity and source functions. These unknowns have a wide range of variability and would result in a large uncertainty in instrument measurements. The risk of information loss incurred in attempting to perform an optimized measurement sequence, considering these uncertainties, was not felt to be justified by a reduction in the measurement matrix size. Therefore the baseline 24 point measurment plan is the preferred approach at this time.

5.0 REFERENCES

The following references are presented to support the technical material contained in this report.

1. *Shuttle/Payload Contamination Evaluation Program Version II*, JSC NAS9-15826, MCR-81-509, Martin Marietta Corporation, Denver Aerospace, January 1981.

2. *Thermal Radiation Analysis System (TRASYS)*, JSC NAS9-15304, MCR-73-105, Rev. 2, Martin Marietta Aerospace, Denver Division, June 1979.

3. Gebhart, B.: *Unified Treatment for Thermal Radiation Transfer Process - Gray, Diffuse Radiators and Absorbers*, Paper No. 57-A-34, ASME, December 1957.

4. Spieth, B. E.: *DISSPLA Plot Capability Addition to the SPACE Computer Program*, Martin Marietta Aerospace, Denver Division, February, 1980.

5. Taeusch, D. R.: *Orbiter Calibration System - IECM Mass Spectrometer*.

6. *IECM Contamination Monitoring - RMS Joint Angles/IECM Position/ Attitude*, JSC Informal Data Transmittal, January 11, 1980.

Appendix A

SPACE II Multiple Reflection Algorithm Description

This appendix contains the results of trade studies and analyses describing the development of the SPACE II multiple reflection algorithms. The appendix comprises three parts: Part 1 (p. A-3) is a memo describing the multiple reflection approach and a functional comparison of the new approach to GBCAL; Parts 2 (p.A-14) and 3 (p. A-22) describe trade studies whose objectives were to evaluate the convergence characteristics of the multiple reflection approach compared to GBCAL for a variety of typical payloads.

MARTIN MARIETTA AEROSPACE

January 28, 1980

To: National Aeronautics and Space Administration
Lyndon B. Johnson Space Center
Houston, Texas 77058

Attention: Mr. S. Jacobs - ES-5

Subject: SPACE Multiple Reflection Option

Objective: The objective of this analysis is to describe the new SPACE multiple reflection option. The approach presented is expected to replace the GBCAL subroutine which was limited to direct flux applications and outgassing species only.

Approach: Consider a two node configuration with parameters shown below.
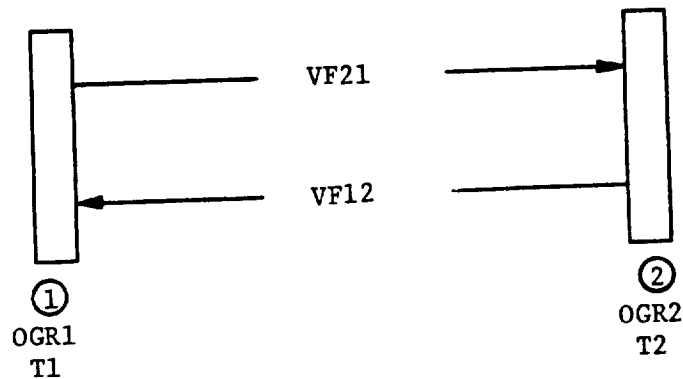
Assume that surface ① is designated as the critical surface. The flux incident on ①, assuming no reflections, is given by:

$$\psi 1(0) = OGR2 * VF12$$

This expression is the basis for contamination flux computations. The subscript will indicate the number of reflections considered for the remainder of this analysis.

A-3

For 1 reflection the flux on ① becomes the direct contribution from ② (OGR2 * VF12) plus a fraction of the flux incident on ② then reemitted back to ①. This can be expressed by:

$$\psi 1(1) = \psi 1(0) + OGR1 * VF21 * (1-S12) * VF12 \tag{2}$$

where S12 is the sticking coefficient from ① to ② and (1-S12) is therefore the fraction of incident flux reflected from ②. Then VF12 * (1-S12) is the fraction of flux reflected from ② incident on ①.

Substituting for $\psi 1(0)$ and simplifying yields:

$$\psi 1(1) = \left[OGR2 + OGR1 * VF21 * (1-S12) \right] * VF12 \tag{3}$$

The term in the brackets can be considered as a new effective mass loss rate for surface ② consisting of the original source rate OGR2 and a component from another source, in this case, the receiver itself.

If two reflections are considered, then an additional component is added to the source rate of surface ② consisting of the portion of flux emitted from ②, reflected from ① back to ②, then reflected from ② back to ①. The component can be expressed by

$$\Delta\psi 1(2) = OGR2 * VF12 * (1-S21) * VF21 * (1-S12) * VF12 \tag{4}$$
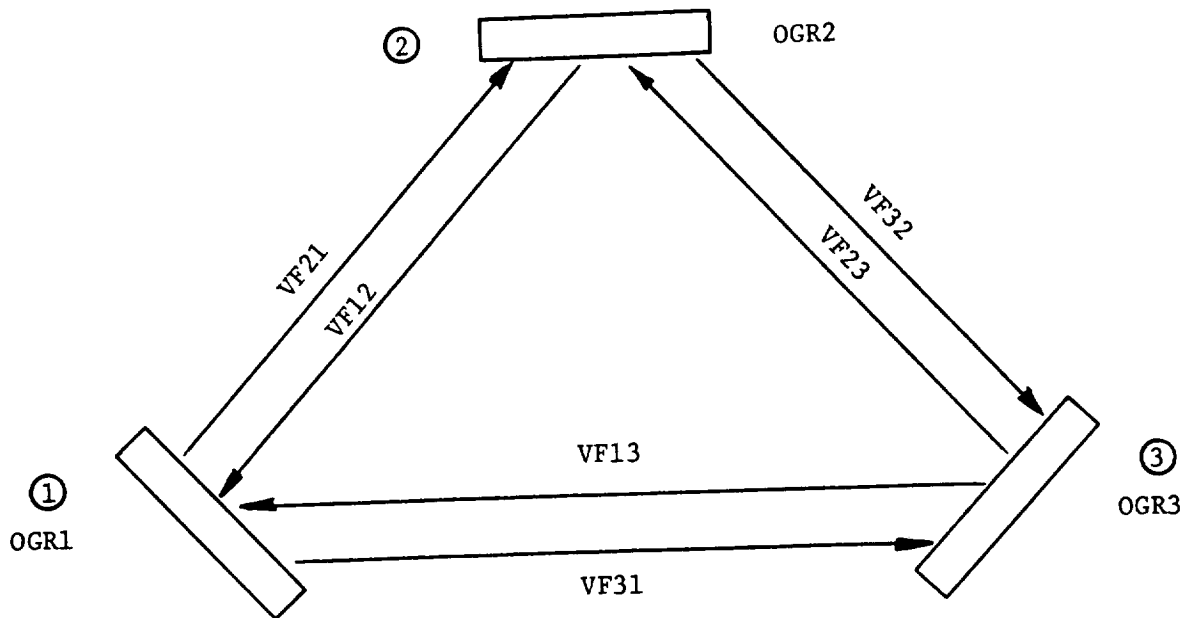
Schematically this can be shown by:
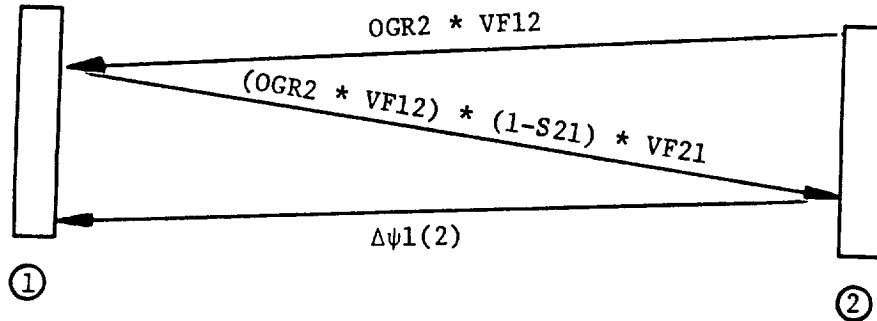
Combining (4) with (3) yields the total flux incident on ① for two reflections.

$$\psi 1(2) = \left[OGR2 + OGR1 * VF21 * (1-S12) + OGR2 * VF12 * (1-S21) * VF21 * (1-S12) \right] * VF12 \tag{5}$$

where again the term in the brackets is a new effective mass loss rate for ② comprising the original rate (n=0) plus two components (n=1,2).

A three node geometry is shown in the next figure.

Assume that all nodes are sources and node ① is the receiver. The effective mass loss rate terms for ② and ③ can be developed on a component basis as a function of the number of reflections by identifying all possible paths for mass transport to ①. The mass loss rate components for surface ② ($\Delta MLR2(n)$) are summarized below:

$$n = 0 \quad \Delta MLR2(0) = OGR2 \tag{6}$$

$$n = 1 \quad \Delta MLR2(1) = OGR1 * VF21(1-S12) + OGR3 * VF23(1-S32) \tag{7}$$

$$n = 2 \quad \Delta MLR2(2) = OGR2 * VF12(1-S21) * VF21(1-S12) + OGR3 *$$
$$VF13(1-S31) * VF21(1-S12) + OGR1 * VF31(1-S13) *$$
$$VF23(1-S32) + OGR2 * VF32(1-S23) * VF23(1-S32) \tag{8}$$

Then:

$$MLR2 = \Delta MLR2(0) + \Delta MLR2(1) + \Delta MLR2(2) \tag{9}$$

The process can be illustrated graphically for node ② as shown in Figure 1. The n = 0 component is the OGR2. The n = 1 components are computed from links ①—② and ③—②. The n = 2 components are developed from links: ②—①—② ; ③—①—② ; ①—③—② ; and ②—③—② . The computational sequence is cumulative in n (i. e. if 1 reflection is desired the n = 1 link is computed; if 2 reflections are desired the n = 1 and n = 2 links are computed and summed). Equation (4) is illustrated by the link ②—①—② .

The same computational sequence is followed for all nodes which have a non-zero viewfactor to node ① . The total effective mass loss rates are then used in the direct flux and column density routines in place of the original surface OGR. The advantage of this approach over GBCAL is that all species can be analyzed for both surface/point sources and the column density routines remain functional.
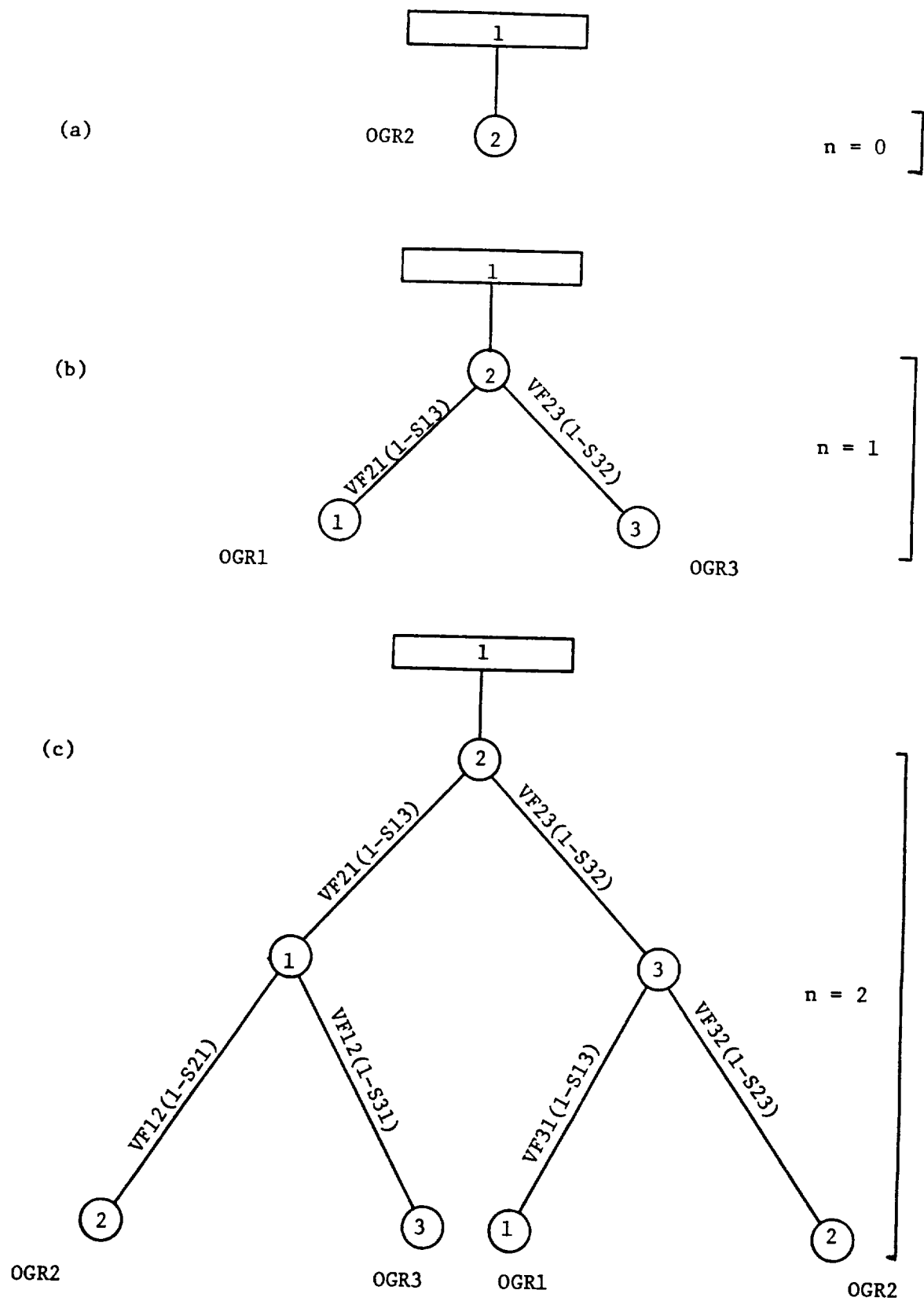
Figure 1 Three Node Tree Diagram

Application: The application of this approach for evaluating multiple reflections is limited by the convergence of equations (9) which establishes the final accuracy of the surface effective mass loss rate. Typical spacecraft simulations have shown excellent convergence after 2 or 3 reflections. However, artificial geometries can be generated which illustrate divergence of (9) unless a large number of reflections are used. Consider the following geometry
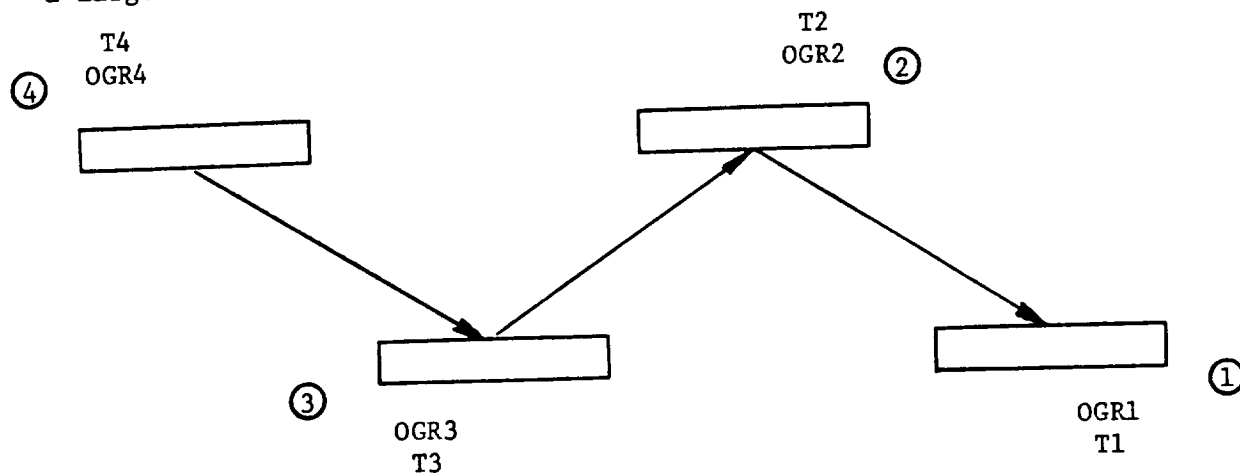
If we designate node ① as the receiver we can examine the mass loss rate of ② as a function of n reflections. The applicable tree diagram is shown in Figure 2. If we assume the following parameters

$$VF12 = VF21 = VF32 = VF23 = VF34 = VF43 = 0.5$$

$$VF13 = VF31 = VF14 = VF41 = VF24 = VF42 = 0$$

$$T4 = 200, \; T3 = 100, \; T2 = 0, \; T1 = -100$$

The cumulative contribution to the mass loss rate of ② is

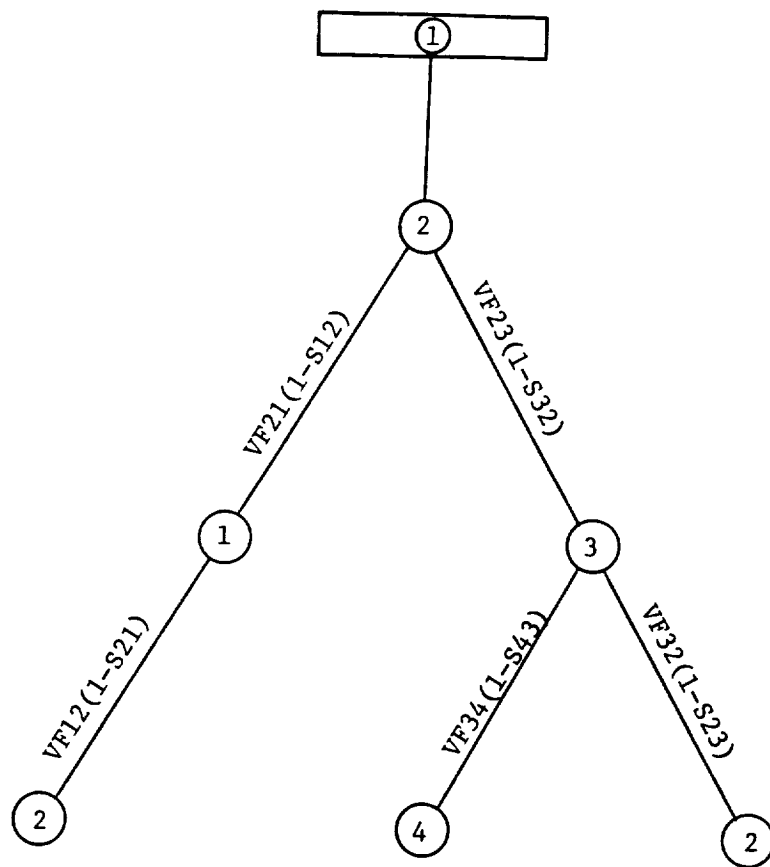| n	ΔMLR2(n)
0	OGR2
1	.25 OGR3 + .5 OGR1 + OGR2
2	1.188 OGR2 + .25 OGR3 + .5 OGR1 + .125 OGR4

Figure 2   Four Node Tree Diagram

If we assign relative outgassing rates

$$OGR1 = OGR3 = .1$$
$$OGR2 = 1$$
$$OGR4 = 10$$

Then the mass loss rate as a function of n is:

n	$MLR2(n)$
0	1.0
1	1.08
2	2.51

Obviously the high outgassing rate of node ④ has a significant impact on MLR2 and requires a minimum of two reflections to reach node ②. The principal reasons for this are the series of large viewfactors together with a high outgassing rate. Outgassing rates can easily vary by an order of magnitude. However, a series of very large viewfactors (~.5) in a realistic spacecraft simulation has never been observed and based on limited experience, seems very unlikely to occur. The impact on the example of reducing the viewfactor to .2 (still quite large) is substantial as shown below:

n	$MLR2(n)$
0	1.0
1	1.03
2	1.20

This approach has been evaluated against the closed form solution of GBCAL for an abbreviated IECM/DFI/Payload Bay geometry (38 nodes). The results of the analysis showed that excellent convergence was obtained after 3 reflections with 2 reflections providing adequate accuracy for typical mission analysis. (See attachment for detailed results.)
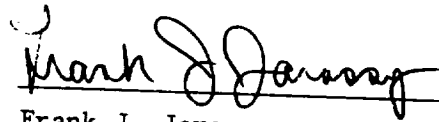
Conclusions/Recommendations - As a result of the trade study documented herein, there exists strong evidence to support the inclusion of the multiple reflection option into the SPACE code. The major advantages of this option include: a)   the multiple reflection option provides the user with the capability to evaluate any combination of ten (10) molecular contaminant species as opposed to the outgassing-only capability of GBCAL;

b)   the multiple reflection option provides the capability to evaluate surface to surface contaminant transport as well as molecular column density and return flux while GBCAL provides the limited capability of evaluating surface to surface transport only;

c)   the current GBCAL capability is limited to 38 nodes in the unblocked format (blocking will increase run times significantly) while multiple reflection can evaluate up to 300 nodes as currently designed;

d)   for the conditions/configurations evaluated to date, the multiple reflection option appears to converge rapidly to the closed form GBCAL values in 2 to 3 reflections and

e) parallel surface to surface checkout runs using GBCAL and multiple reflection with $n = 3$ indicate a computer run time savings of up to 80% with the multiple reflection option for 38 nodes. As mentioned previously, for configurations with a greater number of nodes (requiring GBCAL blocking), the savings could be even more significant.

Based upon the data presented, it is therefore recommended that the multiple reflection option be integrated into the SPACE II program for delivery to JSC and be maintained as the baseline approach to evaluating surface reflection of emitted contaminants. We feel, however, that until more experience is obtained in applying this approach to real spacecraft, the GBCAL capability (38 nodes maximum) should be retained and applied as a check by reducing complex configurations to 38 nodes of worst case sources.

Very truly yours,

Frank J. Jarossy

Attachment

A simplified IECM/DFI/Orbiter P/L Bay geometry was used to compare the accuracy of the multiple reflection approach to GBCAL as a function of the number of reflections (n). The maximum number of nodes which GBCAL can accomodate without blocking is 38. Table I summarizes the deposition rates as a function of n for the multiple reflection option. Nodes >1000 represent IECM critical surfaces. Nodes 11 and 13 are the bulkheads which were included in order to evaluate large node effects. IECM critical surfaces were assigned temperatures of -200°C resulting in sticking coefficients of 1.0. Other IECM/DFI surfaces were assigned a temperature of $+100^\circ$C. P/L bay nodes were assigned a variety of temperatures corresponding to the Orbiter T_{max} case.

The accuracy of multiple reflections is compared to the closed form solution (GBCAL) in Table II. The accuracy of the approximation increases rapidly with n resulting in excellent correlation for n = 3 with acceptable correlation for n = 2 (>85%). A plot of these results is shown in the figure which indicates that increasing n past three provides a slow increase in accuracy.

TABLE I   DEPOSITION RATE (g/cm^{2}sec)

Node	GBCAL	n = 0	n = 1	n = 2	n = 3
11 *	.644E-11			.566E-11	
13 *	.906E-11			.801E-11	
1040	.340E-10	.197E-10	.276E-10	.311E-10	.327E-10
1050	.272E-13	.735E-14	.187E-13	.230E-13	.252E-13
1060	.355E-13	.973E-14	1244E-13	.300E-13	.330E-13
1070	.395E-13	.109E-13	.271E-13	.334E-13	.366E-13
1080	.309E-10	.226E-10	.275E-10	.294E-10	.302E-10
1090	.229E-10	.165E-10	.200E-10	.216E-10	.223E-10
1100	.227E-10	.116E-10	.174E-10	.210E-10	.215E-10

TABLE II   NORMALIZED DEPOSITION RATE $(\dot{D}_{NFLCT}/\dot{D}_{GBCAL})$

Node	n = 0	n = 1	n = 2	n = 3
11 *			.88	
13 *			.88	
1040	.58	.81	.91	.96
1050	.27	.69	.85	.93
1060	.27	.69	.85	.93
1070	.28	.69	.85	.93
1080	.73	.89	.95	.98
1090	.72	.87	.94	.97
1100	.51	.77	.93	.95

* Deposition values for these nodes require manual calculation due to sticking coefficient considerations. A single check point (n = 2) was computed to determine if large nodes followed a trend similar to that of the small nodes.
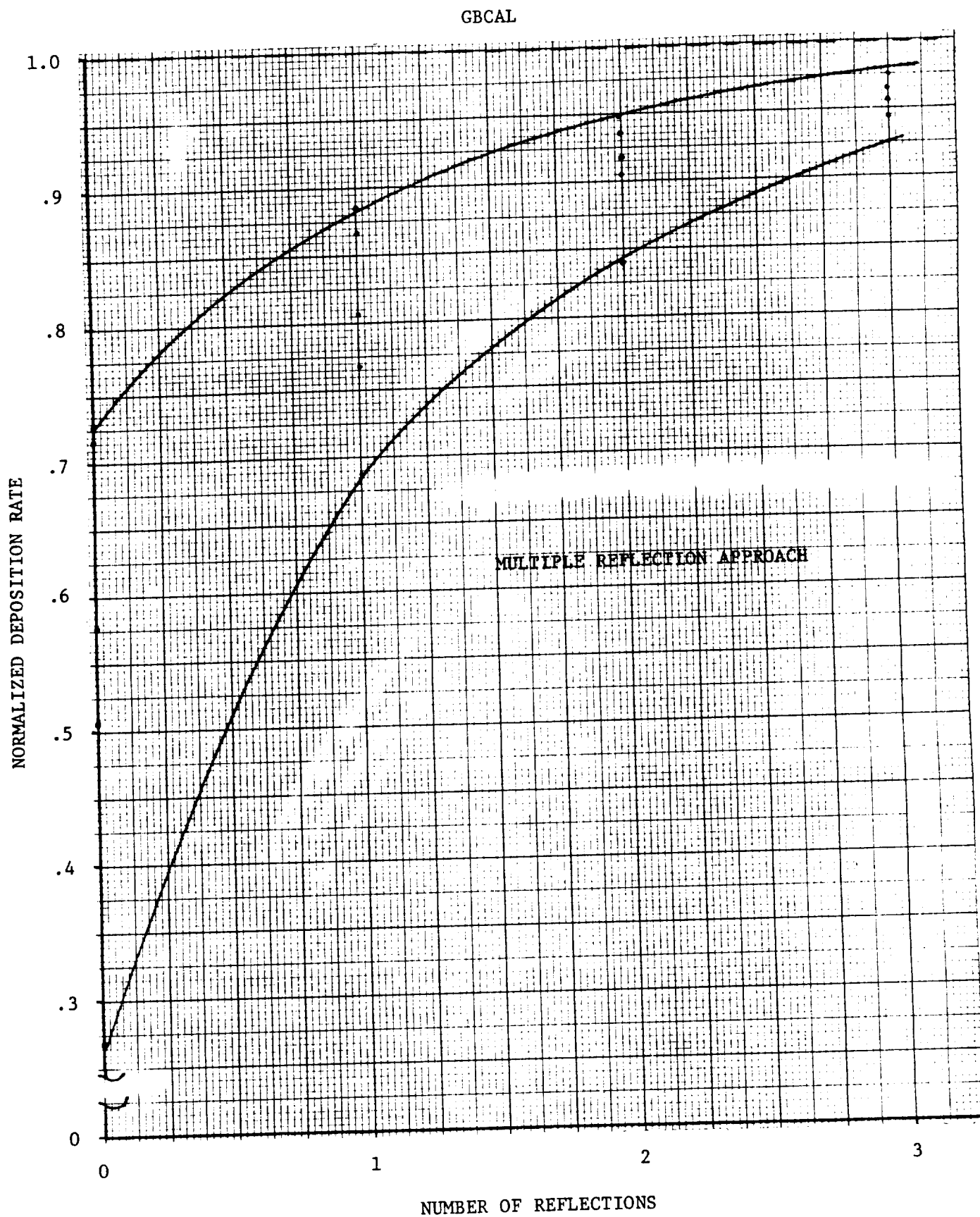
Figure 1   CONVERGENCE ENVELOPE

GBCAL/Multiple Reflection Trade Study Update

Objective

The convergence characteristics of the SPACE II direct flux with multiple reflections capability have been evaluated for the STS Orbiter/IECM/DFI payload configuration, using results from the closed form GBCAL solution technique as convergence criteria. Convergence characteristics for this payload are compared with those observed for the previously evaluated P80-1 and DSP payloads. In addition, the computer costs associated with the IECM/DFI analysis are evaluated and compared with those incurred in evaluating the P80-1 and DSP payloads.

Approach

The IECM/DFI geometrical configuration used in Figure 1 had been previously developed to model the schedules OFT-1 payload. Thermal and nonmetallic materials data were supplied by NASA-JSC. Two thermal profiles were evaluated, corresponding to maximum and minimum surface temperatures occurring during one complete orbit beginning at 24 hours after launch. As in the previous analyses conducted for the P80-1 and DSP payloads, only outgassing direct flux was evaluated. The full payload bay/IECM/DFI configuration was reduced to a 38 node subset by eliminating the forward and top TQCM, the CQCM, the mass spectrometer aperture, and a small portion of the payload bay liner.

Computer runs were made according to the same plan used previously, first obtaining baseline predictions with
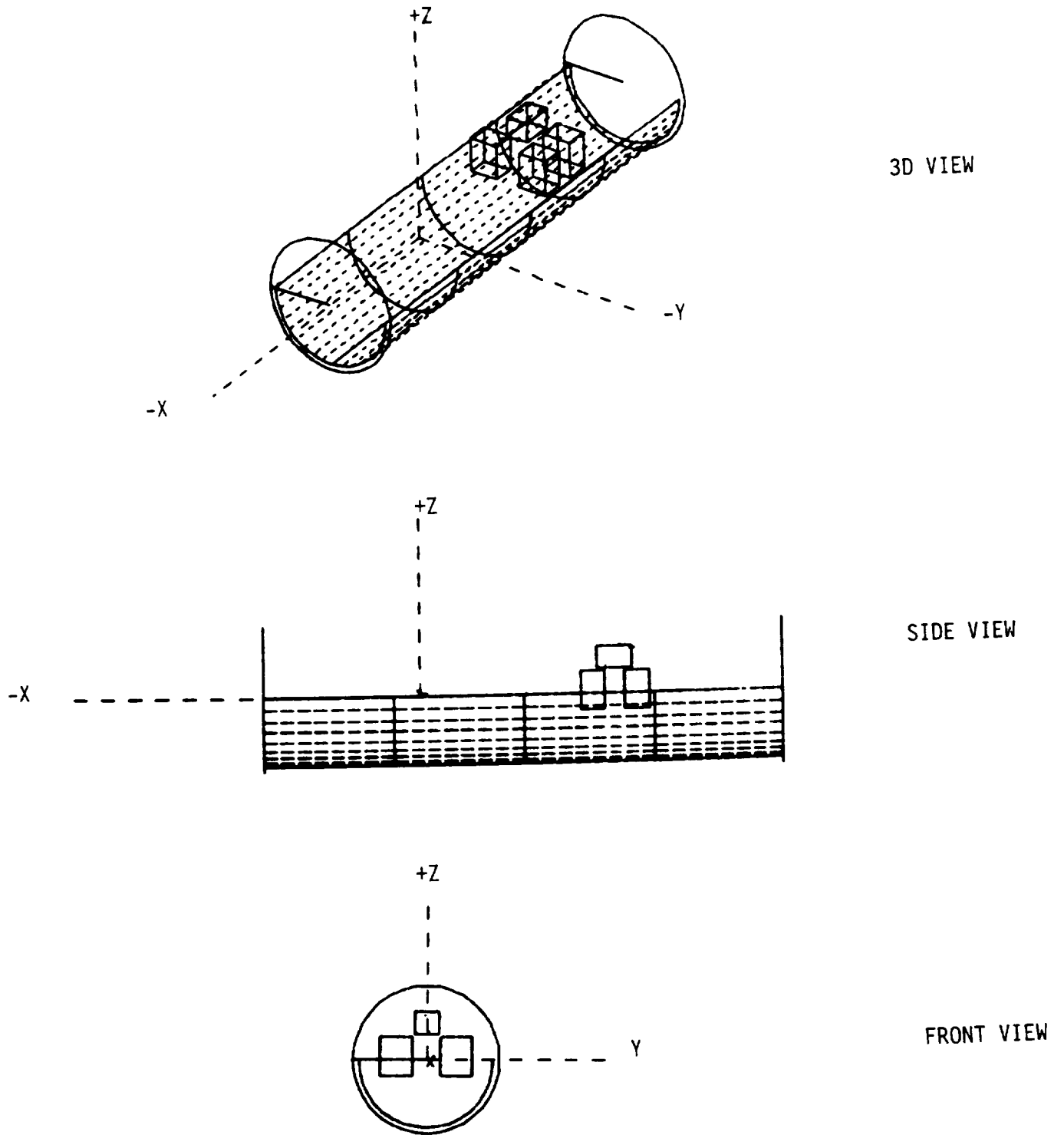
3D VIEW

SIDE VIEW

FRONT VIEW

Figure 1. IECM/DFI/Payload Bay Modeled Configuration

with GBCAL, then using the SPACE II multiple reflection logic, gradually increasing the number of reflections performed until better than 95% average convergence was achieved.

Results

Figures 2 and 3 show convergence results for the IECM/DFI hot and cold thermal profiles, respectively. Depicted are the mimimum and maximum convergence observed for specific surfaces, as well as the average convergence for all surfaces. Figure 4 presents the average results for each payload configuration/thermal profile thus far evaluated. Figure 5 shows the computer CPU time vs number of reflections relationship for each configuration.

Discussion

From Figure 4, the convergence behavior of the IECM/DFI payload is similar to that of the P80-1, although not quite as rapid. On the average, only four reflections were required to achieve better than 95% convergence.

In order to evaluate the observed convergence behavior, we must consider the three factors previously identified as most significantly influencing this behavior.

The first factor is the number of body-to-body viewfactor pairs divided by the number of nodes in the configuration, interpreted as the average number of surfaces "seen" by a given receiver. For the IECM/DFI configuration, this factor has the value 288/38 or about 7.6, compared to 9.5 for the DSP and 3.0 for the P80.

The second critical factor is the average magnitude of the body-to-body viewfactor pairs. All of the IECM/DFI viewfactors are less than 0.5, and the distribution of magnitudes more closely resembles that of the DSP than that
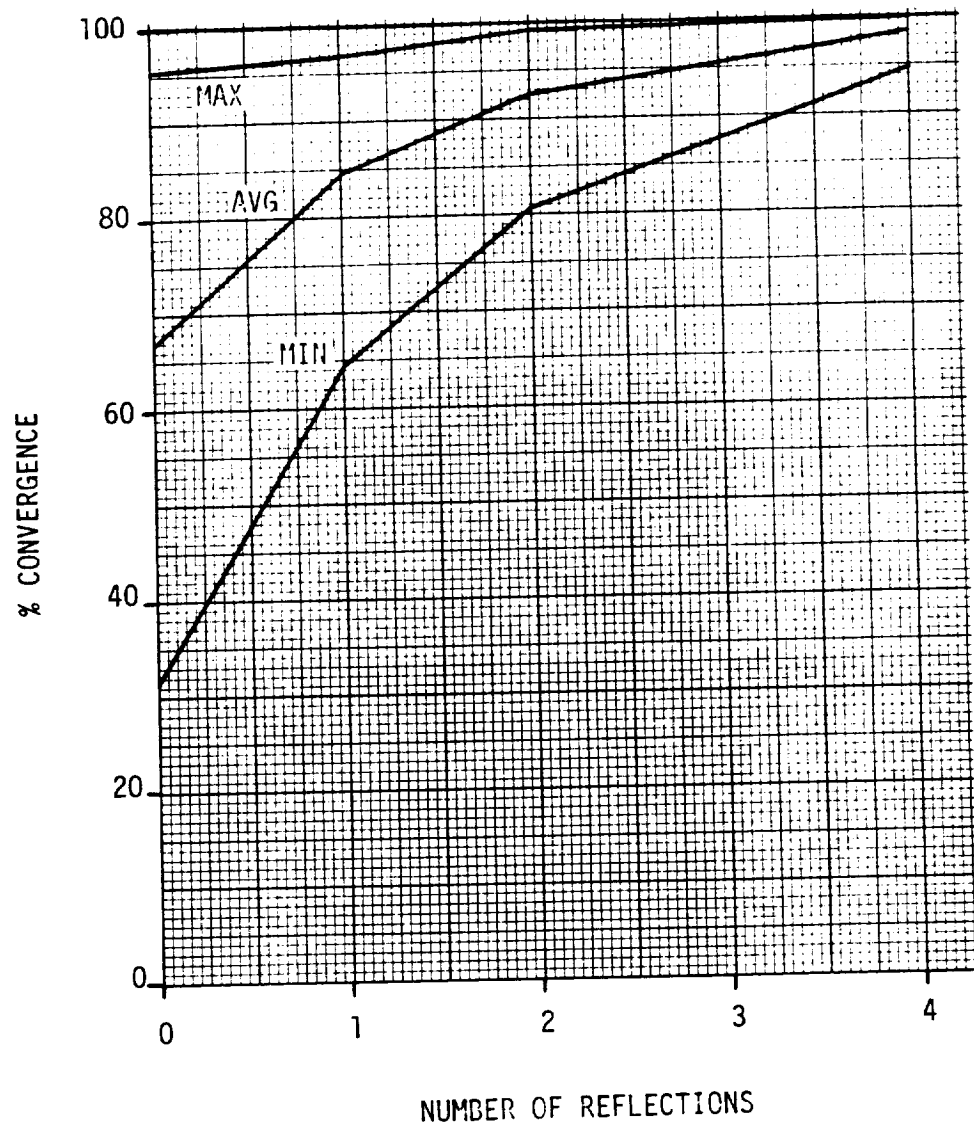
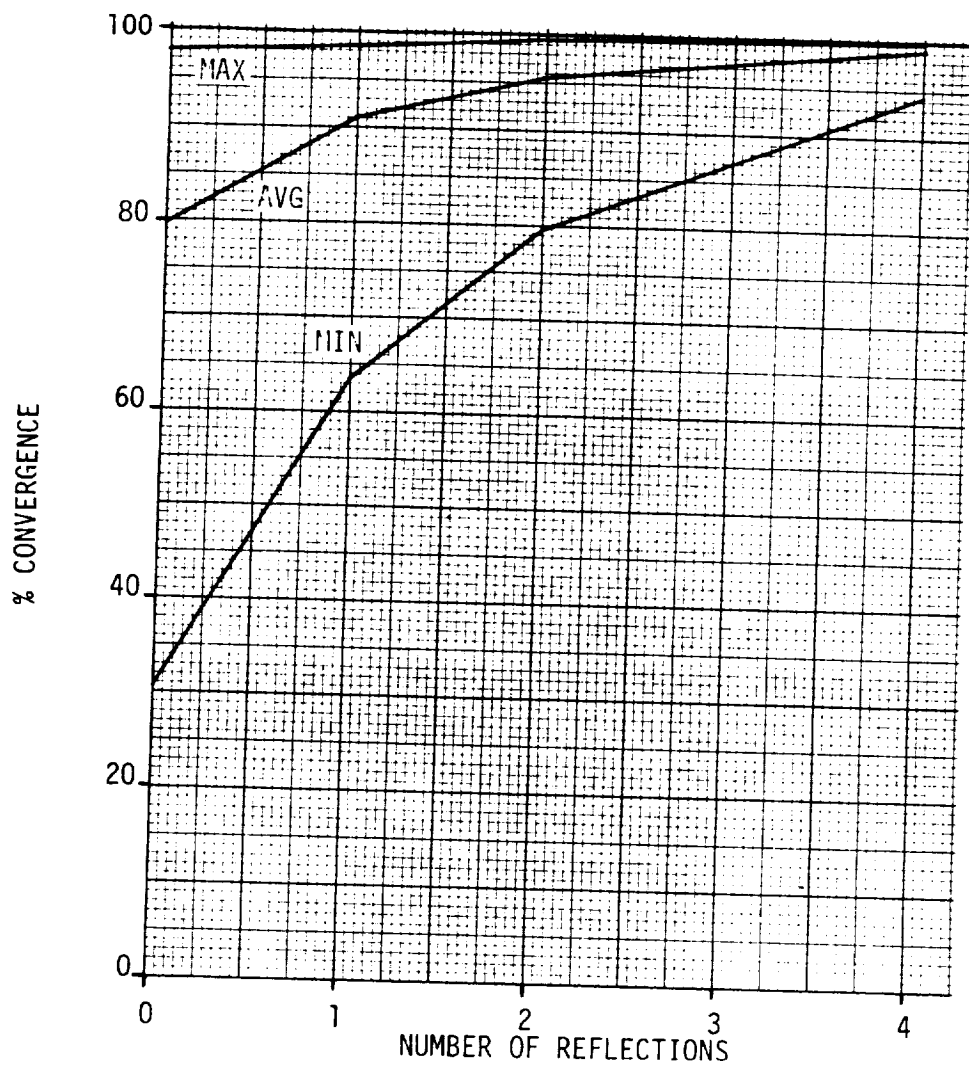Figure 2. Convergence Results: IECM/DFI, Hot Profile

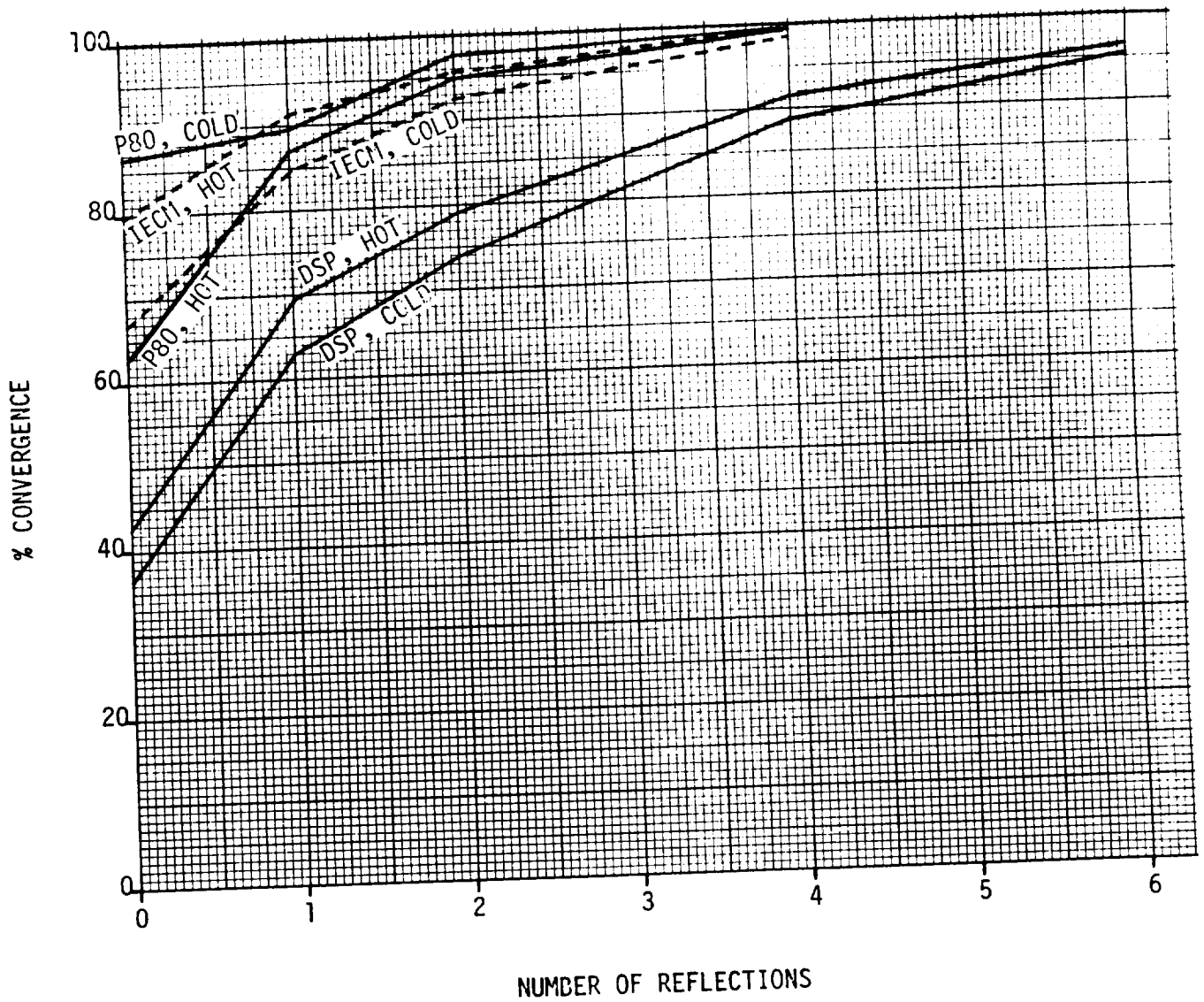Figure 3. Convergence Results: IECM/DFI, Cold Profile
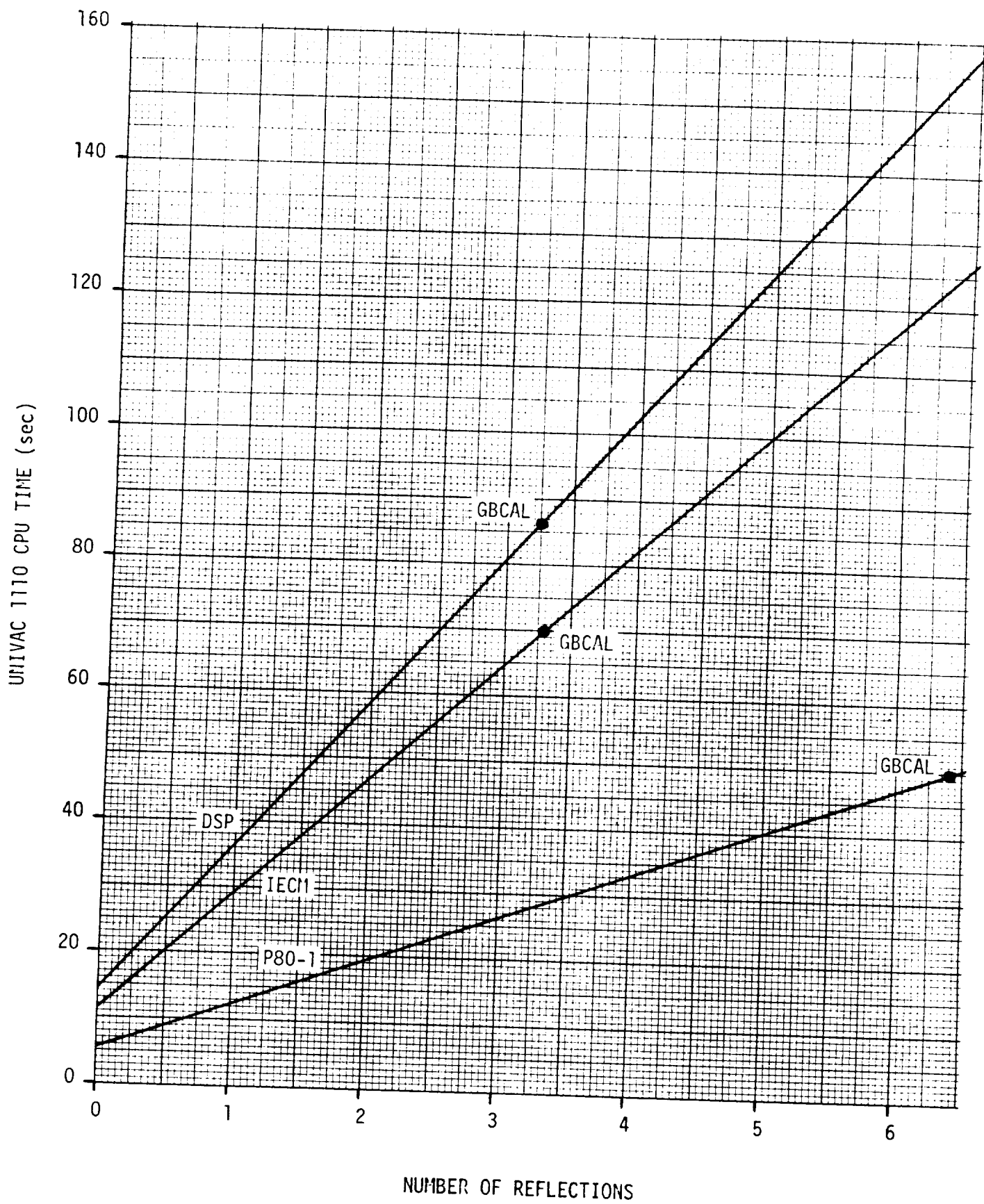
Figure 4. Average Results For All Configurations

Figure 5. CPU Time vs. Number of Reflections

A-20

of the P80.

The final consideration is the average temperature difference between node pairs. While the IECM/DFI configuration does not exhibit the extreme temperature differences observed for the P80, average temperature differences are much greater than those occurring in the DSP configuration.

Consideration of the first two factors would indicate that the IECM/DFI convergence should be relatively slow, more like the DSP than the P80. Since, however, the opposite is the case, it is apparent that the third consideration outweighs the first two. It appears, then, that the thermal profile of a payload configuration is the best indicator of the convergence characteristics to be expected.

In evaluating the cost of performing multiple reflection analyses, figure 5 lends support to the conclusion that the number of viewfactor pairs (size of tape 12) is the driving parameter and best indicator of the expected cost.

Conclusions

All of the conclusions drawn from the IECM/DFI evaluation agree with those developed from the DSP and P80 investigations (number of reflections considered adequate, parameters influencing convergence and applicability of GBCAL as an analytical tool), with the additional result that the payload thermal profile is the most significant parameter influencing convergence.

# GBCAL/MULTIPLE REFLECTION TRADE STUDY RESULTS

OBJECTIVE

The purpose of this analysis was to evaluate the convergence characteristics of the SPACE II direct flux with multiple reflections capability for a range of typical STS Orbiter/payload configurations, identifying those factors which either aid or hinder convergence with predictions obtained with the closed form GBCAL solution technique. In addition, the computer cost associated with multiple reflection analyses was compared with that incurred using the GBCAL software.

APPROACH

Two payload configurations were selected for analysis: 1) the Defense Support Program (DSP) satellite, and 2) the P80-1 satellite. The DSP is a relatively large, essentially cylindrical payload, occupying a significant portion of the payload bay volume, and, for a nominal mission, experiences a relatively benign thermal environment. The P80, on the other hand, is a relatively small payload situated in close proximity to the aft bulkhead, and encompasses a wide range of temperatures, including several cryogenic surfaces. Because of the geometrical and thermal extremes represented by these two satellites, it was felt that their selection would serve to bracket the resulting convergence characteristics, facilitating the development of universally applicable convergence criteria by which the convergence characteristics of an arbitrary payload could be predicted.

For each payload, two thermal profiles (hot/cold) were evaluated for their impact on convergence. Input data (geometry, materials, and thermal profiles) for each configuration were obtained from previous contamination analyses performed for these payloads.

Due to inherent limitations of the GBCAL closed form solution technique (see Discussion), only outgassing direct flux could be evaluated and each configuration had to be limited to a maximum of 38 nodes. A review of previously developed thermal profiles and body-to-body viewfactors for the two payloads was conducted to determine which 38 node subset of each configuration should be retained for analysis. Figure 1 depicts the complete DSP/payload bay configuration and Figure 2 presents the 38 node subset retained. Similarly, Figure 3 shows the complete P80/payload bay configuration, while Figure 4 shows the 38 node subset selected.

+Z

−X

−Y
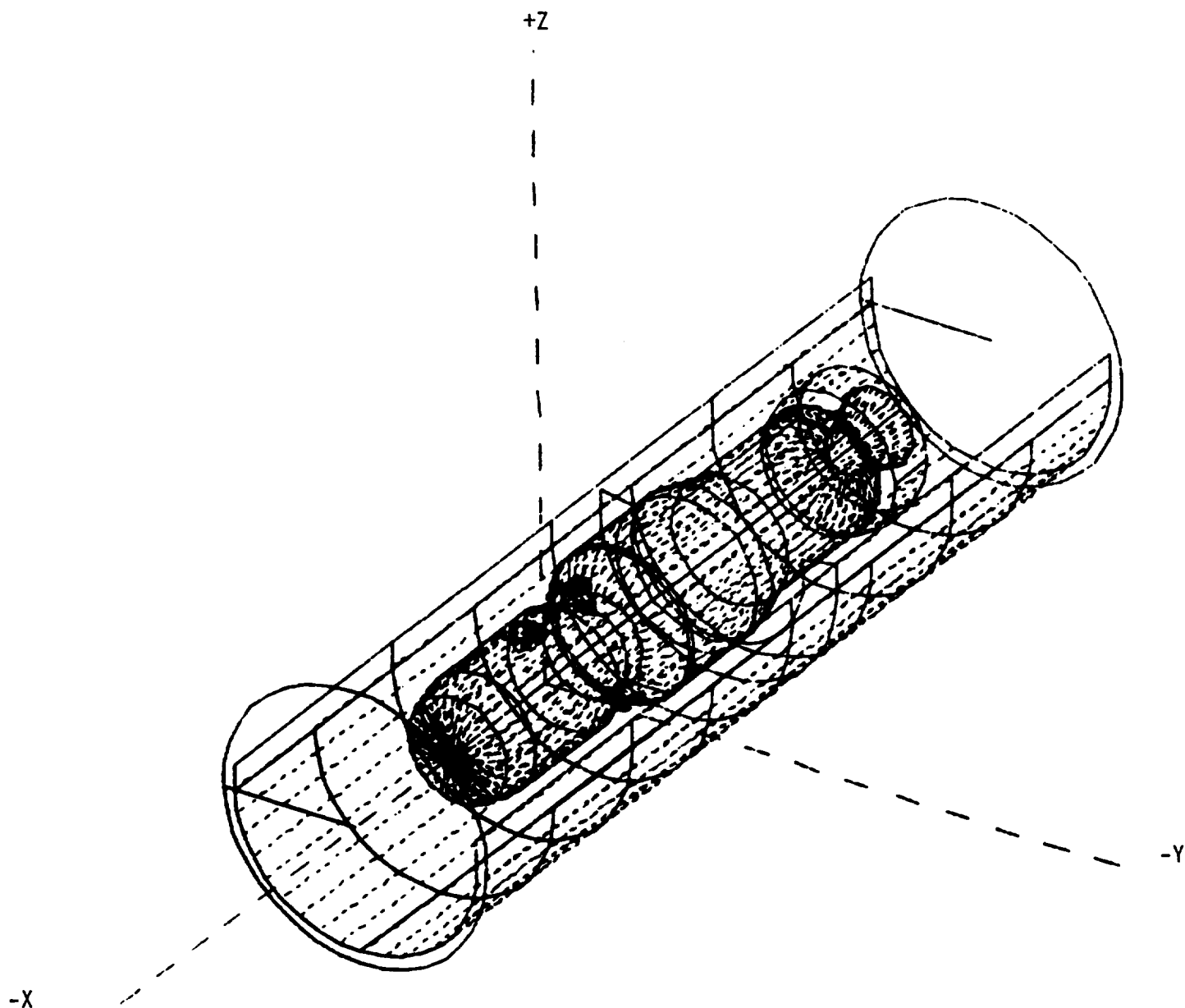
3-D VIEW
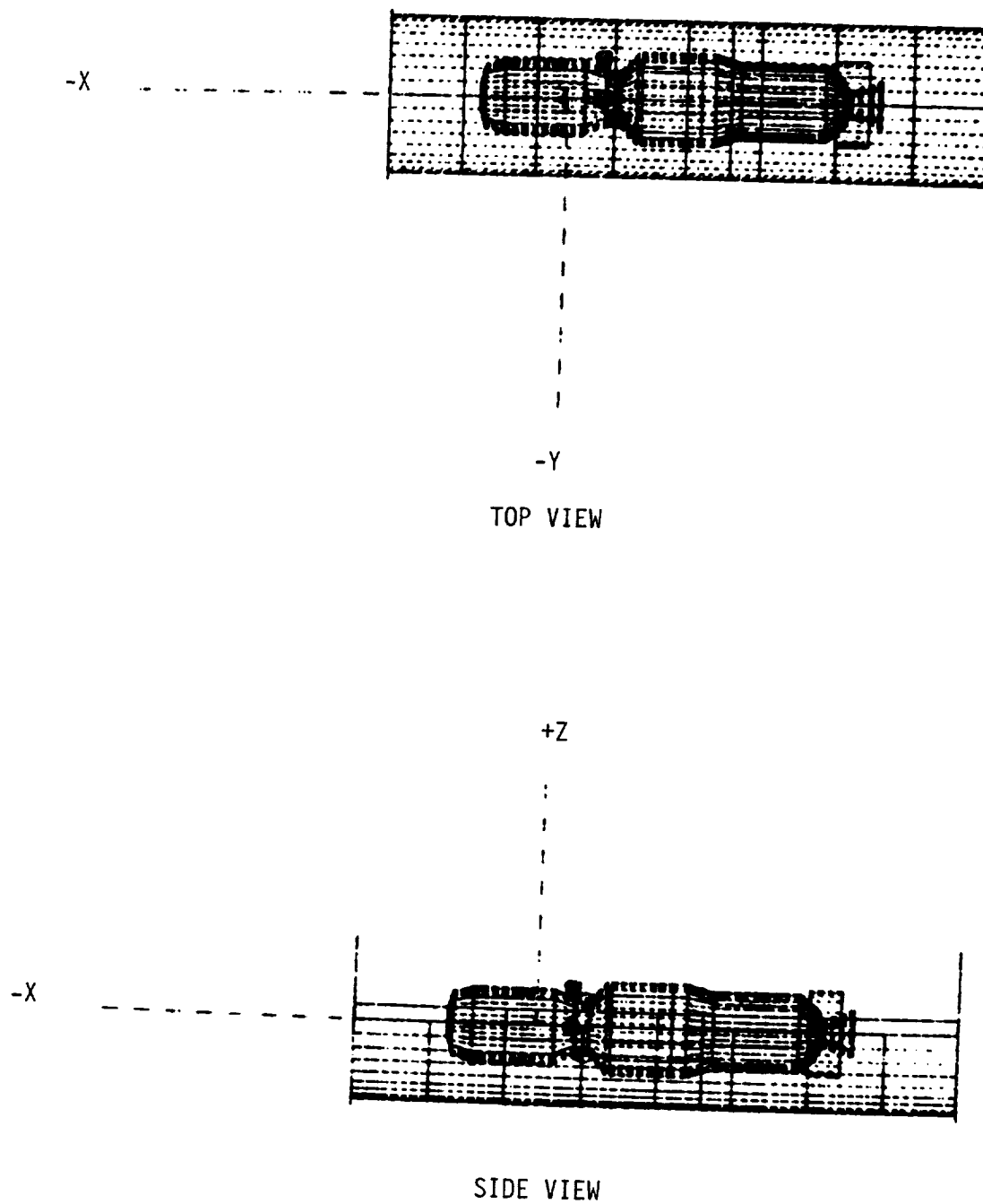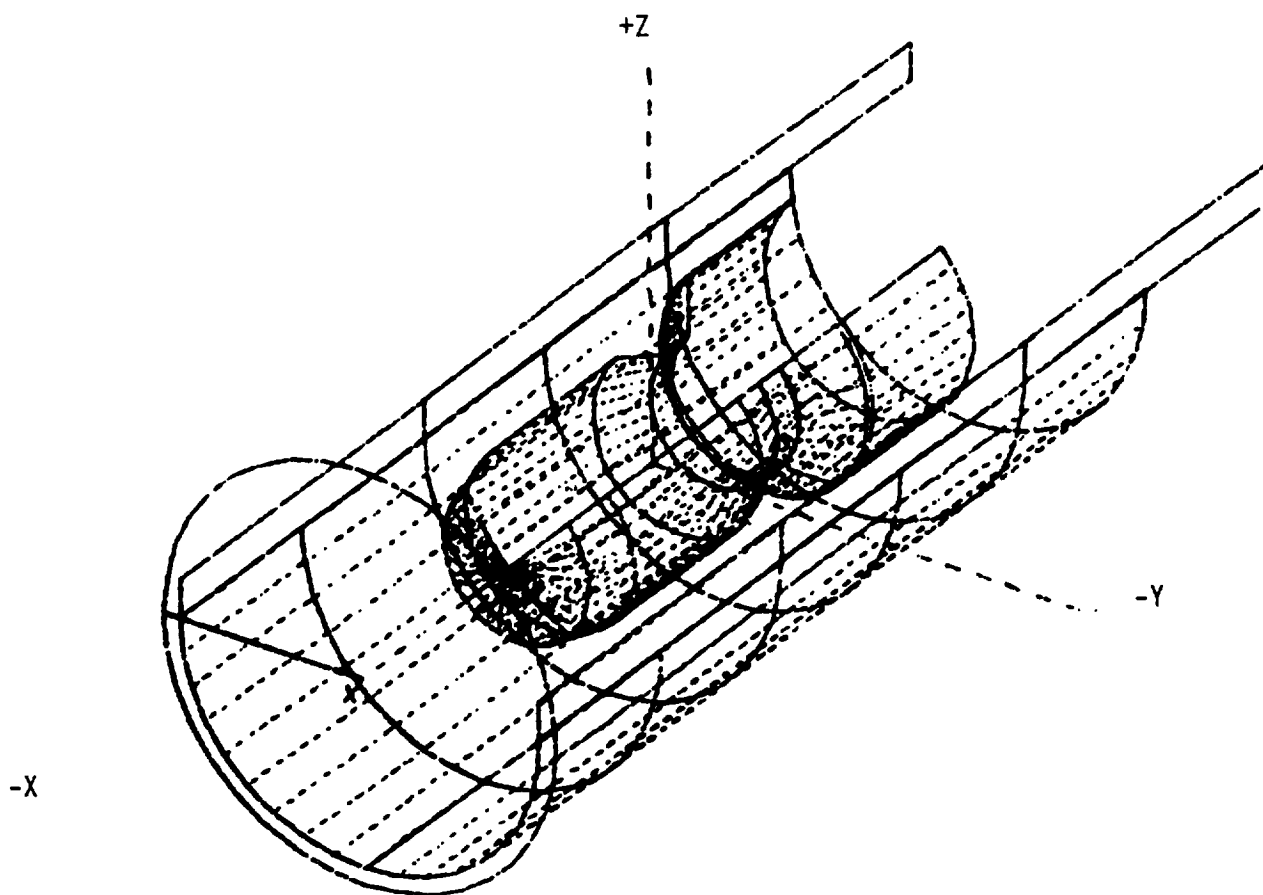
Figure 1. Unmodified DSP Configuration

-X — · — · — · — · — · — · — · —

|
|
|
|
|
|
-Y

TOP VIEW

+Z
:
|
|
|
|

-X — — — — — — — — —

SIDE VIEW

Figure 1.   Unmodified DSP Configuration (cont'd)

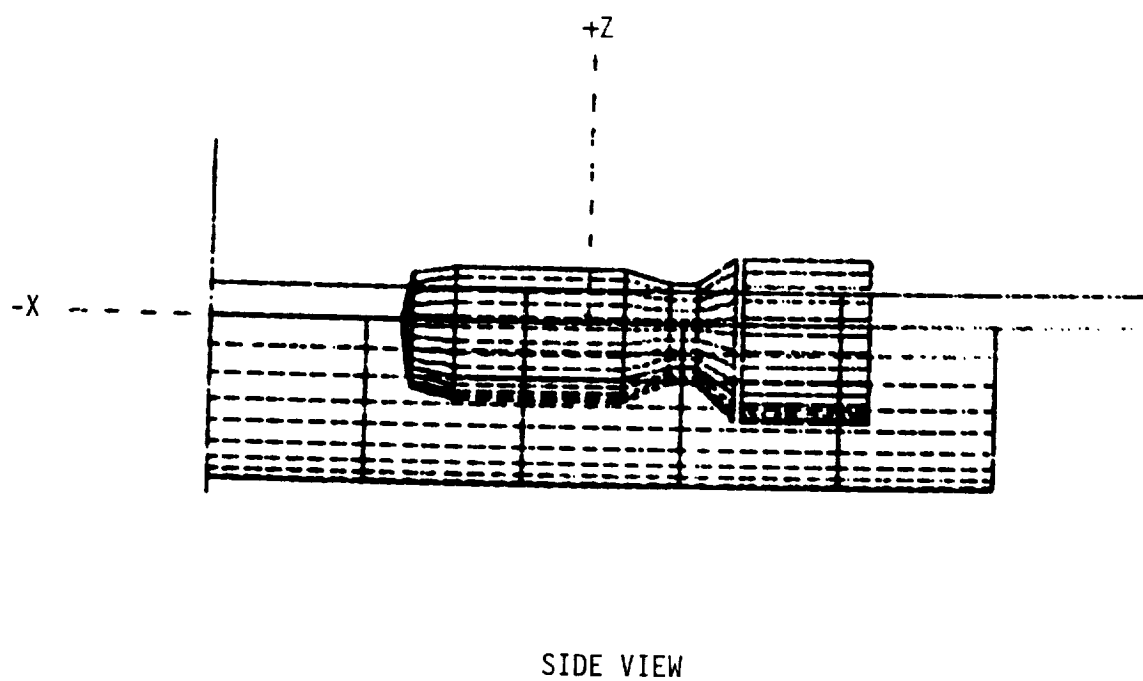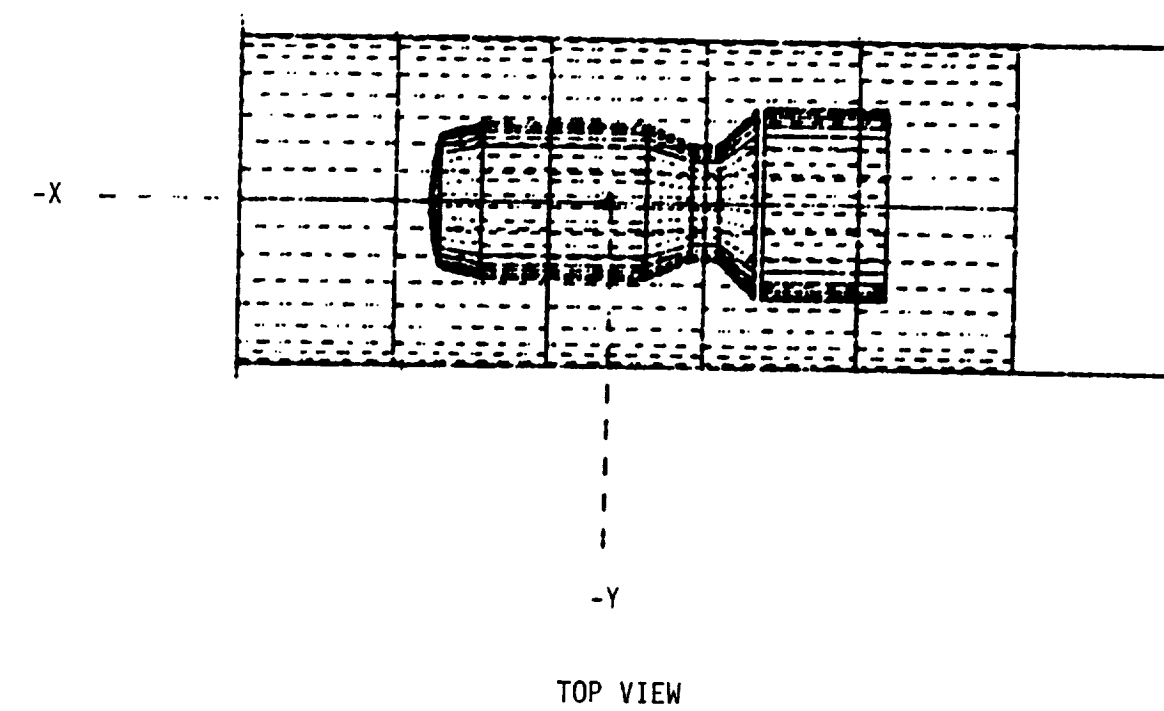3-D VIEW

Figure 2. DSP 38 Node Subset
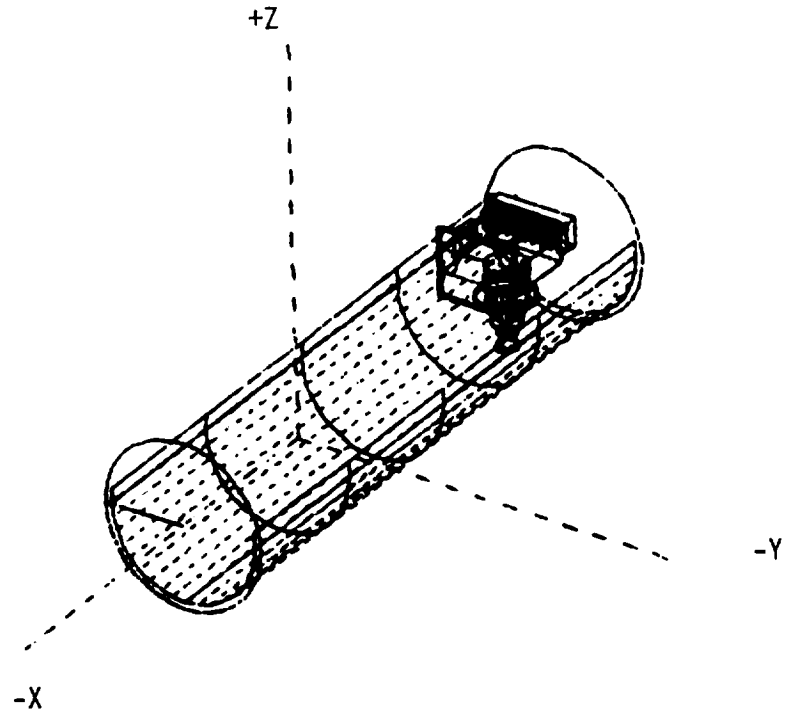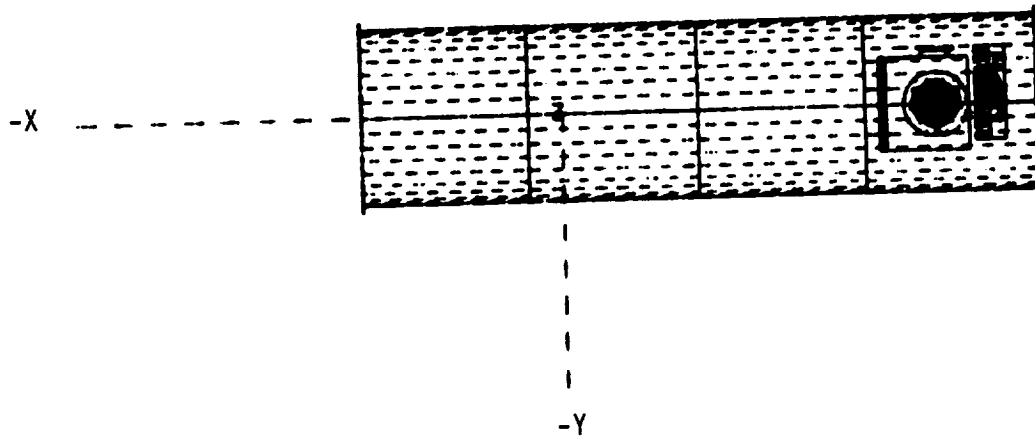
-X

-Y

TOP VIEW

+Z

-X

SIDE VIEW

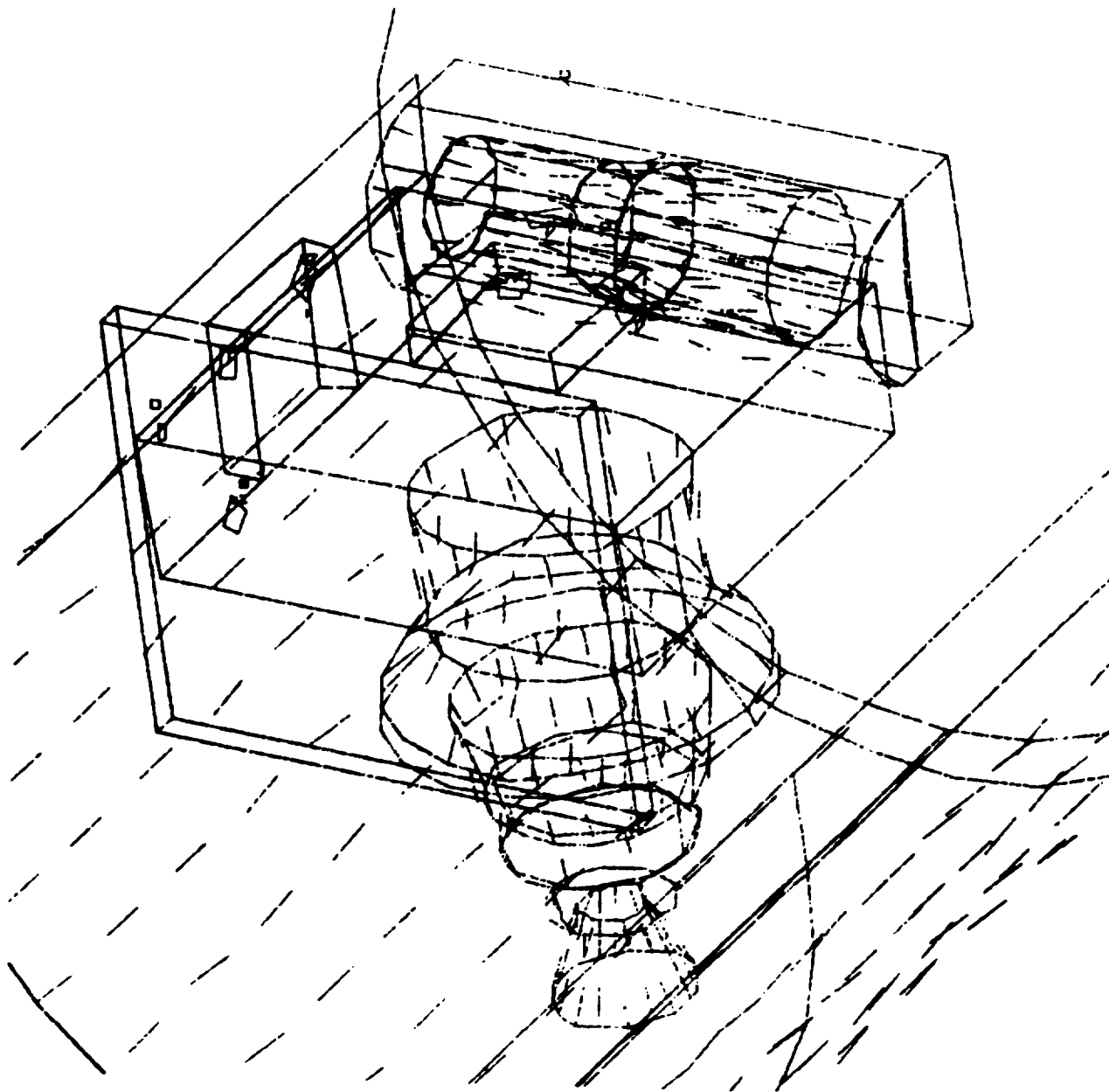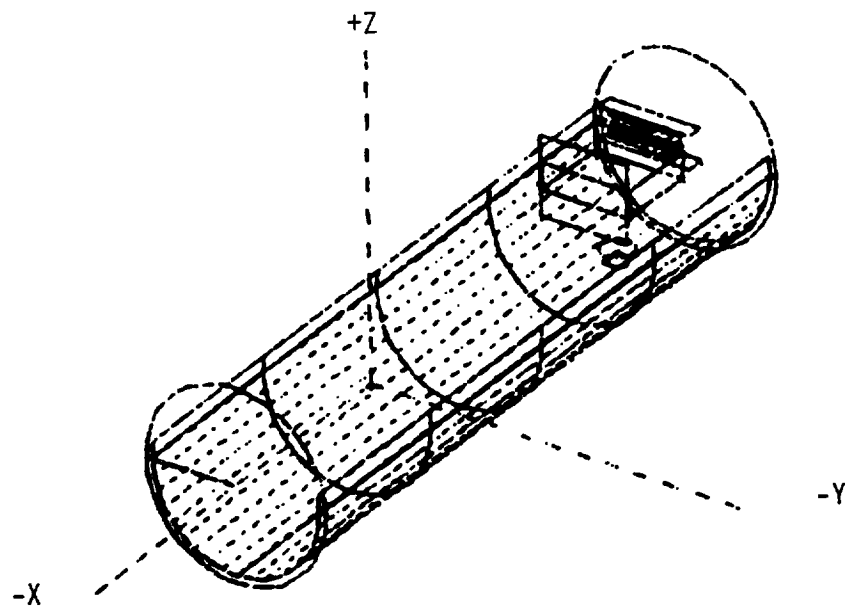*Figure 2.   DSP 38 Node Subset (cont'd)*

3-D VIEW

TOP VIEW

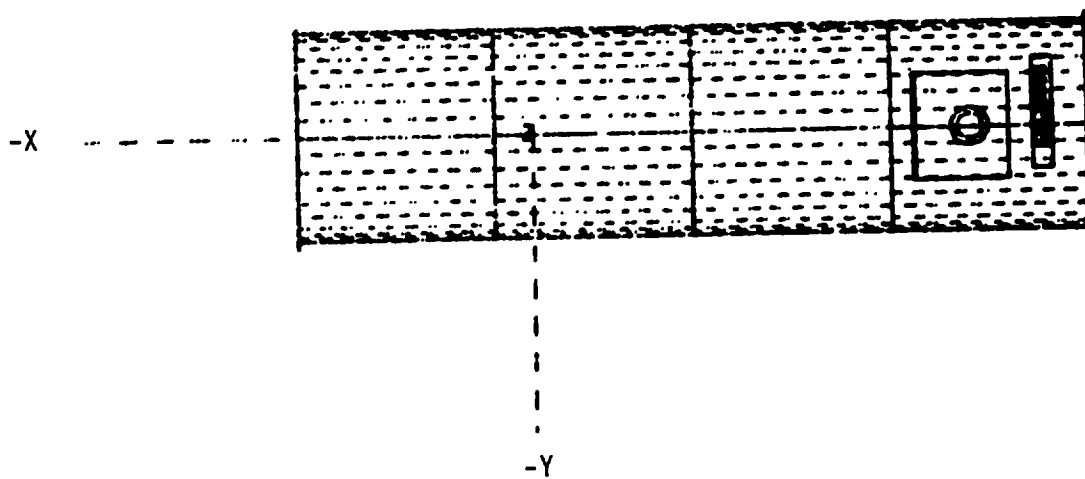Figure 3. Unmodified P80-1 Configuration

A-27

3-D BLOWUP

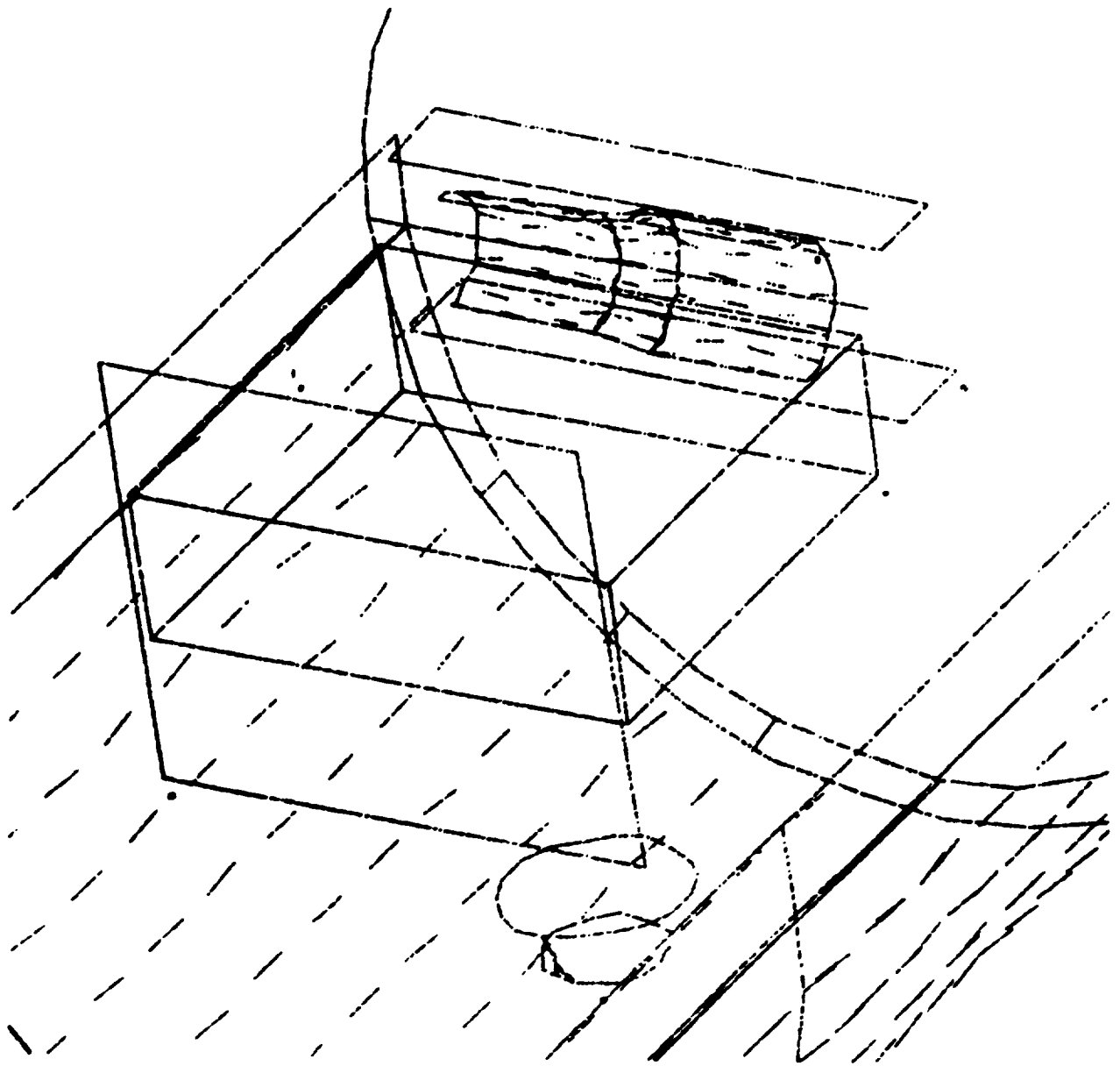Figure 3.   Unmodified P80-1 Configuration (cont'd)

3-D VIEW

TOP VIEW

Figure 4.   P80-1 38 Node Subset

3-D BLOWUP

Figure 4.   P80-1 38 Node Subset (cont'd)

For each configuration/thermal profile, the GBCAL computer code was run to obtain baseline deposition predictions for all payload surfaces. Runs were then made using the SPACE II multiple reflection capability, gradually increasing the number of reflect- ions performed until better than 95% average convergence was achieved. All runs were made on the UNIVAC 1110 computer at Electron Information Systems (EIS) so that direct cost comparisons could be made.

Finally, results were analyzed in order to identify those payload characteristics which tended to increase or decrease the rate of convergence.

In addition to the two payloads evaluated, preparations are being made to evaluate the convergence characteristics of the NASA IECM/DFI configuration for OFT-1.

RESULTS

Figures 5 through 8 show convergence results for the four configurations evaluated (DSP-hot, DSP-cold, P80-hot, and P80-cold). Depicted in these figures are the minimum and maximum convergence observed for specific surfaces, as well as the average convergence for all payload surfaces. Figure 9 presents the average results for each configuration. Figure 10 shows the computer CPU time required as a function of the number of reflections performed, as well as the CPU time required to run GBCAL. No significant difference in CPU time was observed for evaluating either thermal profile for a given payload.

DISCUSSION

The results presented in Figures 5 through 8 indicate a significant difference in the rates of convergence for the DSP and P80 configurations. For each configuration, the cold thermal profile resulted in slightly faster convergence than the warm thermal profile. In general, only two reflections were required to achieve 95% or better convergence for the P80 configura- tion, while six reflections were required to achieve the same level of convergence for the DSP configuration. Since each configuration consists of the same number of nodes, the different rates of convergence observed must therefore be a function of the thermal and geometrical relationships among the surfaces in each configuration.
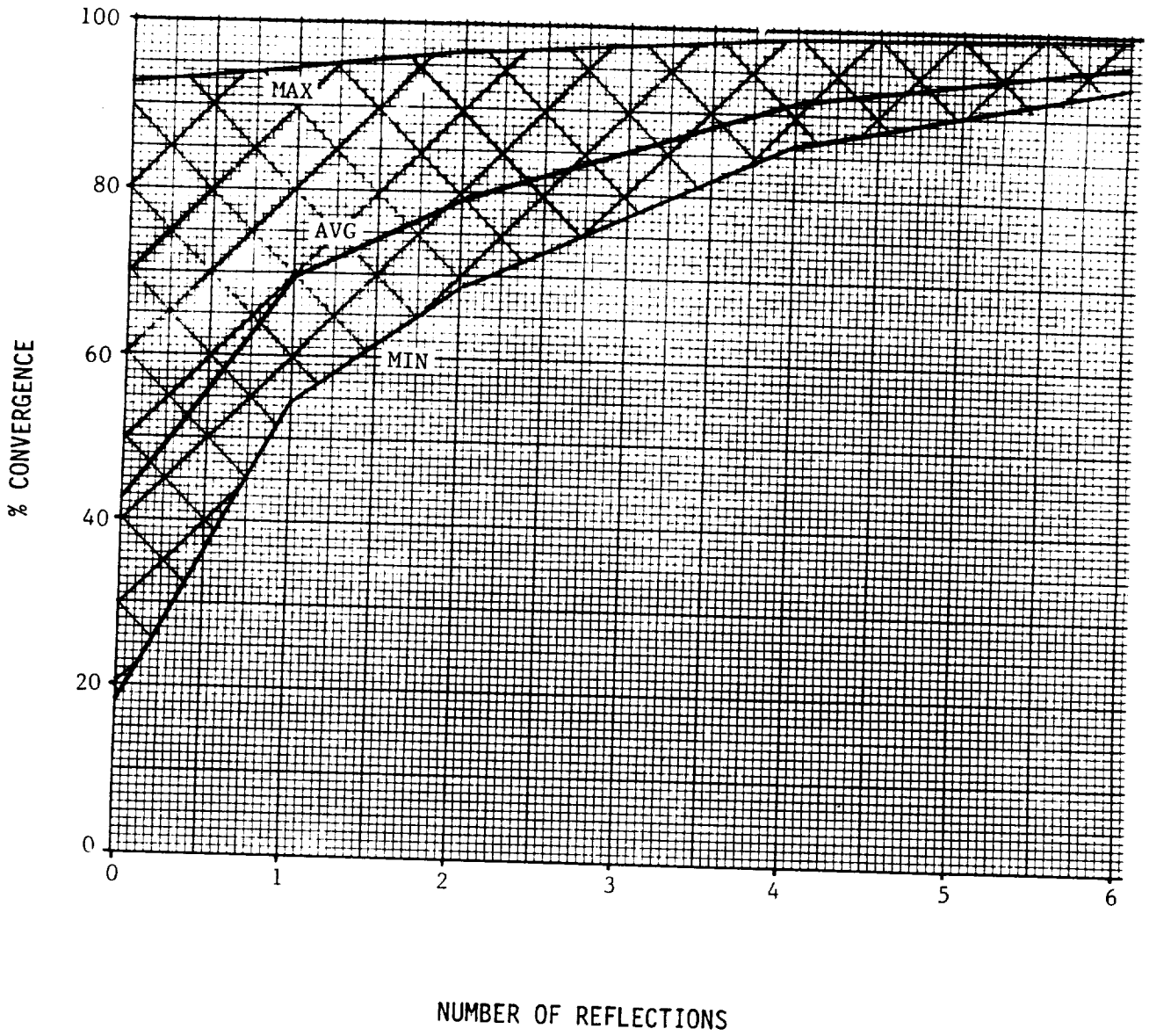
A-31

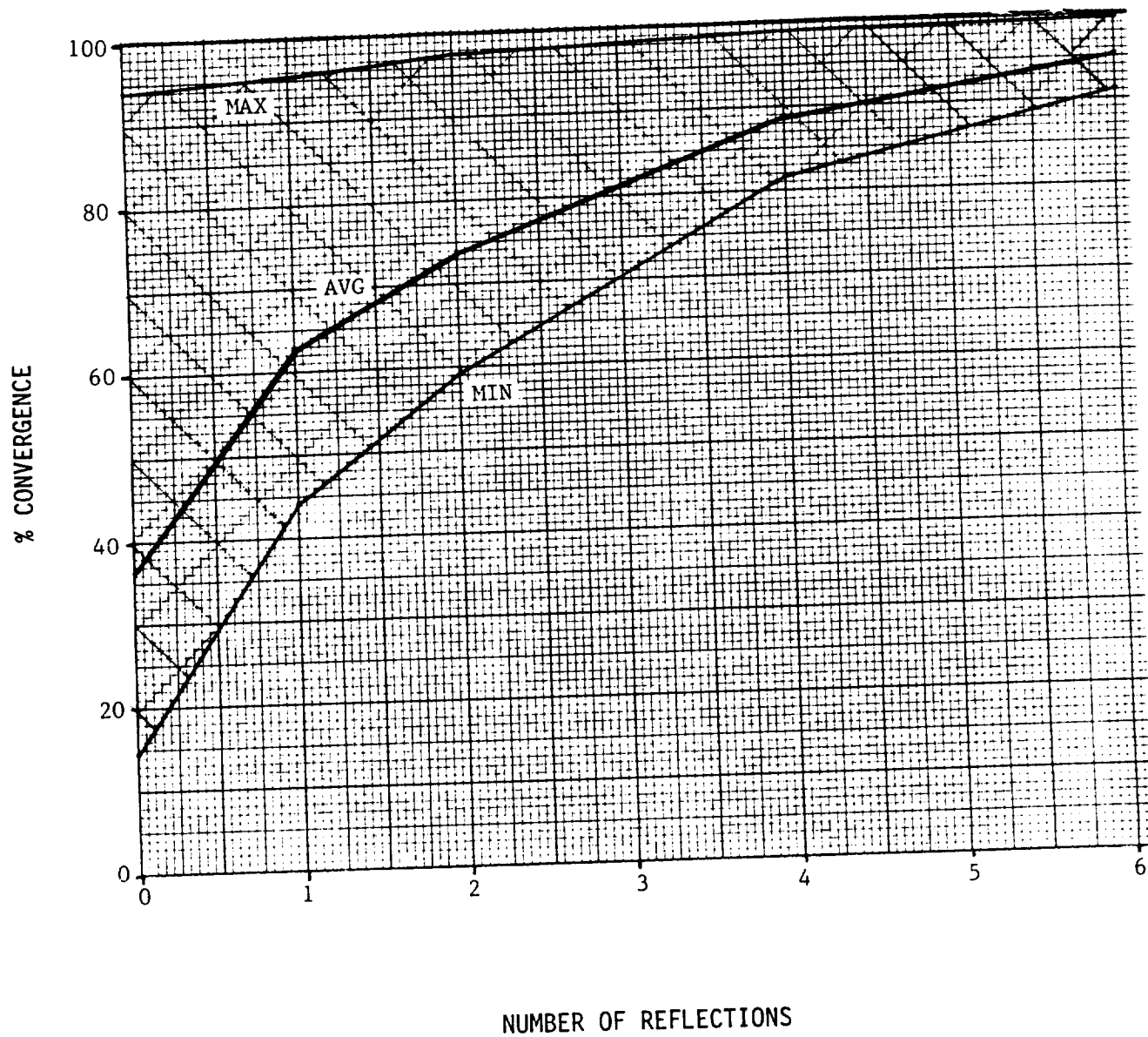*Figure 5.   Convergence Results: DSP, Hot Profile*
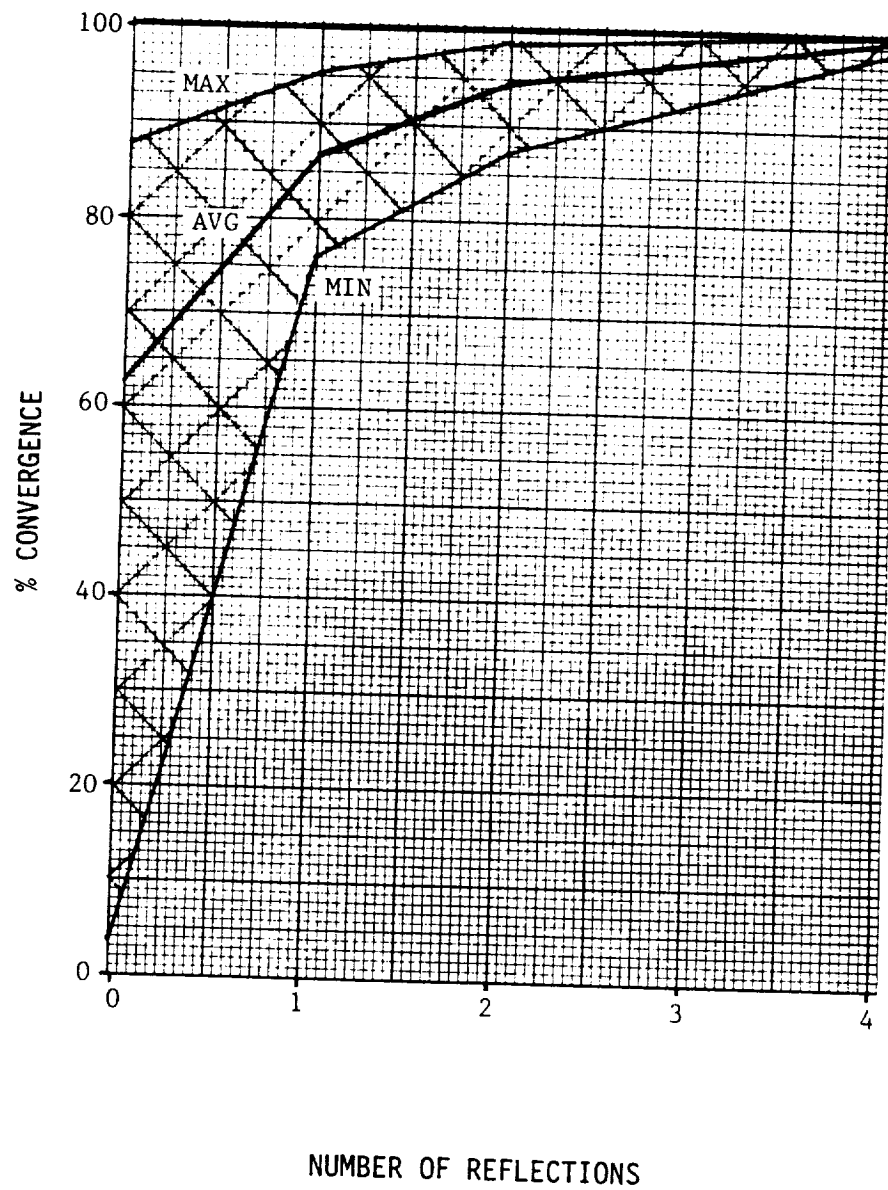
Figure 6. Convergence Results: DSP, Cold Profile

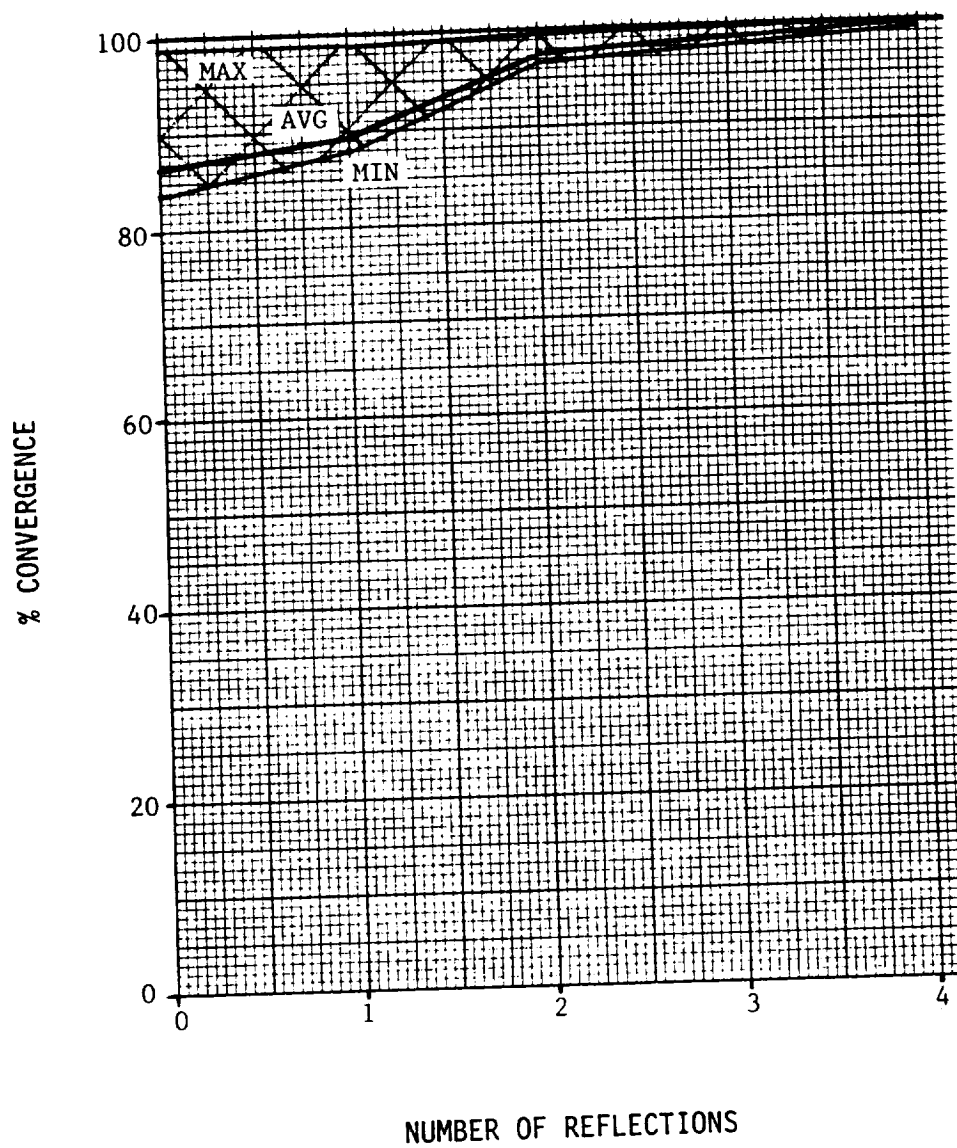Figure 7. Convergence Results: P80, Hot Profile

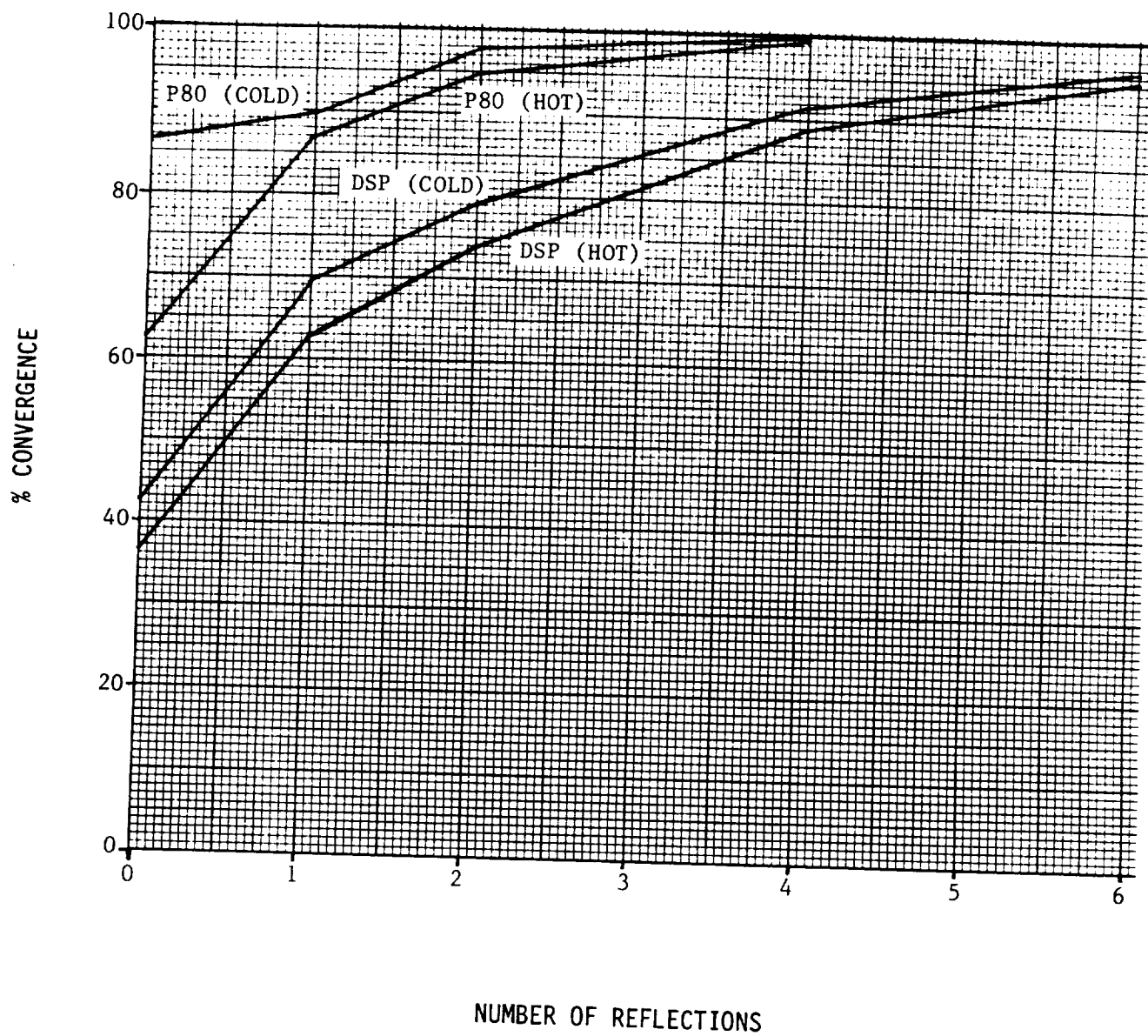Figure 8. Convergence Results: P80, Cold Profile

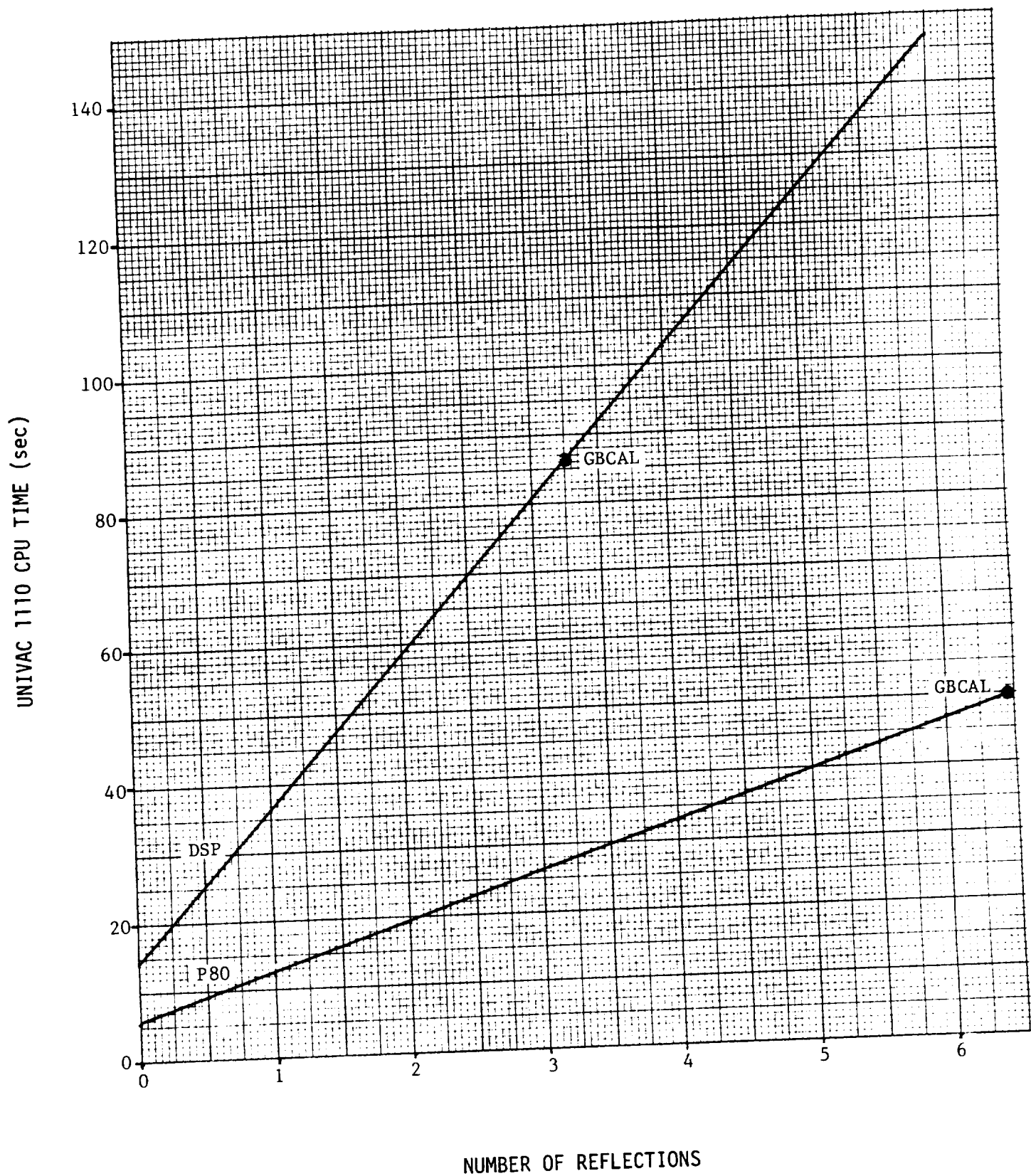Figure 9. Average Results For Each Configuration

Figure 10.   CPU Time vs. Number of Reflections

Analysis of the results has identified three factors which are most significant in influencing the rate of convergence.

First, the greater the number of surfaces that "see" a particular critical surface, the slower the convergence will be. Since more surfaces are contributing to direct flux, more reflections are required to adequately account for all possible paths by which mass can arrive at the critical surface.

For an arbitrary payload, an appropriate measure of this factor can be obtained by dividing the number of viewfactor pairs (i.e., size of tape 12) by the number of nodes in the configuration. Thus, for the DSP configuration, each node "sees" (on the average) 360/38 or 9.5 other surfaces. For the P80 configuration, each node sees 112/38 or about 3 other surfaces. From this, we would expect that the P80 configuration would converge more rapidly than the DSP configuration.

The second critical factor is the average magnitude of the viewfactors between surfaces. If the viewfactor between a source and a receiver is relatively large, a greater proportion of the emitted mass will impinge on the receiver, resulting in fewer reflections being required to attain a given level of convergence. In the DSP configuration, only a few node pairs have viewfactors as large as 0.5, while a significant number of P80 node pairs have viewfactors in the 0.5 to 0.8 range.

Finally, the higher the average temperature difference between node pairs is, the higher the rate of convergence will be. This occurs because large temperature differences result in relatively large sticking coefficients, thus requiring fewer reflections to characterize the steady-state mass exchange among surfaces. For the DSP configuration, the average temperature difference between surfaces is only about 2°C, while the P80 configuration consists of a wide range of temperatures, including several cryogenic surfaces.

Thus, for the two payloads evaluated, these factors combine so as to favor rapid convergence for the P80 configuration while hindering convergence for the DSP configuration. In general, however, four or five reflections would appear adequate to guarantee better than 90% convergence for typical payload geometries and thermal profiles.

In evaluating the cost of performing multiple reflection analyses, several points are of significance. For a given configuration, the computer time is a linear function of the number

of reflections performed. The cost of performing zero reflections (straight direct flux) is a function of the number of nodes in the configuration, the number of body-to-body viewfactors pairs, and the number of receiving (critical) surfaces evaluated. The slope of the linear relationship is proportional to the number of body-to-body viewfactor pairs.

For the DSP and P80 configurations, the number of nodes (38) and receiving surfaces (20) are the same. Thus, we would expect that the cost of performing a given number of reflections, as well as the slope of the cost vs. number of reflections relationship for the DSP configuration would be approximately 360/112 or 3.2 times that of the P80 configuration. Examination of Figure 10 shows that, indeed, this is the case.

Comparing the cost of running GBCAL with that of performing multiple reflections, we see that, for the DSP, the "break-even" point occurs at 3 reflections, and for the P80, at 6 reflections. Since 3 reflections yields only about 85% convergence for the DSP configuration, it appears that GBCAL is more cost-effective for slowly converging configurations. However, it must be emphasized that GBCAL is inherently limited in its capabilities and cannot meet total mission analysis requirements for the following reasons:

- GBCAL is limited to 38 node configurations; "Multi-reflect," possesses a full 300 node capability.

- Only outgassing species can be evaluated with GBCAL. With Multireflect, a 10 specie capability exists, including early desorption and engine exhaust constituents.

- Only direct flux can be evaluated with GBCAL, while the multiple reflection logic also addresses column density and return flux.

In order to provide adequate resolution for contamination analysis, most configuration models contain many more than 38 nodes. Stripping a configuration down to a 38 node subset could drastically alter deposition predictions for two primary reasons: 1) the mass which would have been contributed by the deleted nodes will not be available to reflect and ultimately deposit on critical surfaces, and 2) the deleted nodes result in there being fewer reflective paths by which mass can arrive at a critical surface.

Thus, even when a configuration can be expected to exhibit slow convergence, we do not recommend that GBCAL be used to evaluate a subset of the configuration.

CONCLUSIONS

Based on the study results to date, the following conclusions have been drawn:

- four to five reflections appear to be adequate for typical payload geometries/thermal profiles, yielding at least 90% convergence,

- the fewer surfaces "seen" by a critical surface, the faster will convergence occur,

- the higher the relative magnitude of the configuration's body-to-body viewfactors, the faster will convergence occur,

- the greater the average temperature difference between surfaces, the faster will convergence occur, and

- because of its inherent limitations, GBCAL is not recommended, even for slowly converging configurations-- GBCAL should be considered only as a valid calibration source for the multireflect option as opposed to a viable contamination analysis tool.

Appendix B

Deposition Summation Algorithm Description

This appendix describes the deposition summation logic and its implementation in the SPACE II code.

Deposition Summation Routine

Objective

The objective of this activity was to develop and incorporate additional logic into the SPACE code to accumulate deposition for discrete mission intervals executed during any one SPACE run. Deposition was to be computed for both direct and return flux transport mechanisms using existing sticking coefficient and sublimation algorithms and summed over all mission intervals.

Approach

Mission time intervals are defined by the input variables TSTART(3) and TSTOP(3). The mission interval establishes the exposure time duration for all surface sources. The ONTIME (50) variable defineds the exposure time duration for point sources. Thus, point sources can be operational for a full mission interval (i.e. evaporator) or only a small portion of a mission interval (i.e. VCS).

A stacked run (i.e. a six interval full-orbit simulation) input is assembled by first developing a full set of namelist inputs for the first time interval identifying the desired source characteristics, transport mechanisms, mission parameters, report options, etc. For the remaining intervals, the only inputs required are the new point source parameters (PNTSC(50), ONTIME(50)), the new velocity vector orientation (not required if a ZLV attitude is being simulated), and a new temperature file selected from TAPE10 through proper selection of oneof the following: MINTMP,

MAXTMP, or ATCODE = 1, 2, 3, 4, or 5.

The logic flow is illustrated in Figure 1. The title card is first read from the input deck (in subroutine MAIN). If the titles is not 'STOP' then $CONTRL is read. If DIRECT = .TRUE., the normal direct flux calculations are performed for each receiver and REPORT(21) and (22) are written and the deposition for each receiver (per specie) is stored in common. If the first stack of the run is being evaluated the deposition perreceiver that is stored is that from REPORT(24). If it is not the first stack, the sublimation of light species multiplied by (TSTOP - TSTART) is subtracted from the old deposition already stored, and the total new deposition is the old sublimated deposition plus the new deposition for that stack. If REPORT(51) = .TRUE., REPORT(51) is then written. If RFAS2 or RFSS = .TRUE. the return flux calculations are performed for RECEVR(I) and the return flux reports are written. If REPORT(49) and (50) = .TRUE., the reports are written, deposition stored (and sublimated if not first stack) and the accumulated deposition is computed. After all receivers have been evaluated for retrun flux, if REPORT(51) = .TRUE. REPORT(51) is written and the next stack title is read. This logic is then repeated for each stack until the title card is 'STOP'.

The new reports 23, 24, 49, 50, and 51 have the following contents and formats:

Report 23 'Direct Flux Deposition Rates on Surface (RECEVR)'
There are three sections to this report:

1. 'Direct Flux Surface Source Deposition Rates' - contains deposition rates for all surface source have a non-zero flux to the receiver

B-4
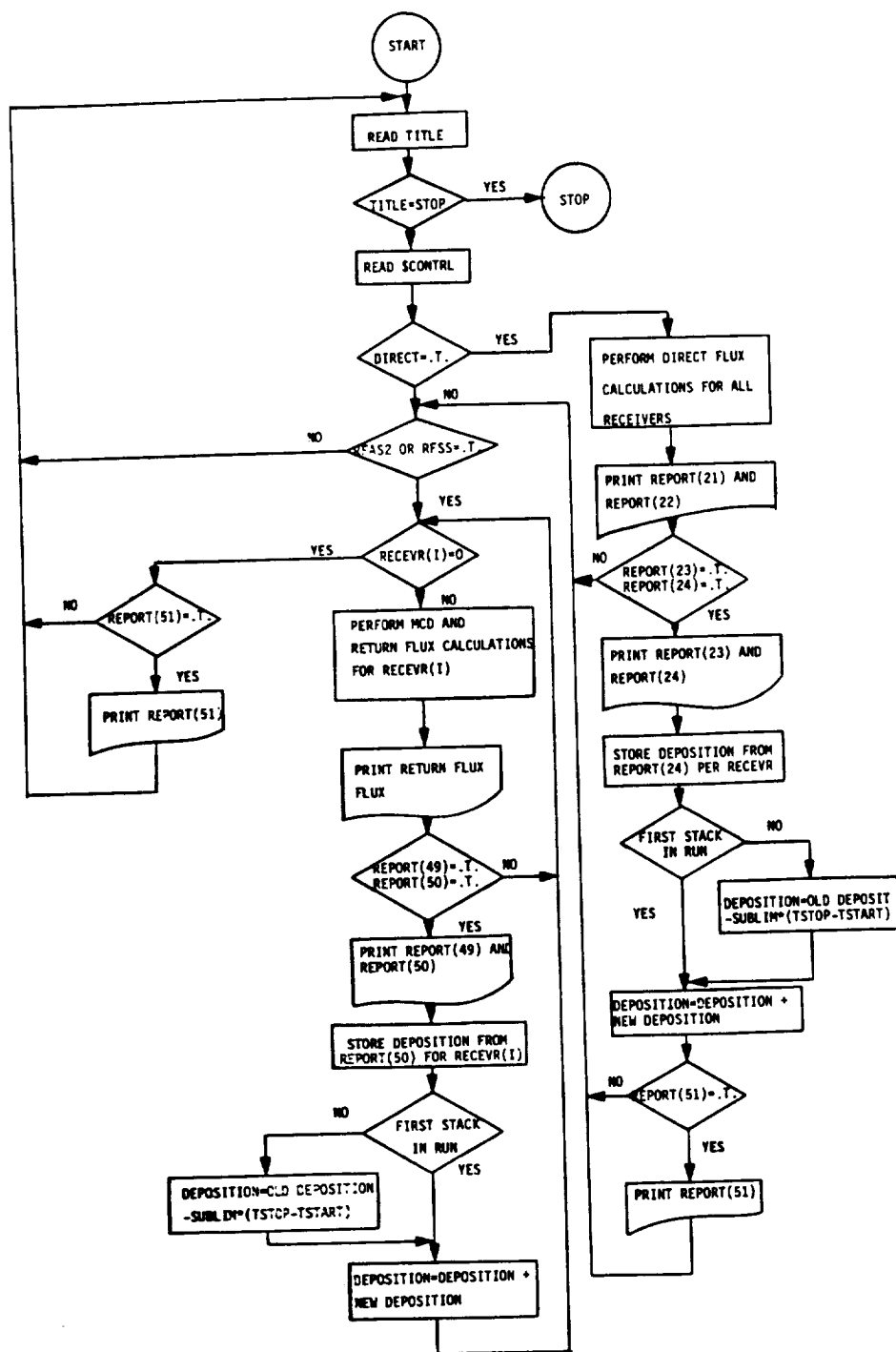
Figure 1 Deposition Summation Algorithm Logic Flow

(by specie),

2. 'Direct Flux Point Source Deposition Rates' - contains deposition rates for every point source having a flux contribution to the rates for every point source having a flux contribution to the receiver,

3. 'Grand Total' - contains the total deposition rate for sections 1) and 2) for each specie.

Report 24 'Direct Flux Deposition on Surface (RECEVR)' - same format as Report 23 except deposition rates are multiplied by appropriate exposure times to compute deposition values for the total time slice. Surface source deposition rates are multiplied by (TSTOP(3) - TSTART(3)) and point source deposition rates are multiplied by the proper value of ONTIME(50).

Report 49 'Return Flux Deposition Rate'

There are four sections to this report:

1. 'Return Flux-Ambient Scattering-Surface Source Deposition Rates' - contains all surface source contributions for return flux due to ambient scattering to the receiver.

2. 'Return Flux-Ambient Scattering' - Point Source Deposition Rates' - contains all point source contributions for return flux due to ambient scattering.

3. 'Return Flux-Self-Scattering' - Point Source Deposition Rates' - contains all point source contributions for return flux due to self-scattering.

4. 'Grand Total' - contains the sum of sections 1), 2), and 3) by specie.

Report 50 'Return Flux Deposition on Surface (RECEVR)' - same format as Report 49 except deposition values are presented (see Report 24 deposition).

Report 51 'Total Accumulated Deposition Direct and/or Return Flux

Combined - Report 51 has one section containing the total of all deposition arrays stored in common by receiver and specie. These values represent a cumulative summary of deposition for all prior time slices.

The following subroutines have have been modified for the deposition logic:

COLLCT	PRINTD
DIRCT	RFASS
DFLUX	RFSSS
MAIN	RTFMCD

A new subroutine TOTDEP' has been added after subroutine MAIN.

Appendix C

OFT-1/OFT-3 Mission Analysis

Thermal Data (Tape 10)

This appendix is a listing of the SPACE II input data file TAPE 10. The file contains the Shuttle Orbiter/IECM/DFI/payload bay nodal temperature data used for the OFT-1 and OFT-3 mission analyses.

OFT-1 Shuttle Orbiter/IECM Temperature File

| NODEJ | MAXTMP | MINTMP | ATCODE | | | | |
			1	2	3	4	5
1	-12.84	-2.17	3.00	-7.39	-20.55	-4.67	17.97
2	-9.46	-.47	-3.72	-16.18	-17.21	-4.07	-9.48
3	-9.89	.07	-3.04	-14.74	-16.83	-12.25	-9.90
4	-10.56	.35	-2.27	-12.32	-17.37	-15.54	-10.57
5	-11.98	-5.84	-8.28	-18.70	-19.29	3.27	-12.01
6	-9.75	-.74	-3.96	-16.42	-17.45	-4.65	-9.77
7	-9.90	.07	-3.01	-14.73	-16.83	-15.73	-9.91
8	-10.72	.21	-2.38	-12.49	-17.54	-15.73	-10.73
11	-17.78	-17.78	-17.78	-17.78	-17.78	-17.78	-17.78
13	-16.79	-15.47	-15.86	-17.77	-17.96	-15.18	-16.80
20	-17.78	-17.78	-17.78	-17.78	-17.78	-17.78	-17.78
22	-17.78	-17.78	-17.78	-17.78	-17.78	-17.78	-17.78
24	-17.78	-17.78	-17.78	-17.78	-17.78	-17.78	-17.78
26	-17.78	-17.78	-17.78	-17.78	-17.78	-17.78	-17.78
30	-17.78	-17.78	-17.78	-17.78	-17.78	-17.78	-17.78
32	-17.78	-17.78	-17.78	-17.78	-17.78	-17.78	-17.78
34	-17.78	-17.78	-17.78	-17.78	-17.78	-17.78	-17.78
36	-17.78	-17.78	-17.78	-17.78	-17.78	-17.78	-17.78
40	20.40	23.19	24.77	22.63	20.78	20.04	20.40
42	-20.37	-13.71	-14.34	-21.22	-24.60	-17.48	-20.37
44	20.40	23.19	24.77	22.63	20.78	20.04	20.40
46	-13.82	-5.68	-6.54	-15.05	-18.88	-10.11	-13.82
50	20.58	23.37	24.95	22.80	20.95	20.22	20.58
52	-13.81	-5.64	-6.51	-15.06	-18.90	-10.12	-13.81
54	20.58	23.37	24.95	22.80	20.95	20.22	20.58
56	-19.55	-12.81	-13.46	-20.46	-23.81	-16.77	-19.56
60	-29.50	-26.98	-25.49	-26.21	-28.20	-30.78	-29.51
62	-29.17	-26.85	-25.53	-26.25	-28.09	-30.42	-29.17
64	-32.61	-31.63	-29.27	-28.38	-29.93	-32.42	-32.63
66	-13.86	-14.29	-14.46	-13.45	-12.81	-13.47	-13.86
67	10.22	7.11	5.91	13.12	17.69	12.98	10.21
68	10.83	8.06	6.76	11.28	16.45	13.08	10.82
70	-9.99	-10.81	-10.77	-8.67	-7.30	-9.05	-9.99
72	7.93	5.13	4.53	11.27	15.60	10.70	7.93
74	10.22	7.11	5.91	13.12	17.69	12.98	10.21
76	-2.42	-4.05	-3.96	.17	2.87	-.57	-2.43
77	9.16	6.23	5.32	12.03	16.54	11.87	9.15
80	-29.51	-26.98	-25.49	-26.21	-28.20	-30.78	-29.51
82	-29.51	-26.98	-25.49	-26.21	-28.20	-30.78	-29.51
84	-32.57	-31.58	-29.22	-28.33	-29.89	-32.38	-32.58
86	10.74	7.93	6.64	11.53	16.62	13.07	10.74
87	10.37	7.26	6.08	13.29	17.85	13.13	10.36
88	10.81	8.04	6.73	11.25	16.42	13.06	10.80
90	8.78	6.16	5.37	10.40	15.12	11.19	8.77
92	8.26	5.46	4.89	11.63	15.94	11.02	8.25
94	10.37	7.26	6.08	13.29	17.85	13.13	10.36
96	7.38	4.84	4.53	10.14	14.53	9.97	7.37
97	9.38	6.46	5.56	12.27	16.77	12.09	9.37
100	-18.77	-8.02	-12.55	-22.82	-27.11	-25.68	-18.94
102	-18.77	-8.02	-12.55	-22.82	-27.11	-25.68	-18.94
104	-12.47	-11.52	-10.53	-10.51	-11.30	-12.45	-12.59
110	-10.16	-2.69	-3.59	-9.48	-15.74	-10.40	-10.24
112	-10.86	-10.03	-9.07	-9.42	-10.12	-10.99	-11.01
115	-18.77	-8.02	-12.55	-22.82	-27.11	-25.68	-18.94
117	-9.95	-2.38	-3.14	-9.31	-15.51	-9.38	-10.02
118	-9.43	-1.60	-2.02	-8.89	-14.94	-6.84	-9.48
119	-9.21	-9.25	-8.88	-8.63	-8.73	-9.19	-9.39
121	-9.95	-2.38	-3.14	-9.31	-15.51	-9.38	-10.02
106	-10.13	12.78	22.09	9.18	-6.13	-16.05	-10.15
107	-3.95	20.18	29.70	13.58	-1.85	-11.76	-3.97
122	-9.43	-1.60	-2.02	-8.89	-14.94	-6.84	-9.48
130	-18.77	-8.03	-12.56	-22.81	-27.10	-25.67	-18.94

NODEJ	MAXTMP	MINTMP	ATCODE				
			1	2	3	4	5
132	-18.77	-8.03	-12.56	-22.81	-27.10	-25.67	-18.94
134	-12.23	-11.28	-10.30	-10.28	-11.07	-12.22	-12.36
140	-10.18	-2.71	-3.61	-9.49	-15.75	-10.42	-10.25
142	-10.82	-9.99	-9.03	-9.38	-10.08	-10.95	-10.97
145	-18.77	-8.03	-12.56	-22.81	-27.10	-25.67	-18.94
147	-9.97	-2.40	-3.16	-9.32	-15.52	-9.40	-10.04
148	-9.45	-1.63	-2.04	-8.90	-14.95	-6.86	-9.50
149	-9.20	-9.25	-8.88	-8.62	-8.72	-9.18	-9.38
151	-9.97	-2.40	-3.16	-9.32	-15.52	-9.40	-9.38
136	-10.04	12.90	22.21	9.28	-6.05	-15.97	-10.04
137	-3.93	20.20	29.71	13.60	-1.83	-11.74	-10.06
152	-9.45	-1.63	-2.04	-8.90	-14.95	-6.86	-3.96
450	-10.20	-10.20	-9.49	-9.09	-9.29	-10.03	-9.50
451	-10.20	-10.20	-9.49	-9.09	-9.29	-10.03	-10.33
452	-10.20	-10.20	-9.49	-9.09	-9.29	-10.03	-10.33
453	-10.20	-10.20	-9.49	-9.09	-9.29	-10.03	-10.33
454	-10.20	-10.20	-9.49	-9.09	-9.29	-10.03	-10.33
455	-13.70	-12.75	-11.35	-10.86	-11.79	-13.40	-10.33
456	-13.70	-12.75	-11.35	-10.86	-11.79	-13.40	-13.74
457	-13.70	-12.75	-11.35	-10.86	-11.79	-13.40	-13.74
458	-13.70	-12.75	-11.35	-10.86	-11.79	-13.40	-13.74
459	-13.70	-12.75	-11.35	-10.86	-11.79	-13.40	-13.74
460	-10.19	-10.19	-9.48	-9.07	-9.28	-10.02	-13.74
461	-10.19	-10.19	-9.48	-9.07	-9.28	-10.02	-10.32
462	-10.19	-10.19	-9.48	-9.07	-9.28	-10.02	-10.32
463	-10.19	-10.19	-9.48	-9.07	-9.28	-10.02	-10.32
464	-10.19	-10.19	-9.48	-9.07	-9.28	-10.02	-10.32
465	-13.67	-12.71	-11.31	-10.82	-11.75	-13.36	-10.32
466	-13.67	-12.71	-11.31	-10.82	-11.75	-13.36	-13.71
467	-13.67	-12.71	-11.31	-10.82	-11.75	-13.36	-13.71
468	-13.67	-12.71	-11.31	-10.82	-11.75	-13.36	-13.71
469	-13.67	-12.71	-11.31	-10.82	-11.75	-13.36	-13.71
301	-25.07	-24.17	-22.96	-23.06	-23.74	-24.82	-13.71
305	-17.36	-16.36	-15.28	-15.34	-16.17	-17.35	-25.15
306	-17.22	-16.23	-15.16	-15.22	-16.04	-17.22	-17.52
307	-20.90	-20.58	-19.93	-19.74	-19.90	-20.70	-17.38
311	-25.40	-24.50	-23.29	-23.39	-24.08	-25.16	-20.80
315	-16.94	-16.04	-15.03	-15.10	-15.83	-16.93	-25.49
316	-18.32	-17.50	-16.62	-16.76	-17.38	-18.30	-17.10
316	-16.13	-16.05	-15.91	-15.84	-15.95	-16.15	-18.44
317	-20.79	-20.45	-19.80	-19.64	-19.83	-20.63	-16.18
420	-16.04	-16.83	-16.53	-15.40	-14.34	-15.11	-20.72
425	-16.91	-17.67	-17.38	-16.32	-15.32	-16.04	-15.94
250	-4.16	-4.56	-3.99	-3.23	-3.07	-3.70	-16.84
260	-3.10	-3.98	-4.13	-3.25	-2.25	-2.61	-4.30
202	-16.69	-16.77	-16.81	-16.75	-16.61	-16.61	-3.23
203	-16.71	-16.79	-16.82	-16.76	-16.64	-16.65	-16.67
380	-43.24	-42.98	-42.74	-42.94	-43.35	-43.90	-16.70
381	-43.32	-43.06	-42.82	-43.02	-43.43	-43.98	-43.74
382	-50.56	-49.59	-48.50	-48.85	-49.76	-50.96	-43.82
383	-50.60	-49.63	-48.54	-48.89	-49.80	-51.00	-50.93
384	-54.09	-53.19	-51.46	-51.03	-52.46	-54.09	-50.96
385	-57.31	-56.56	-54.92	-54.34	-55.62	-57.18	-54.32
386	-62.34	-62.14	-60.81	-59.94	-61.03	-62.23	-57.51
387	-62.36	-62.16	-60.83	-59.96	-61.05	-62.25	-62.57
388	-35.67	-34.70	-33.51	-33.37	-34.59	-36.13	-62.59
389	-35.81	-34.84	-33.66	-33.52	-34.73	-36.27	-35.94
390	-37.39	-36.59	-35.45	-34.86	-36.01	-37.63	-36.07
391	-37.48	-36.69	-35.55	-34.96	-36.10	-37.72	-37.62
392	-32.49	-31.91	-31.28	-31.46	-32.18	-33.07	-37.71
393	-32.36	-31.78	-31.14	-31.32	-32.05	-32.94	-32.85
160	17.13	52.27	28.81	-8.62	-30.26	-46.33	-32.72
161	-16.22	-15.62	-15.00	-15.32	-16.06	-16.95	17.13
162	-17.84	-17.24	-16.61	-16.92	-17.65	-18.55	-16.30
							-17.90

NODEJ	MAXTMP	MINTMP	ATCODE 1	2	3	4	5
163	-16.76	-15.87	-15.23	-15.22	-15.85	-16.84	-16.82
164	-17.02	-16.12	-15.47	-15.45	-16.07	-17.06	-17.05
165	-16.37	-15.36	-14.39	-14.09	-14.68	-16.12	-16.46
166	-16.08	-15.07	-14.06	-13.74	-14.33	-15.77	-16.13
167	-24.50	-23.57	-22.68	-22.55	-23.12	-24.33	-24.63
168	-23.63	-22.63	-21.64	-21.47	-22.08	-23.38	-23.72
169	-14.91	-14.76	-14.08	-13.67	-13.81	-14.71	-15.16
170	-15.24	-15.10	-14.41	-14.00	-14.14	-15.03	-15.48
171	-6.14	-6.43	-6.12	-5.63	-5.51	-6.03	-6.43
172	-6.40	-6.69	-6.39	-5.88	-5.76	-6.28	-6.68
174	-26.07	-25.55	-24.86	-24.99	-25.50	-26.24	-26.13
175	-27.97	-27.85	-27.39	-27.09	-27.23	-27.88	-28.18
177	-24.86	-24.67	-24.14	-23.83	-24.01	-24.75	-25.07
180	-18.24	-17.85	-17.59	-17.97	-18.55	-18.95	-18.42
181	-18.24	-17.85	-17.59	-17.97	-18.55	-18.95	-18.42
182	-18.35	-18.24	-18.09	-18.05	-18.18	-18.53	-18.52
183	-17.66	-17.55	-17.40	-17.36	-17.49	-17.84	-17.82
184	-17.51	-17.12	-16.86	-17.23	-17.80	-18.20	-17.67
185	-17.51	-17.12	-16.86	-17.23	-17.80	-18.20	-17.67
190	-19.05	-18.59	-18.13	-18.02	-18.40	-19.10	-19.16
230	-15.91	-17.34	-16.89	-10.66	-9.16	-13.98	-15.82
240	-15.51	-16.26	-16.73	-16.09	-14.79	-14.97	-15.45
440	-13.45	-3.73	-5.40	-14.49	-18.73	-17.44	-13.46
441	-12.37	-3.39	-5.49	-15.76	-18.01	-13.53	-12.38
442	-12.00	-4.01	-6.23	-17.22	-18.53	-5.25	-12.03
443	-12.31	-5.24	-7.85	-20.58	-21.60	11.82	-12.34
445	-13.44	-3.75	-5.44	-14.48	-18.73	-17.43	-13.45
446	-12.49	-3.53	-5.64	-15.88	-18.14	-13.62	-12.50
447	-11.91	-3.93	-6.17	-17.15	-18.47	-5.01	-11.94
448	-11.63	-4.57	-7.20	-20.00	-21.02	13.06	-11.67
1010	12.50	53.00	40.20	-5.20	-18.00	1.20	12.50
1015	21.10	57.00	45.70	5.30	-6.00	11.00	21.10
1012	16.80	55.00	42.90	0.10	-12.00	6.10	16.80
1014	16.80	55.00	42.90	0.10	-12.00	6.10	16.80
1011	16.80	55.00	42.90	0.10	-12.00	6.10	16.80
1013	16.80	55.00	42.90	0.10	-12.00	6.10	16.80
1000	19.00	64.00	49.80	-0.80	-15.00	6.30	19.00
1005	25.30	68.00	54.50	6.50	-7.00	13.30	25.30
1002	22.10	66.00	52.10	2.90	-11.00	9.80	22.10
1004	22.10	66.00	52.10	2.90	-11.00	9.80	22.10
1001	22.10	66.00	52.10	2.90	-11.00	9.80	22.10
1003	22.10	66.00	52.10	2.90	-11.00	9.80	22.10
1020	-12.00	0.00	-3.80	-17.20	-21.00	-15.30	-12.00
1025	-4.60	4.00	1.30	-8.30	-11.00	-7.00	-4.60
1022	-8.80	2.00	-1.40	-13.60	-17.00	-11.90	-8.80
1024	-8.80	2.00	-1.40	-13.60	-17.00	-11.90	-8.80
1021	-8.80	2.00	-1.40	-13.60	-17.00	-11.90	-8.80
1023	-8.80	2.00	-1.40	-13.60	-17.00	-11.90	-8.80
1030	30.70	33.00	32.30	29.70	29.00	30.10	30.70
1035	37.30	39.00	38.50	36.50	36.00	36.80	37.30
1032	36.40	37.00	36.80	36.20	36.00	36.30	36.40
1034	36.40	37.00	36.80	36.20	36.00	36.30	36.40
1031	36.40	37.00	36.80	36.20	36.00	36.30	36.40
1033	36.40	37.00	36.80	36.20	36.00	36.30	36.40

Appendix D

Mass Spectrometer/TQCM/CQCM Transfer

Function Analysis

This appendix contains the results of the mass spectrometer and TQCM transfer function analyses relating SPACE II predicted incident flux and deposition to instrument outputs. The appendix comprises two Parts: Part 1 is the mass spectrometer analysis (p. D-3); and Part 2 is the TQCM analysis. The CQCM response is assumed similar to the TQCM response.

PART 1

MASS SPECTROMETER TRANSFER FUNCTION ANALYSIS

Objective: The objective of this analysis is to determine the transfer function relating the SPACE computed flux incident on the mass spectrometer (MS) entrance aperture to the count rate recorded by the MS/IECM data recording system. The transfer function will be used during the mission analysis activity to assess the sensitivity of the MS to predicted contamination levels.

Instrument Description: A schematic of the MS is shown in Figure 1. The function of the collimator section is to limit the field-of-view of the instrument to a 10^0 half angle cone. This is accomplished by a series of chevron baffles. Molecules incident at angles greater than 10^0 are reflected by the baffles and adsorbed by zirconium "getters". The "getters" are essentially molecular pumps serving to eliminate extraneous molecules from the internal MS volume and thus maintaining an acceptable vacuum level. The pumping speed of the "getters" (S_c) is variable and decreases as a function of total number of molecules adsorbed. The reduction in collimator pumping speed serves to increase the density of extraneous molecules in the ion source region.

The function of the ion source is to ionize neutral gas molecules with a regulated electron beam and then direct the ions into the analyzer section. The sensitivity of the MS system is expressed as a function of particle density in the ion source region.

The analyzer comprises a quadrup$\overset{o}{\wedge}$le section to separate and select proper particle masses and an electron multiplier to create the current pulses. Attached to the analyzer section is the appendage pump. This pump also serves to eliminate extraneous particles and has a pumping speed designated S_A.

Analysis: The MS sensitivity data relates the number of counts from the detector electronics to the particle density in the ion source volume. Laboratory calibration has been accomplished for the gases shown below (Ref. 1).
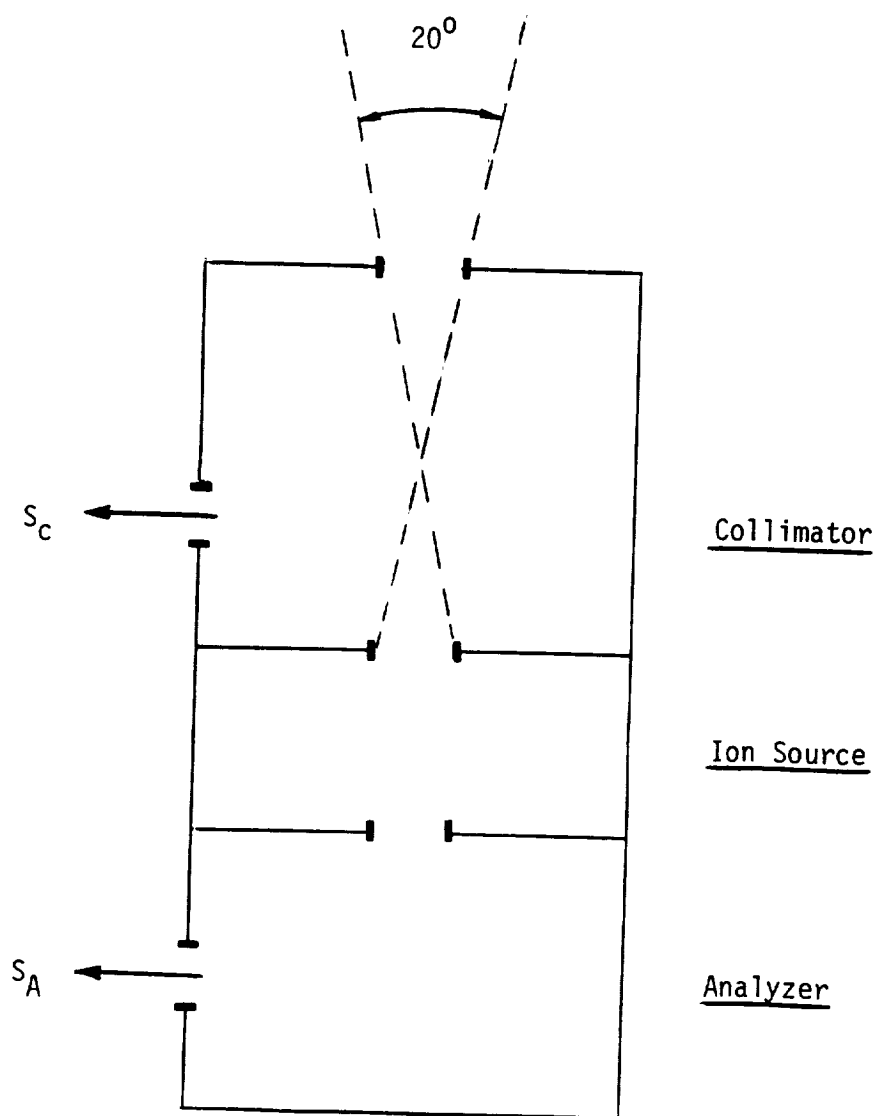
Figure 1.   Mass Spectrometer Functional Schematic

Specie	Sensitivity (counts/sec./particles/cm^3)
He	0.141E-3
H_2O	0.946E-3
N_2	1.05E-3
A_r	1.12E-3

Approximate sensitivities for other gases can be obtained utilizing the data from Figure 2 and Figure 3. Figure 2 relates a N_2 sensitivity multiplier to the normalized molecule electron count. Figure 3 corrects the collimator transmission as a function of molecule AMU. (Ref. 1).

The transfer functions relating ion source particle density to flux incident on the collimator entrance aperture have been derived (Ref. 2) for both random and collimated flux inputs. For the random flux input:

$$N_R = \pi FA \ [f(S_A, S_C)] \tag{1}$$

where

N_R = ion source number density (particles/cm^3)

F = flux incident on the entrance aperture (particles/cm^2/sec/sr)

A = area of entrance aperture (7.07 x 10^{-2}cm^2)

S_A = appendage pump pumping speed (cm^3/sec)

S_C = collimator pump pumping speed (cm^3/sec)

For the collimated flux input

$$N_C = NaVAcos\alpha \ [f(S_A, S_C, L] \tag{2}$$

where

N_C = ion source number density (particles/cm^3)

N_a = ambient number density (particles/cm^3)

V = spacecraft velocity (cm/sec)

α = angle of attack with respect to ambient velocity vector

L = loss coefficient

S_A and S_C are variable and depend on the total integrated gas load to which they have been exposed. Analyses (Ref. 2) have shown that variations in S_A (1000 cm^3/sec. initial value) due to expected gas loads will result in a N_R and N_C variation on the order of 4%. This is a negligible effect compared to other uncertainties.
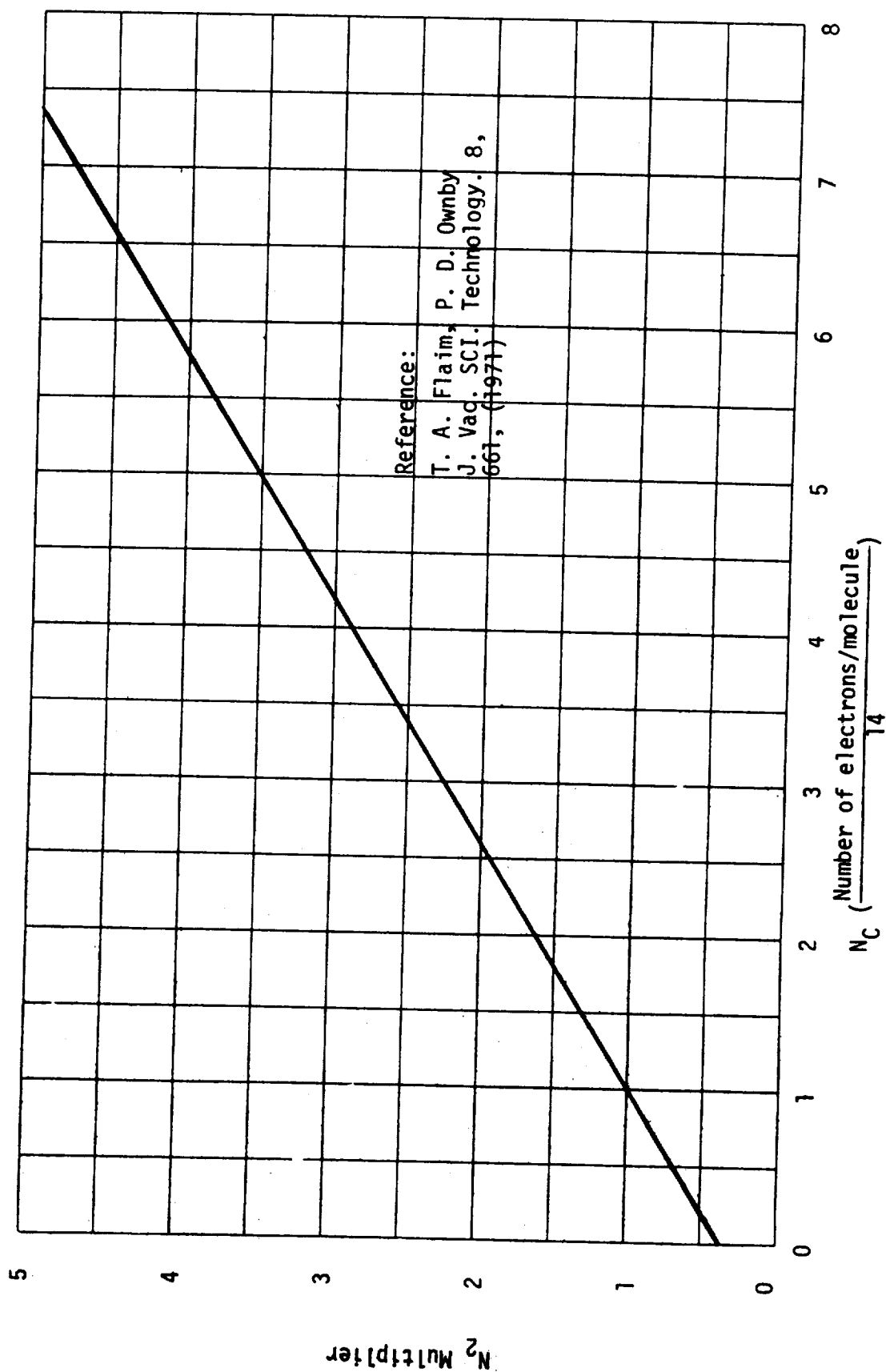
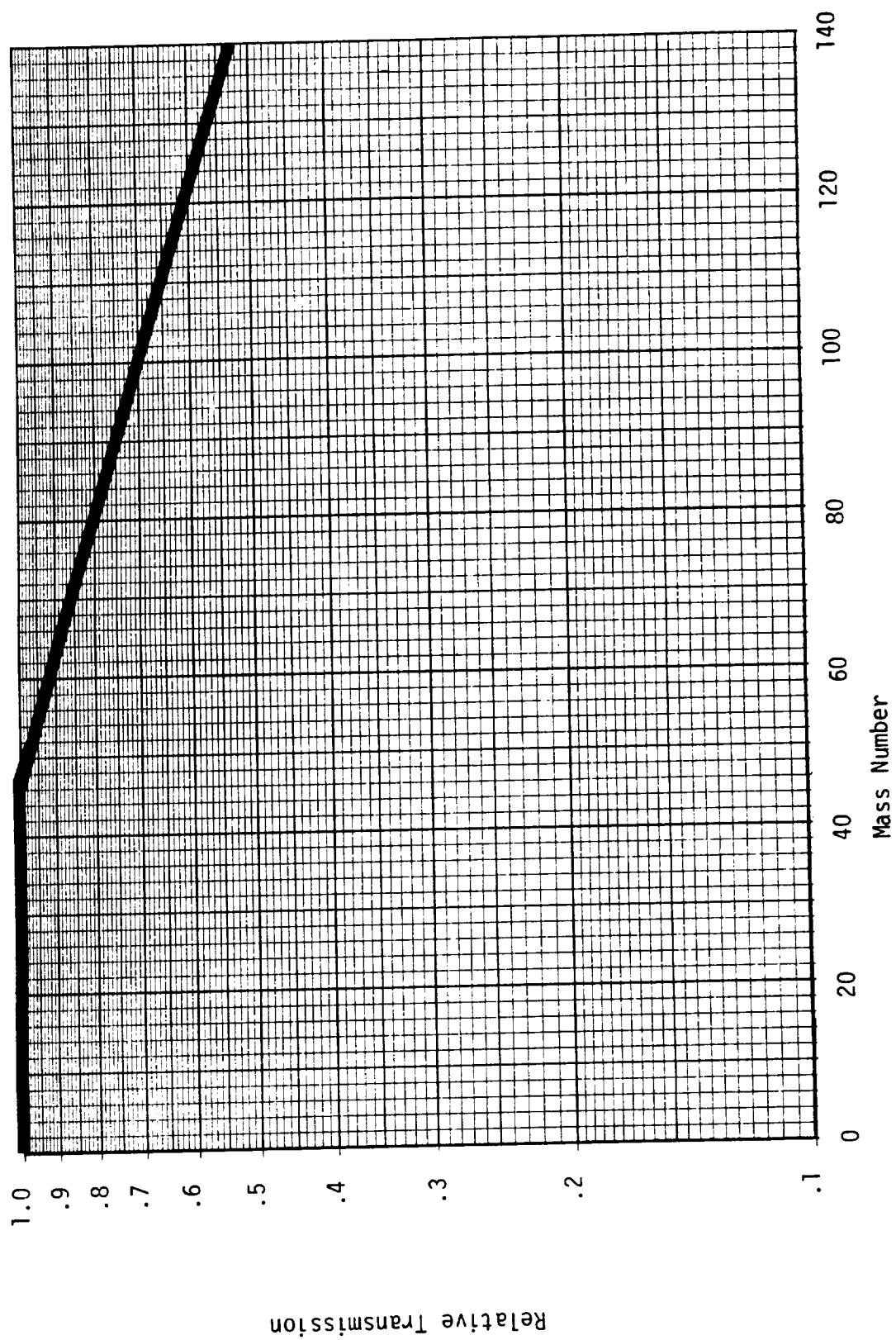Figure 2. Ionization Efficiency Relative to N_2

Figure 3. Transmission Efficiency

Relative Transmission

The effect of the decay of S_c due to expected gas loads can result in ion density variations up to 600%. Calculated reductions in S_c as a function of time for both random and collimated flow are shown in Table I and Table II (Ref. 2).

For the purposes of this analysis we will assume that the MS aperture remains closed until immediately prior to the mapping activity and the undegraded value of the collimator pumping speed will be assumed ($S_c = 7.2 \times 10^4$ cm^3/sec.)

The remaining variable to be determined is the loss coefficient (L). This variable, which applies only to the ram flux sensitivity calculation, is the ratio of the collimator output aperture flux to input aperture flux. Variations in the loss coefficient depend on specie and gas temperature. Values for L can vary from 0.55 for N_2 to 0.35 for atomic oxygen for $\alpha = 0$, $T = 1000^\circ$K. A nominal value of 0.45 will be assumed for this analysis.

Based on these values for S_A, S_c and L, the transfer functions relating incident flux to ion source density can be computed. From Reference 2 for random flux ($\alpha = 90^\circ$),

$$N_R = \pi FA \ \frac{7.15 \times 10^{-4} + \left(\dfrac{38.2}{888 + S_c}\right)}{158 - \left(\dfrac{1.44 \times 10^4}{120 + S_A}\right) - \left(\dfrac{1.46 \times 10^3}{888 + S_c}\right)} \tag{3}$$

Substituting for A, S_c, S_A yields

$$N_R = (1.90 \times 10^{-6}) \ F \tag{4}$$

For collimated flux ($\alpha = 0^\circ$)

$$N_C = N_a VA\cos\alpha \ \frac{4.49 \times 10^{-2} L + 38.2 \left(\dfrac{(1 - 4.49 \times 10^{-2}L)}{(888 + S_c)}\right)}{158 - \left(\dfrac{1.44 \times 10^4}{120 + S_A}\right) - \left(\dfrac{1.46 \times 10^3}{888 + S_c}\right)} \tag{5}$$

Substituting for A, L, S_c, S_A yields,

$$N_c = (1.02 \times 10^{-5}) \, N_a Vcos\alpha \tag{6}$$

Therefore the overall MS transfer functions for the species identified previously becomes

Specie	Transfer function (nominal case) (counts/sec/particles/cm^2/sec)	
	T_{RANDOM}	$T_{COLLIMATED}$
H_e	2.68×10^{-10}	1.42×10^{-9}
H_2O	1.80×10^{-9}	9.55×10^{-9}
N_2	2.00×10^{-9}	1.06×10^{-8}
A_r	2.13×10^{-9}	1.13×10^{-8}

Therefore, the data system recorded count rate (counts/sec.) can be computed for specific species for random (R_R) and collimated (R_C) flux conditions from

$$R_R = T_{RANDOM} * F$$

$$R_C = T_{COLLIMATED} * NaVcos\alpha$$

Conclusions: Transfer functions relating the MS data system to the entrance aperture flux intensities have been developed for both the random flux and collimated (ram) flux cases. Ambient atmosphere data system count rate predictions utilize the collimated flux transfer functions. For example, at an altitude of 240 km the nominal N_2 density is 1.32×10^{-9} particles/cm^3. For a spacecraft velocity of 7.8×10^5 cm/sec and $\alpha = 0^0$ the data system count rate becomes

$$R_C = 1.06 \times 10^{-8} * 1.32 \times 10^9 * 7.8 \times 10^5 * 1$$
$$R_C = 1.09 \times 10^7 \text{ counts/sec}$$

Table I. Collimator Pumping Speed Degradation - Random Flux

α (degrees)	Time (weeks)	S_c (cm^3/sec.)
90	0	72,000
90	1	40,800
90	2	24,000
90	3	14,400

Table II. Collimator Pumping Speed Degradation - Ram Flux

α (degrees)	Time (hours)	S_c (cm^3/sec.)
0	0	72,000
0	10	24,000
0	100	4,200

This count rate is within the maximum calibration rate of 2.5×10^7 counts/sec.

For the contamination measurement case the random flux transfer functions apply. The SPACE computer code will predict flux levels in a region constrained by the 0.1 steradian field-of-view of the MS and therefore the transfer functions can be used directly. For example, assume that the H_2O portion of early desorption is to be measured from the Nomex on the Shuttle Orbiter wing. For a wing temperature of $100^\circ C$ (hot case) and five days into the mission the source rate for H_2O is predicted to be $9.0 \times 10^{-12} g.cm^2/sec$. For a view factor of 0.1 the molecular flux at the MS entrance aperture is $3.0 \times 10^{10} mol/cm^2/sec$. For a transfer function of 1.8×10^{-9} this results in a count rate of 54 counts/sec. This count rate is relatively low but within the sensitivity of the data system.

Detection of direct flux of the more complex molecules of surface outgassing may be far more difficult with the MS due to the fact that the cracking patterns of the Orbiter outgassing species are not clearly defined. For the outgassing contaminant species, reliance on the TQCMs and CQCMs may be required.

REFERENCES

1. Taeusch, David R. : Memo, IECM Sensitivity, University of Michigan, May 1, 1979.

2. Taeusch, David R. : Memo, Analysis of Data for a Pumped Ante-Chamber Mass Spectrometer System 015803-2-R, University of Michigan.

TEMPERATURE-CONTROLLED QUARTZ CRYSTAL MICROBALANCE (TQCM)

Objective - The objective of this analysis is to determine the transfer function relating the beat frequency output of the TQCM instrument to the contaminant flux impinging on the sensor crystal as predicted by the SPACE computer program.

Instrument Description - The QCM is a mass measuring device which uses an oscillating quartz crystal to measure the changes in deposited mass. Mass deposited or removed from the crystal changes the oscillation frequency. The frequency change is proportional to the mass change. The temperature of the TQCM crystals are controllable. The sticking coefficient (ratio of depositing mass to impinging mass) and desorption rate for various species is a function of substrate temperature. Thus the ability to control substrate temperature will allow accomodation coefficients and activation energies for a variety of species to be analyzed. Temperatures planned for the IECM TQCMs are $+80^{o}C$ (for crystal cleaning) and +30, 0, -30, $-60^{o}C$ for data collection. Since the dwell times for light gas molecules (H_2O, CO_2, N_2, O_2, etc.) are negligible for temperatures above approximately $-120^{o}C$, these species are not expected to deposit on the TQCM sensor.

Analysis - The change in TQCM beat frequency as a function of impinging flux can be expressed by:

$$\Delta F = m_i * s_i * \Delta t * \frac{1}{\sigma} \tag{1}$$

where

ΔF = change in frequency (H_z)
m_i = mass flux of specie i impinging on sensor crystal ($g/cm^2/sec$)
s_i = sticking coefficient for specie i
Δt = exposure time (sec)
σ = TQCM sensitivity (1.56×10^{-9} $g/cm^2/H_z$)

The mass flux (m_i) levels are predicted by the SPACE computer code for up to 10 species as a function of spacecraft material, temperature, and geometry. The sticking coefficient (s_i) is variable in most cases and is a strong function of surface temperature. Typically the deposition rate on

a surface can be expressed by:

$$D = I - E = sI \qquad \text{for } I > E \qquad (2)$$
$$D = 0 \qquad \text{for } I < E$$

where

  D = deposition rate

  I = impingement rate

  E = evaporation rate

The evaporation or sublimation rate (E) is a strong function of surface temperature and for light gases (H_2O, N_2, O_2, CO_2, etc.) is substantially larger than typical values of I at surface temperatures above $-120^{\circ}C$. Therefore, the deposition rates for light gases at TQCM temperatures are expected to be zero.

For generic outgassing species an empirical relationship has to be developed for s based on test data for "typical" spacecraft materials (Reference 1). The sticking coefficient is expressed as:

$$s = \frac{T_S - T_R}{200} \qquad \begin{array}{l} \text{for } T_S > T_R \\ (T_S - T_R) < 200 \end{array} \qquad (3)$$
$$s = 0 \qquad \text{for } T_S < T_R$$

where

  T_S = source temperature ($^{\circ}C$)

  T_R = receiver temperature ($^{\circ}C$)

This algorithm has been incorporated into the SPACE computer program and provides the basis for the majority of deposition calculations.

For the light gas species a relationship based on equation (2) is utilized with the sublimation rate computed as a function of vapor pressure at the temperature of interest.

For engine plume non-volatile residue (NVR) a sticking coefficient of 1 is used since by definition NVR does not evaporate. NVR accounts for up to 1.7% of the MMH/N_2O_4 engine exhaust. Since direct impingement

of engine plumes is not anticipated and this "specie" does not reflect or desorb, negligible collection on the TQCM is anticipated. Under certain attitudes engine NVR (primarily MMH-Nitrate) may impinge upon the TQCMs viewing into the ambient drag vector through return flux of engine effluents, however, this is expected to be very small for the viewing times/locations of the OFT-4 mapping mission.

Conclusions - The results of the previous discussion indicate that the only contaminant specie predicted by the SPACE program and expected to deposit on the TQCM is generic outgassing. Typical outgassing rates for Shuttle Orbiter materials are on the order of 5×10^{-10} g/cm^2/sec (HRSI/LRSI) at a temperature of 100^{0}C. For a TQCM temperature of -60^{0}C the sticking coefficient becomes 0.8. If we assume a view factor of 0.3 (relatively large) the frequency change on a per second exposure time basis can be computed from

$$\frac{\Delta f}{\Delta t} = \frac{m * s}{\sigma} \tag{4}$$

$$\frac{\Delta f}{\Delta t} = \frac{5 \times 10^{-10} * 0.3 * 0.8}{1.56 \times 10^{-9}}$$

$$\frac{\Delta f}{\Delta t} = 0.077 \; H_z/sec$$

Or conversely a 13 second exposure time is required to record a frequency change of 1 H_z. Clearly, considering smaller, more realistic view factors and lower source temperatures, exposure times substantially greater than 13 seconds could be required in order to record outgassing deposition.

REFERENCES

1. Shuttle/Payload Contamination Evaluation Program Users Manual, Martin Marietta Corporation, Denver, Colorado, April 1977.

D-14

Appendix E

OFT-4 Mission Analysis Plan

MARTIN MARIETTA AEROSPACE

DENVER DIVISION
POST OFFICE BOX 179
DENVER, COLORADO 80201
TELEPHONE (303) 979-7000

29 April 1980

To: National Aeronautics and Space Administration
        Lyndon B. Johnson Space Center
        Houston, Texas 77058

        Attention: Mr. S. Jacobs ES-5

From: Mr. F. Jarossy

cc: Dr. H. Ehlers ES-5

Subject: Preliminary OFT-4 IECM Contamination Analysis Plan

Introduction - The objectives of the IECM measurement activity on OFT-4 are twofold. The primary objective is to define the contamination environment induced by the Shuttle Orbiter contamination sources. The secondary objective is to validate the ability of the SPACE computer program to predict the contamination environment as a function of source and mission parameters. Subsequent to validation, the SPACE program will then be used to predict the contamination environment for future missions.

The SPACE computer program is the only mechanism presently available capable of evaluating IECM instrument performance in the vicinity of the Shuttle Orbiter. The code will be used to: 1) predict contamination levels at various IECM locations to allow assessment of IECM mass spectrometer (MS) and temperature controlled quartz crystal microbalance (TQCM) sensitivities; 2) identify dwell times at each location required to obtain adequate measurement statistics; and 3) provide sufficient parametric data relating instrument sensitivities to predicted flux levels to allow the development of an optimized IECM contamination mapping program.

Objective - The purpose of the OFT-4 analysis activity is to establish an optimized measurement location matrix for the IECM. The results of that analysis will comprise: 1) recommended location/orientation coordinates; 2) measurement durations for each point; and 3) the predicted instrument output data.

The objective of this plan is to define the approach for performing the OFT-4 analysis. The approach will consider both the primary objective of general contamination environment definition and the secondary objective

1) assure that adequate measurement statistics are obtained based on pre-dicted contaminant sensitivities and; 2) assure that adequate spatial resolution is obtained for development of the contamination environment map in response to the primary IECM objective.

Measurement matrix points required to obtain data necessary for contamination model verification (i.e. spatial/temperal/thermal variations in source characteristics, flux attenuation due to ambient scattering) will also be identified. It is anticipated that the majority of these points will be included in a subset of existing points and therefore result in a minimum impact to the overall size of the matrix.

Instrument sensitivities and transfer functions (input flux/output data) are summarized in the attachments for the mass spectrometer and TQCM. Since the number of matrix points to be analyzed has increased substantially from previous estimates (6), the IECM will be represented by a 4 node geometry. These nodes will include a cylinder and a disc for each of the two instruments. The disc represents the sensitive surface and the cylinder acts as a shadowing surface to limit the instrument fields-of-view. It is anticipated that a maximum of fifty points (i.e., locations/orientations) will be addressed.

Conclusions - The proposed OFT-4 IECM mapping mission analysis approach will remain flexible. The general approach outlined here together with the flexi-bility of the SPACE computer model will allow the analysis to respond to modified prediction requirements as they become identified while remaining cognizant of the basic IECM objections for this mission.

References
1. Contamination Monitoring Requirements, Informal Data Transmittal, Lyndon B. Johnson Space Center, Houston, Texas, January 1980.

2. Proposed OFT-4 IECM Point Map Assessment, Memo, Martin Marietta Corporation, Denver, Colorado, March 21, 1980.

Frank J. Jarossy